0-315-01150-5

National Library of Canada
Canadian Theses Division
Ottawa, Canada
K1A 0N4

Bibliothèque nationale du Canada
Division des thèses canadiennes

49008

PERMISSION TO MICROFILM — AUTORISATION DE MICROFILMER

- Please print or type — Écrire en lettres moulées ou dactylographier

Full Name of Author — Nom complet de l'auteur
LANA LEE

Date of Birth — Date de naissance
11 OCTOBER 1951

Country of Birth — Lieu de naissance
U.S.A.

Permanent Address — Résidence fixe
80 FAYETTE STREET,
~~EDMONTON,~~ 1
CAMBRIDGE, MASSACHUSETTS 02139

Title of Thesis — Titre de la thèse
A LANTHANIDE SHIFT PROBE NMR STUDY OF THE THREE DIMENSIONAL STRUCTURE OF CARP PARVALBUMIN

University — Université
THE UNIVERSITY OF ALBERTA

Degree for which thesis was presented — Grade pour lequel cette thèse fut présentée
PH. D.

Year this degree conferred — Année d'obtention de ce grade
1980

Name of Supervisor — Nom du directeur de thèse
DR. BRIAN D. SYKES

Permission is hereby granted to the NATIONAL LIBRARY OF CANADA to microfilm this thesis and to lend or sell copies of the film.

The author reserves other publication rights, and neither the thesis nor extensive extracts from it may be printed or otherwise reproduced without the author's written permission.

L'autorisation est, par la présente, accordée à la BIBLIOTHÈQUE NATIONALE DU CANADA de microfilmer cette thèse et de prêter ou de vendre des exemplaires du film.

L'auteur se réserve les autres droits de publication; ni la thèse ni de longs extraits de celle-ci ne doivent être imprimés ou autrement reproduits sans l'autorisation écrite de l'auteur.

Date
3 October 1980

Signature
Lana Lee

NL-91 (4/77)

National Library of Canada
Collections Development Branch

Canadian Theses on
Microfiche Service

Bibliothèque nationale du Canada
Direction du développement des collections

Service des thèses canadiennes
sur microfiche

NOTICE

The quality of this microfiche is heavily dependent upon the quality of the original thesis submitted for microfilming. Every effort has been made to ensure the highest quality of reproduction possible.

If pages are missing, contact the university which granted the degree.

Some pages may have indistinct print especially if the original pages were typed with a poor typewriter ribbon or if the university sent us a poor photocopy.

Previously copyrighted materials (journal articles, published tests, etc.) are not filmed.

Reproduction in full or in part of this film is governed by the Canadian Copyright Act, R.S.C. 1970, c. C-30. Please read the authorization forms which accompany this thesis.

THIS DISSERTATION
HAS BEEN MICROFILMED
EXACTLY AS RECEIVED

AVIS

La qualité de cette microfiche dépend grandement de la qualité de la thèse soumise au microfilmage. Nous avons tout fait pour assurer une qualité supérieure de reproduction.

S'il manque des pages, veuillez communiquer avec l'université qui a conféré le grade.

La qualité d'impression de certaines pages peut laisser à désirer, surtout si les pages originales ont été dactylographiées à l'aide d'un ruban usé ou si l'université nous a fait parvenir une photocopie de mauvaise qualité.

Les documents qui font déjà l'objet d'un droit d'auteur (articles de revue, examens publiés, etc.) ne sont pas microfilmés.

La reproduction, même partielle, de ce microfilm est soumise à la Loi canadienne sur le droit d'auteur, SRC 1970, c. C-30. Veuillez prendre connaissance des formules d'autorisation qui accompagnent cette thèse.

LA THÈSE A ÉTÉ
MICROFILMÉE TELLE QUE
NOUS L'AVONS REÇUE

Ottawa, Canada
K1A 0N4

NL-339 (Rev. 8/80)

THE UNIVERSITY OF ALBERTA

A LANTHANIDE SHIFT PROBE NMR STUDY OF THE THREE DIMENSIONAL STRUCTURE OF CARP PARVALBUMIN

by

© LANA LEE

A THESIS
SUBMITTED TO THE FACULTY OF GRADUATE STUDIES AND RESEARCH
IN PARTIAL FULFILMENT OF THE REQUIREMENTS FOR THE DEGREE
OF DOCTOR OF PHILOSOPHY

BIOCHEMISTRY

EDMONTON, ALBERTA
FALL 1980

THE UNIVERSITY OF ALBERTA

FACULTY OF GRADUATE STUDIES AND RESEARCH

The undersigned certify that they have read, and recommend to the Faculty of Graduate Studies and Research, for acceptance, a thesis entitled A LANTHANIDE SHIFT PROBE NMR STUDY OF THE THREE DIMENSIONAL STRUCTURE OF CARP PARVALBUMIN submitted by LANA LEE in partial fulfilment of the requirements for the degree of DOCTOR OF PHILOSOPHY.

Brian D. Sykes
Supervisor

Wayne F. Anderson

Cyril M. Kay

Dallas Rabenstein

Stanley J. Opella
External Examiner

Date 12 September 1980

To My Family

Abstract

The interaction of selected lanthanides, such as ytterbium (Yb^{3+}), with the calcium binding protein parvalbumin from carp results in a series of ^1H NMR resonances which are shifted far outside the envelope of the ^1H NMR spectrum of the diamagnetic form of the protein. These shifted resonances are sensitive monitors of the behavior and geometry of the metal binding sites of the protein in solution and have become the focus of a methodology I have developed, the final goal of which is the ability to ascertain the three dimensional structure of the EF binding site of parvalbumin in solution.

The methodology includes the determination of the stoichiometry of the binding of ytterbium to parvalbumin, an analysis of the linewidths of the shifted resonances, an evaluation of the temperature dependence of the observed shifts, and the elucidation of the principal axis system of the magnetic susceptibility tensor of the metal ion.

When Yb^{3+} is added to Ca^{2+} saturated parvalbumin, up to a total Yb^{3+} to total protein ratio of 1/1, a series of shifted resonances appear corresponding to nuclei in the vicinity of the first site filled. At higher ratios in the range of 1/1 to 2/1, a new set of resonances appear corresponding to nuclei in the vicinity of the second site filled. These results indicate that Yb^{3+} sequentially replaces the two Ca^{2+} ions of parvalbumin. Thus at low protein to metal ratios, a single protein metal binding site

is filled by Yb^{3+}. The assignment of the first site filled as the EF site is supported by previously published studies. The ^{1}H NMR data have been further analyzed to yield the relative affinities of the CD and EF sites for ytterbium with respect to Ca^{2+}. The dissociation constants for Yb^{3+} are calculated to be $K^{CD}_{Yb^{3+}} = (4\text{-}7) \times 10^{-10}$ and $K^{EF}_{Yb^{3+}} = (2\text{-}6) \times 10^{-10}$ M from known dissociation constants for calcium[1]. The approximate equality of these constants is verified by Yb^{3+} titrations of apo parvalbumin. The focus of this thesis is on the determination of the structure of the EF binding site in solution using the Yb^{3+} induced shifted resonances.

The linebroadening of the shifted resonances has been measured at 200, 270, 400, and 600 MHz, and the spin lattice relaxation times, at 270 MHz. The analysis of the relaxation rates based upon the theories of Vega and Fiat[2] and Gueron[3] indicates that the susceptibility relaxation mechanism is the major source of spin spin relaxation. From this contribution, individual metal to proton distances are measured.

The diamagnetic shift positions have been determined by an analysis of the temperature dependence of the observed chemical shift positions of the Yb^{3+} induced ^{1}H NMR resonances.

---

[1] Haiech, J., Derancourt, J., Pechere, J.-F., & Demaille, J.G. (1979) *Biochemistry 18*, 2752.
[2] Vega, A.J., & Fiat, D. (1976) *Mol. Phys. 31*, 347.
[3] Gueron, M. (1975) *J. Magn. Reson. 19*, 58.

The paramagnetic shifts of three assigned resonances, the C-2 and C-4 protons of Histidine 26, and the amino terminal acetyl protons, as well as a number of methyl groups, have been used to determine the orientation and principal elements of the magnetic susceptibility tensor of the bound Yb^{3+}. The elucidation of these parameters are needed for the comparison of the observed spectrum of the nuclei surrounding the EF Ca^{2+} binding site of parvalbumin with the calculated spectrum based upon the X-ray crystallographic structure. I observe a significant number of the calculated shifts to be larger than any of the observed shifts. In the future, I shall be able to refine the X-ray based proton coordinates using the geometric information contained in these lanthanide induced shifted resonances.

Acknowledgements

It is with great pleasure and sincere appreciation that I acknowledge my debt to Brian D. Sykes. Throughout this work, he provided foresight, ideas, understanding, enthusiasm, and bright optimism. His developments on and maintenance of the NMR spectrometer enabled me to obtain the superb spectra presented here. I shall always value our friendship. I just wish he could sing in tune. I have relished the cheerful hospitality both he and his wife Nancy have extended to the Group and me.

Other members of the Group have aided me during my stay here. I have greatly benefitted from discussions with Brian F. P. Edwards. He has been a constant source of support and encouragement. He was always helpful in troubleshooting numerous computer programs, but he can't sing either.

On the other hand, Edward R. Birnbaum can sing any song in key besides cook a mean enchilada. His observation of the ^{1}H NMR spectrum of the troponin C CB-9 Pr^{3+} complex began this work. I am grateful to him for many stimulating discussions.

I thank Timothy D. Marinetti for sharing his knowledge of the lanthanides and NMR.

Thanks to Gerry McQuaid, the magnet, the machine, and the entire operation continues to run smoothly.

Joining me in enduring many, many, many Mr. Mikeburgers were other members of the lab: John Baldo, Fred Brauer, Heather Dettman, Scott Hagen, Poul Hansen, Judith Shelling,

John Shriver, and Grayson Snyder. Their contributions to the lab and to Group cooperative dinners are appreciated.

Members of the X-ray crystallographic lab have always been helpful. Dr. Louis Delbaere was instrumental in running the proton generation programs. Koto Hayakawa grew the parvalbumin crystals and determined their unit cell dimensions; she and Dr. Gary Brayer helped me prepare many Ortep plots and a Byron's Bender model of parvalbumin. Colin Broughton introduced me to the three dimensional structure of parvalbumin on the MMS graphics display system.

I thank Drs. Krishna Bose and Aksel Bothner-By for their generous gift of the fluorinated parvalbumin.

I thank Lois Serink for teaching me protein purification techniques and Mr. Mike Natriss for running numerous amino acid analyses for me.

This work required spectra at several frequencies. I thank Dr. Josef Dadok for the 600 MHz spectra, Dr. William E. Hull for the 400 MHz spectra, and Dr. Tom Nakashima and Glen Bigam for the 200 MHz spectra.

Special thanks go to Terry Butler of the University of Alberta Computing Sciences Department for guiding me through the intricacies of Textform, the program used to prepare this thesis.

I thank Lottie Rutkowski and Susan Toy for their friendship and home cooking which contributed greatly to my enjoyment of Edmonton.

This work was supported by the Medical Research Council

of Canada Group on Protein Structure and Function, and The University of Alberta in the form of Teaching Assistantships and the Dissertation Fellowship.

Table of Contents

Chapter Page

I. Introduction 1

A. Calcium Binding Proteins 1

B. Lanthanides as Structural NMR Probes 15

C. Objectives of this Project 20

II. An Overview of the NMR Methodology 23

A. Introduction 23

B. Diamagnetic Spectrum 23

C. Paramagnetic Spectrum 23

D. Paramagnetic Shifts and Diamagnetic Positions .26

E. The Binding of Ytterbium to Parvalbumin 27

F. Metal to Proton Distances 30

G. Magnetic Susceptibility Tensor 31

H. General Conclusions 31

I. Advantages and Disadvantages 32

III. Experimental Methods 39

A. Protein Purification 39

1. Extraction 40

2. Ammonium Sulfate Fractionation 40

3. Gel Exclusion Chromatography 41

4. Ion Exchange Chromatography 41

B. General Methods 43

1. Polyacrylamide gel electrophoresis 43

2. NMR Procedures 45

3. Protein Concentration Determination 46
4. Lanthanide Solution Preparation 47
C. Protein Characterization 48
1. Polyacrylamide gel electrophoresis 48
2. Amino Acid Analysis 50
3. Ultraviolet Absorption Spectroscopy 50
4. Nuclear Magnetic Resonance Spectroscopy .52
5. X-ray Crystallography 57
IV. The Binding of Ytterbium to Parvalbumin 60
A. Introduction 60
B. Experimental Procedures 61
C. Results 67
D. Discussion 75
V. The Analysis of the Linebroadening 87
A. Introduction 87
B. Theory 87
C. Experimental Procedures 93
D. Results 94
E. Discussion 104
VI. The Temperature Dependence of the Observed Shifts 119
A. Introduction 119
B. Experimental Procedures 120
C. Results 123
D. Discussion 123
VII. The Paramagnetic Shifts of Assigned Resonances ..148
A. Introduction 148
B. Experimental Procedures 149

C. Results 152

D. Discussion 161

VIII. Data Summary 167

A. Introduction 167

B. Region I 167

C. Region II 173

D. Region III 178

IX. The Elucidation of the Principal Axis System 183

A. Introduction 183

B. Theory of the Lanthanide Induced Shifts 183

C. Experimental Procedures 189

D. Results 196

E. Discussion 201

X. Conclusions 208

A. Introduction 208

B. Discussion 208

C. The Future 215

Bibliography 217

Appendix 1 227

Appendix 2 228

Appendix 3 229

List of Tables

Page

Table 1. Carp Parvalbumin Isozyme Nomenclature............9

Table 2. The Amino Acid Compositions of Three Isozymes of Carp Parvalbumin....................................11

Table 3. Properties of the Rare Earths....................16

Table 4. A Comparison of the Observed and Published Unit Cell Dimensions of Carp Parvalbumin Crystals..........59

Table 5. Yb^{3+} Titration of Ca^{2+} Saturated Parvalbumin.....72

Table 6. Yb^{3+} Titration of Apo Parvalbumin...............74

Table 7. The Calcium Dissociation Constants of Parvalbumin I...79

Table 8. The Calcium Dissociation Constants of Parvalbumin II..80

Table 9. The Magnesium Dissociation Constants of Parvalbumin...81

Table 10. Additional Dissociation Constants of Parvalbumin...82

Table 11. Magnetic Properties of the Rare Earths..........91

Table 12. The Observed Spin Spin Relaxation Rates of the Ytterbium Shifted Parvalbumin Resonances as a Function of the ^1H NMR Resonance Frequency 99

Table 13. Relative Contributions of Various Mechanisms to Spin Spin Relaxation of Shifted ^1H NMR Resonances in Ytterbium Substituted Parvalbumin Determined from ^1H NMR Resonance Frequency Dependence of the Observed Linewidths...............101

Table 14. Measured Spin Lattice Relaxation Times for Ytterbium Shifted ^1H NMR Resonances of Parvalbumin...103

Table 15. The Observed Spin Spin Relaxation Rates of the Downfield Ytterbium Shifted Parvalbumin Resonances as a Function of ^1H NMR Frequency........106

Table 16. Relative Contributions of Various Mechanisms to Spin Spin Relaxation of Shifted ^{1}H NMR Resonances in Ytterbium Substituted Parvalbumin Determined from ^{1}H NMR Resonance Frequency Dependence at 200, 270, 400, and 600 MHz of the Observed Linewidths....................107

Table 17. Relative Shifting and Broadening Contributions in Lanthanide Complexes................116

Table 18. The Temperature Dependence of the Observed Chemical Shift Positions I..................127

Table 19. The Temperature Dependence of the Observed Chemical Shift Positions II.................128

Table 20. The Temperature Dependence of the Observed Chemical Shift Positions III................129

Table 21. The Temperature Dependence of the Observed Chemical Shift Positions IV.................130

Table 22. The Temperature Dependence of the Observed Chemical Shift Positions V..................131

Table 23. The Temperature Dependence of the Observed Chemical Shift Positions VI.................132

Table 24. The Temperature Dependence of the Observed Chemical Shift Positions VII................133

Table 25. The Temperature Dependence of the Observed Chemical Shift Positions VIII...............134

Table 26. The Temperature Dependence of the Observed Chemical Shift Positions IX.................135

Table 27. The Temperature Dependence of the Observed Chemical Shift Positions X..................136

Table 28. The Temperature Dependence of the Observed Chemical Shift Positions XI.................137

Table 29. The Temperature Dependence of the Observed Chemical Shift Positions XII................138

Table 30. The Temperature Dependence of the Observed Chemical Shift Positions XIII...............139

Table 31. The Temperature Dependence of the Observed Chemical Shift Positions XIV................140

Table 32. Diamagnetic Positions of the Downfield Shifted Resonances in Region I of the ^{1}H NMR Spectrum of the Yb^{3+} Parvalbumin Complex............141

Table 33. Diamagnetic Positions of the Upfield Shifted Resonances in Region II of the ^{1}H NMR Spectrum of the Yb^{3+} Parvalbumin Complex............142

Table 34. Diamagnetic Positions of the Upfield Shifted Resonances in Region III of the ^{1}H NMR Spectrum of the Yb^{3+} Parvalbumin Complex............143

Table 35. The NMR Titration Data for the Histidine C-2 Protons of Carp Parvalbumin in the Presence of Ca^{2+} and Yb^{3+}....................................155

Table 36. The NMR Titration Data for the Histidine C-4 Protons of Carp Parvalbumin in the Presence of Ca^{2+} and Yb^{3+}....................................157

Table 37. Least Squares Analysis of the NMR pH Titration Data for the C-2 and C-4 Protons of Histidine 26 of Carp Parvalbumin....................159

Table 38. Paramagnetic Shifts for the Assigned Resonances of Carp Parvalbumin.......................163

Table 39. Chemical Shifts of the Downfield Shifted Resonances in Region I of the ^{1}H NMR Spectrum of the Yb^{3+} Parvalbumin Complex....................170

Table 40. Metal to Proton Distances of the Downfield Shifted Resonances in Region I of the ^{1}H NMR Spectrum of the Yb^{3+} Parvalbumin Complex............171

Table 41. Additional Data of the Downfield Shifted Resonances in Region I of the ^{1}H NMR Spectrum of the Yb^{3+} Parvalbumin Complex....................172

Table 42. Chemical Shifts of the Upfield Shifted Resonances in Region II of the ^{1}H NMR Spectrum of the Yb^{3+} Parvalbumin Complex....................175

Table 43. Metal to Proton Distances of the Upfield Shifted Resonances in Region II of the ^{1}H NMR Spectrum of the Yb^{3+} Parvalbumin Complex............176

Table 44. Additional Data of the Upfield Shifted Resonances in Region II of the ^{1}H NMR Spectrum of the Yb^{3+} Parvalbumin Complex....................177

Table 45. Chemical Shifts of the Upfield Shifted Resonances in Region III of the ^{1}H NMR Spectrum of the Yb^{3+} Parvalbumin Complex........................180

Table 46. Metal to Proton Distances of the Upfield Shifted Resonances in Region III of the ^{1}H NMR Spectrum of the Yb^{3+} Parvalbumin Complex.............181

Table 47. Additional Data of the Upfield Shifted Resonances in Region III of the ^{1}H NMR Spectrum of the Yb^{3+} Parvalbumin Complex......................182

Table 48. Paramagnetic Shift Data of the Assigned Histidine and N-acetyl Resonances of Parvalbumin.....197

Table 49. A Comparison of the Observed and Calculated Paramagnetic Shifts and Distances for the Seven Methyl Groups within 10A of the EF Site..............199

Table 50. A Comparison of the Most Upfield and Most Downfield Observed and Calculated Paramagnetic Shifts..................................200

List of Figures

Page

Figure 1. The amino acid sequence of carp parvalbumin, pI=4.25 3

Figure 2. An alpha-carbon stereo-drawing of carp parvalbumin, pI=4.25 4

Figure 3. The EF calcium binding domain of carp parvalbumin; the EF hand 6

Figure 4. The amino acid sequences of the calcium binding regions of carp parvalbumin 7

Figure 5. The coordination of the CD and EF calcium ions of parvalbumin 8

Figure 6. The amino acid sequences of carp parvalbumins with isoelectric points of 4.47, 4.25, and 3.95 10

Figure 7. A comparison of putative calcium binding site sequences of different calcium binding proteins 13

Figure 8. A comparison of putative calcium binding site sequences of different calcium binding proteins 14

Figure 9. The diamagnetic ^{1}H NMR spectrum of calcium saturated parvalbumin 24

Figure 10. The 270 MHz ^{1}H NMR spectrum of carp parvalbumin in the presence of calcium and in the presence of ytterbium 25

Figure 11. A comparison between the 270 MHz ^{1}H NMR spectra of the lutetium parvalbumin complex and the calcium parvalbumin complex 28

Figure 12. A comparison between the aromatic regions of the 270 MHz ^{1}H NMR spectra of the lutetium parvalbumin complex and the calcium parvalbumin complex 29

Figure 13. Theoretical spectra illustrating the NMR fast exchange limit 33

Figure 14. Theoretical spectra illustrating the NMR slow exchange limit 36

Figure 15. Sephadex G-75 chromatography of ammonium sulfate fractionated carp myogen 42

Figure 16. DE-52 cellulose chromatography of the low molecular weight proteins of carp myogen..............44

Figure 17. The isolation of parvalbumin: polyacrylamide gel electrophoresis in SDS urea......................49

Figure 18. The ultraviolet absorption of parvalbumin, pI=4.25..51

Figure 19. The 270 MHz ^{1}H NMR spectrum of parvalbumin obtained from tubes 86-95 in the DE-52 cellulose fractionation of the low molecular weight proteins of carp myogen..................................53

Figure 20. The 270 MHz ^{1}H NMR spectrum of parvalbumin obtained from tubes 110-120 in the DE-52 cellulose fractionation of the low molecular weight proteins of carp myogen..................................54

Figure 21. The 270 MHz ^{1}H NMR spectrum of parvalbumin obtained from tubes 130-140 in the DE-52 cellulose fractionation of the low molecular weight proteins of carp myogen..................................55

Figure 22. A comparison of the aromatic regions of the 270 MHz ^{1}H NMR spectra of carp parvalbumins isolated by DE-52 cellulose chromatography.....................56

Figure 23. Precession photograph of a carp parvalbumin crystal, depicting the hko diffraction plane to the limit of 2 angstrom resolution.........................58

Figure 24. An outline of the mechanism for the binding of ytterbium and calcium to parvalbumin..............65

Figure 25. The downfield portion of the ^{1}H NMR spectrum of carp parvalbumin as a function of total Yb^{3+} to total protein ratio.....................68

Figure 26. The upfield portion of the ^{1}H NMR spectrum of carp parvalbumin as a function of total Yb^{3+} to total protein ratio.....................69

Figure 27. The areas of three representative peaks as a function of (Yb^{3+}/P) ratio in the Yb^{3+} titration of calcium saturated parvalbumin...........71

Figure 28. The area of a representative peak as a function of (Yb^{3+}/P) ratio in the Yb^{3+} titration of apo parvalbumin................................73

Figure 29. The 270 MHz ^1H NMR spectrum of carp parvalbumin in the presence of calcium and in the presence of ytterbium....................................95

Figure 30. The downfield region of the 270 MHz ^1H NMR spectrum of ytterbium substituted parvalbumin. ...97

Figure 31. The upfield region of the 270 MHz ^1H NMR spectrum of ytterbium substituted parvalbumin. ...98

Figure 32. Plot of the observed spin spin relaxation rates versus the square of the resonance frequency in units of radians s^{-1}..............................100

Figure 33. Representative metal to proton distances calculated from the field dependent contribution to the linewidth...................................102

Figure 34. Plot of the observed spin spin relaxation rates versus the square of the resonance frequency in units of radians s^{-1}..............................105

Figure 35. The ^1H NMR spectrum of three different parvalbumin lanthanide complexes....................118

Figure 36. Calibration of the methanol NMR thermometer...121

Figure 37. The downfield region of the 270 MHz ^1H NMR spectrum of parvalbumin in the presence of Yb^{3+} as a function of temperature.........................124

Figure 38. The upfield region of the 270 MHz ^1H NMR spectrum of parvalbumin in the presence of Yb^{3+} as a function of temperature.........................125

Figure 39. The temperature dependence of the observed shift positions indicated by a plot of the observed shift position vs. temperature......................126

Figure 40. The temperature dependence of the resonance with an observed chemical shift position of 15.17 ppm indicated by a plot of the log of its paramagnetic shift vs. log temperature...............144

Figure 41. The downfield portion of the 270 MHz ^1H NMR spectrum of carp parvalbumin.........................153

Figure 42. The pH titration curves of the C-2 protons of histidine 26 of carp parvalbumin in the presence of saturating levels of calcium and in the presence of Yb^{3+} at a total Yb^{3+} to total protein ratio of 0.80.....................................154

Figure 43. The pH titration curves of the C-4 protons of histidine 26 of carp parvalbumin in the presence of saturating levels of calcium and in the presence of Yb^{3+} at a total Yb^{3+} to total protein ratio of 0.80 156

Figure 44. The 270 MHz ^1H NMR spectrum of the N-acetyl terminus of carp parvalbumin 160

Figure 45. The 254 MHz ^{19}F NMR spectrum of carp parvalbumin chemically modified at cysteine 18 with the reagent 2-trifluoroacetoxymercuri-4-fluorophenol 162

Figure 46. The ^1H NMR spectrum of the Yb^{3+} parvalbumin complex divided into the three Regions I, II, and III 168

Figure 47. Region I of the ^1H NMR spectrum of the Yb^{3+} parvalbumin complex 169

Figure 48. Region II of the ^1H NMR spectrum of the Yb^{3+} parvalbumin complex 174

Figure 49. Region III of the ^1H NMR spectrum of the Yb^{3+} parvalbumin complex 179

Figure 50. Definitions of the spherical coordinates......185

Figure 51. Definitions of the direction cosines..........188

Figure 52. The ^1H NMR spectrum of the methyl resonances observed for the parvalbumin-Yb^{3+} complex 190

Figure 53. A stereodiagram of the alpha carbon backbone of parvalbumin indicating the diverse angular orientations of residues 1, 18, and 26.......194

Figure 54. The methyl proton centroid model.............195

Figure 55. The orientation of the ligands in the EF metal binding site of carp parvalbumin in the principal axis system of the magnetic susceptibility tensor of the ytterbium ion...........................205

Figure 56. The orientation of the ligands in the EF metal binding site of carp parvalbumin in the principal axis system of the magnetic susceptibility tensor of the ytterbium ion...........................206

List of Abbreviations and Symbols

A	absorbance
A	angstrom
Abs	absorbance
Ac	acetyl
C	carboxyl
cm	centimeter
D_2O	deuterium oxide
DEAE	diethylaminoethyl
DSS	sodium 2,2-dimethyl-2-silapentane-5-sulfonate
DTNB	5,5′ dithiobis(2-nitrobenzoic acid)
DTT	dithiothreitol
EDTA	ethylenediamine tetraacetic acid
EGTA	ethyleneglycol-bis-(beta-aminoethyl ether) N,N′-tetraacetic acid
g	gram
g_L	Lande g factor
H_0	applied magnetic field
Hepes	N-2-hydroxyethylpiperazine-N′-3-propanesulfonic acid
His	histidine
hr	hour
Hz	hertz
I	nuclear spin quantum number
k	Boltzmann constant

kHz	kilohertz
kV	kilovolt
l	liter
MCBP	muscle calcium binding protein
Mes	(2-(2-morpholino)ethanesulfonic acid)
M	molar
mg	milligram
min	minute
ml	milliliter
mm	millimeter
mM	millimolar
MHz	megahertz
mA	milliampere
N	amino
nm	nanometer
NMR	nuclear magnetic resonance
no	number
P	protein
pI	isoelectric point
Pipes	piperazine-N,N'-bis(2-ethanesulfonic acid)
ppm	parts per million
rpm	revolutions per minute
s	second
S	electron spin quantum number
SDS	sodium dodecyl sulfate
T1	spin lattice relaxation time

T2	spin spin relaxation time
temp	temperature
tricine	N-[tris-(hydroxymethyl)methyl]glycine
tris	tris-(hydroxymethyl)aminomethane
UV	ultraviolet
x g	times gravity
Yb^{3+}	tripositive ytterbium ion
Yb┌*o*┐/P┌*o*┐	total Yb^{3+} to total protein ratio
Yb/P	total Yb^{3+} to total protein ratio
°C	degrees Celsius
°K	degrees Kelvin
β	nuclear magneton
γ	gyromagnetic ratio
δ ┌*OBS*┐	observed chemical shift position
δ ┌*d*┐	diamagnetic chemical shift position
δ ┌*p*┐	paramagnetic chemical shift
λ	wavelength
τ ┌*R*┐	rotational correlation time
$\bar{\chi}$	trace of the magnetic susceptibility tensor
ω┌*I*┐	resonance frequency in radians per second

Amino acid nomenclature is documented in Appendix 1. The chemical structures of Mes, Pipes, dithizone, and xylenol orange are shown in Appendix 2. Expressions (in italics) enclosed within the following brackets ┌ and ┐ are intended to denote subscripts.

I. Introduction

A. Calcium Binding Proteins

Calcium binding proteins play an important role in the regulation of many biochemical processes (Rasmussen & Goodman, 1972; Kretsinger, 1976; Smith, 1977; Geisow, 1978). Among the most studied of these proteins are the skeletal and cardiac troponins which regulate contraction of striated muscle (Potter *et al.*, 1977a; Hincke *et al.*, 1978), the myosin light chains which regulate contraction of some smooth muscles (Wagner & Weeds, 1977), and calmodulin which regulates the following enzymes: bovine brain phosphodiesterase (Lin *et al.*, 1974), brain adenylate cyclase (Westcott *et al.*, 1979), chicken gizzard myosin light chain kinase (Dabrowska *et al.*, 1978), rabbit skeletal myosin light chain kinase (Yagi *et al.*, 1978), human platelet phospholipase A2 (Wong & Cheung, 1979), rabbit skeletal phosphorylase kinase (Shenolikar *et al.*, 1979), erythrocyte Ca^{2+}-ATPase (Jarrett & Penniston, 1978; Lynch & Cheung, 1979), and a number of other enzymes (for recent reviews, see Cheung, 1980; Klee *et al.*, 1980; Means & Dedman, 1980).

Another class of calcium binding proteins which has been studied intensively is the parvalbumins. Parvalbumins are calcium binding proteins found in fish such as carp (Konusu *et al.*, 1965), hake (Pechere *et al.*, 1971b), thornback ray (Parello & Pechere, 1971), pike (Rao & Gerday, 1973), coelacanth (Jauregui-Adell & Pechere, 1978), perch (Lehky & Stein, 1979), and other vertebrates such as frog (Pechere *et al*., 1973), rabbit (Blum *et al*., 1977), and chicken (Heizmann & Strehler, 1979). Their properties include: high solubility in water, low molecular weight (~11,000), acidic isoelectric points, 10% phenylalanine and 20% alanine amino acid compositions, an acetylated amino terminus, and a capacity to bind two moles of calciums per mole of protein (Coffee *et al*., 1974). Although the exact function of the parvalbumins is unknown, studies indicate (Pechere *et al*., 1977; Haiech *et al*., 1979b) that their metal binding properties are vital in their proposed role as the 'soluble relaxing factor' in muscle contraction. In resting muscle, magnesium is bound to the two metal binding sites of parvalbumin. When contraction is initiated by the release of calcium ions from the sarcoplasmic reticulum, the slow Mg^{2+} dissociation enables the free Ca^{2+} ions to bind to the Ca^{2+} specific sites of troponin C (which are not occupied by Mg^{2+}). Subsequently, the Ca^{2+} - Mg^{2+} binding sites of parvalbumin can remove the Ca^{2+} ions from troponin C. The sarcoplasmic reticulum then removes the Ca^{2+} ions bound to parvalbumin (for a discussion on muscle contraction, see (Hasselbach, 1964; Taylor, 1972; Murray & Weber, 1974); for a discussion on the calcium binding properties of troponin, see (McCubbin & Kay, 1980)).

The elucidation of the primary structure (Figure 1) and tertiary structure (Figure 2) of carp parvalbumin with

1 ALA PHE ALA GLY VAL LEU ASN ASP ALA ASP
11 ILE ALA ALA ALA LEU GLU ALA CYS LYS ALA
21 ALA ASP SER PHE ASN HIS LYS ALA PHE PHE
31 ALA LYS VAL GLY LEU THR SER LYS SER ALA
41 ASP ASP VAL LYS LYS ALA PHE ALA ILE ILE
51 ASP GLN ASP LYS SER GLY PHE ILE GLU GLU
61 ASP GLU LEU LYS LEU PHE LEU GLN ASN PHE
71 LYS ALA ASP ALA ARG ALA LEU THR ASP GLY
81 GLU THR LYS THR PHE LEU LYS ALA GLY ASP
91 SER ASP GLY ASP GLY LYS ILE GLY VAL ASP
101 GLU PHE THR ALA LEU VAL LYS ALA

Figure 1. The amino acid sequence of carp parvalbumin, pI=4.25 (Coffee & Bradshaw, 1973).

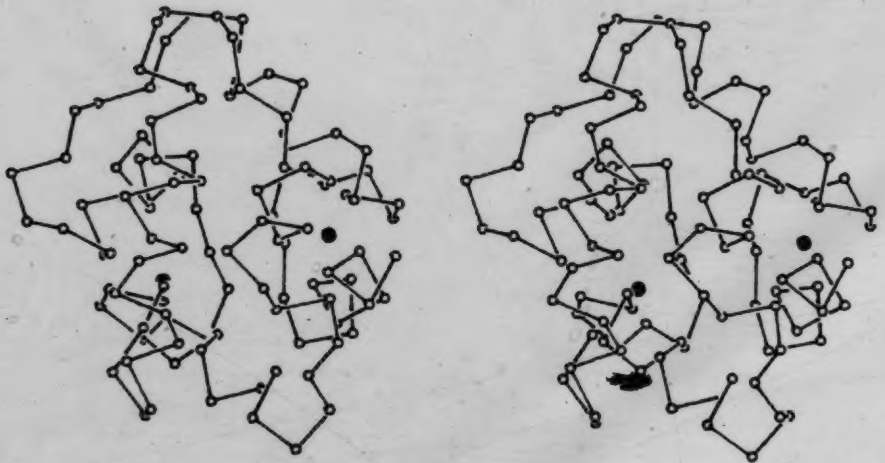

Figure 2. An alpha-carbon stereo-drawing of carp parvalbumin, pI=4.25. The molecule contains six alpha helices designated helices A to F. The CD calcium binding domain (shown on the left side of the stereodrawing) consists of the C helix, the CD calcium binding loop, and the D helix; the EF calcium binding domain (shown on the right side of the stereodrawing) consists of the E helix, the EF calcium binding loop, and the F helix. Atomic coordinates available from the Brookhaven Protein Data Bank were used to prepare this figure.

isoelectric point of 4.25 (Coffee & Bradshaw, 1973; Kretsinger & Nockolds, 1973) revealed that this protein consists of six alpha helices, labelled A, B, C, D, E, and F. Each of the two calcium binding sites is completely formed from a contiguous polypeptide sequence folded into the homologous "CD and EF hands" (Kretsinger & Nockolds, 1973). For example, as shown in Figure 3, the EF hand contains sequentially, three turns of alpha helix (the E helix), a twelve residue loop around the metal, and a second three turn alpha helix (the F helix). (Note the AB hand does not bind calcium because of two deletions within this loop sequence). The twelve residue loop around both metal ions contains regularly spaced carboxyl, carbonyl, and hydroxyl ligands (Figure 4); the coordination of the CD and EF calcium ions of carp parvalbumin is illustrated in Figure 5.

The white muscle of fish is characterized by a group of highly homologous, but distinct parvalbumins, differing in isoelectric point. Two groups (Pechere *et al.*, 1971a; Kretsinger & Nockolds, 1973) have used different names for these isozymes; Table 1 which correlates the published isozyme nomenclature is included to avoid confusion. The isoelectric point nomenclature will be used throughout this manuscript. The determination of the amino acid sequence of three of the four carp parvalbumins (Figure 6) reveals a high homology (Coffee *et al.*, 1974). Ligands to both calciums of carp parvalbumin 4.25 are all conserved in the three isozymes (Figure 6). Table 2 lists the amino acid

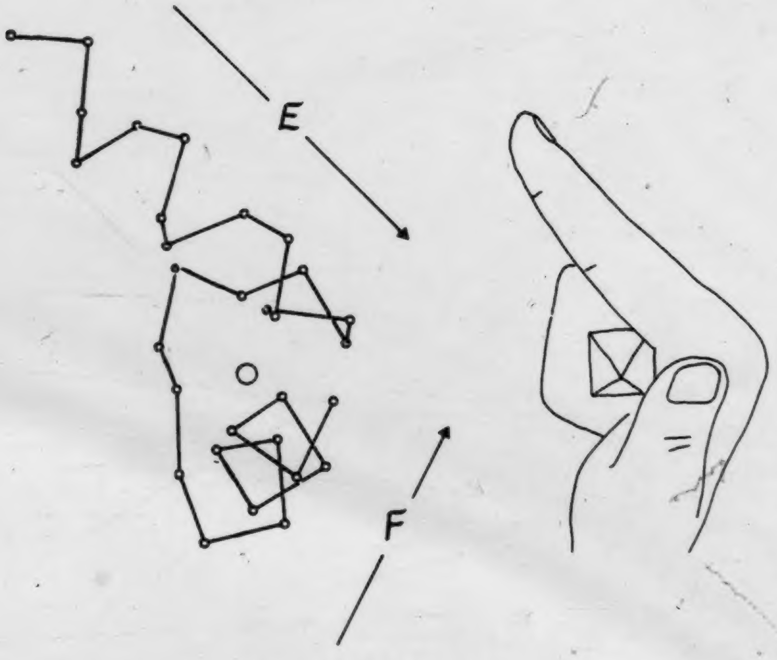

Figure 3. The EF calcium binding domain of carp parvalbumin; the EF hand. The EF hand consists of three elements: the E alpha helix (residues 79-89) represented by the right forefinger, the EF calcium binding loop (residues 90-101) represented by the curled middle finger, and the F alpha helix (residues 99-108) represented by the thumb. The arrows indicate the direction of the carboxyl terminus of the protein. This figure was adapted from Coffee *et al*., 1974.

ASP	GLN	*ASP*	LYS	*SER*	GLY	*PHE*	ILE	*GLU*	GLU	ASP	*GLU*
51	52	53	54	55	56	57	58	59	60	61	62

ASP	SER	*ASP*	GLY	*ASP*	GLY	*LYS*	ILE	*GLY*	VAL	ASP	*GLU*
90	91	92	93	94	95	96	97	98	99	100	101

Figure 4. The amino acid sequences of the calcium binding regions of carp parvalbumin. The upper sequence refers to the CD binding loop; the lower sequence, to the EF binding loop. Residues in italics indicate ligands to the calcium (Kretsinger & Nockolds, 1973).

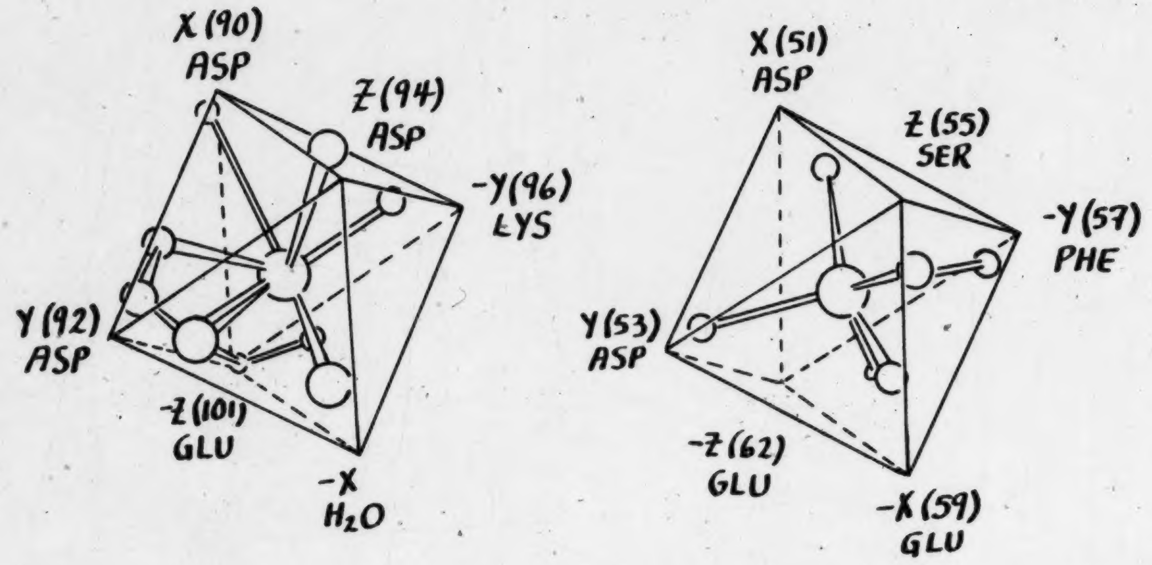
X (90)
ASP
Z (94)
ASP
-Y (96)
LYS
Y (92)
ASP
-Z (101)
GLU
-X
H₂O
X (51)
ASP
Z (55)
SER
-Y (57)
PHE
Y (53)
ASP
-Z (62)
GLU
-X (59)
GLU

Figure 5. The coordination of the CD and EF calcium ions of parvalbumin. Residues ASP 51, ASP 53, SER 55, GLU 59, and GLU 62 coordinate the CD calcium ion (right) with a single side chain oxygen atom. The carbonyl oxygen atom of PHE 57 also coordinates the ion. Residues ASP 90 and ASP 94 coordinate the EF calcium ion (left) with a single side chain oxygen atom; residues ASP 92 and GLU 101 coordinate the ion with two side chain oxygen atoms. In addition, the carbonyl oxygen of LYS 96 and one water molecule coordinate the ion. The letters +/- X, +/- Y, and +/- Z define the vertices of the octahedra. Note that the residues are in register about these vertices in both the CD and EF calcium binding domains. This Figure was adapted from Sowadski *et al*., 1978.

Table 1

Carp Parvalbumin Isozyme Nomenclature

pI[1]	4.47	4.37	4.25	3.95
component[1]	5a	5b	3	2
component[2]	A1	A2	B	C

[1] Pechere *et al*., 1971a.

[2] Kretsinger & Nockolds, 1973.

1	4.47	ALA	PHE	ALA	GLY	VAL	LEU	ASN	ASP	ALA	ASP
	4.25	ALA	PHE	ALA	GLY	VAL	LEU	ASN	ASP	ALA	ASP
	3.95	ALA	TYR	GLY	GLY	ILE	LEU	ASN	ASP	ALA	ASP
11	4.47	ILE	THR	ALA	ALA	LEU	GLU	ALA	CYS	LYS	ALA
	4.25	ILE	ALA	ALA	ALA	LEU	GLU	ALA	CYS	LYS	ALA
	3.95	ILE	THR	ALA	ALA	LEU	GLU	ALA	CYS	GLX	ALA
21	4.47	ALA	ASP	SER	PHE	ASN	HIS	LYS	THR	PHE	PHE
	4.25	ALA	ASP	SER	PHE	ASN	HIS	LYS	ALA	PHE	PHE
	3.95	GLX	ASP	SER	PHE	ASN	ALA	LYS	SER	PHE	PHE
31	4.47	ALA	LYS	VAL	GLY	LEU	THR	SER	LYS	SER	ALA
	4.25	ALA	LYS	VAL	GLY	LEU	THR	SER	LYS	SER	ALA
	3.95	ALA	LYS	VAL	GLY	LEU	SER	ALA	LYS	THR	PRO
41	4.47	ASP	ASP	VAL	LYS	LYS	ALA	PHE	ALA	ILE	ILE
	4.25	ASP	ASP	VAL	LYS	LYS	ALA	PHE	ALA	ILE	ILE
	3.95	ASP	ASP	ILE	LYS	LYS	ALA	PHE	ALA	VAL	ILE
51	4.47	*ASP*	GLN	*ASP*	LYS	*SER*	GLY	*PHE*	ILE	*GLU*	GLU
	4.25	*ASP*	GLN	*ASP*	LYS	*SER*	GLY	*PHE*	ILE	*GLU*	GLU
	3.95	*ASP*	GLN	*ASP*	LYS	*SER*	GLY	*PHE*	ILE	*GLU*	GLU
61	4.47	ASP	*GLU*	LEU	LYS	LEU	PHE	LEU	GLN	ASN	PHE
	4.25	ASP	*GLU*	LEU	LYS	LEU	PHE	LEU	GLN	ASN	PHE
	3.95	ASP	*GLU*	LEU	LYS	LEU	PHE	LEU	GLN	ASN	PHE
71	4.47	LYS	ALA	GLY	ALA	ARG	ALA	LEU	THR	ASP	GLY
	4.25	LYS	ALA	ASP	ALA	ARG	ALA	LEU	THR	ASP	GLY
	3.95	SER	ALA	GLY	ALA	ARG	ALA	LEU	THR	ASP	ALA
81	4.47	GLU	THR	LYS	THR	PHE	LEU	LYS	ALA	GLY	*ASP*
	4.25	GLU	THR	LYS	THR	PHE	LEU	LYS	ALA	GLY	*ASP*
	3.95	GLU	THR	LYS	ALA	PHE	LEU	LYS	ALA	GLY	*ASP*
91	4.47	SER	*ASP*	GLY	*ASP*	GLY	*LYS*	ILE	*GLY*	VAL	ASP
	4.25	SER	*ASP*	GLY	*ASP*	GLY	*LYS*	ILE	*GLY*	VAL	ASP
	3.95	SER	*ASP*	GLY	*ASP*	GLY	*LYS*	ILE	*GLY*	VAL	ASP
101	4.47	*GLU*	PHE	THR	ALA	LEU	VAL	LYS	ALA		
	4.25	*GLU*	PHE	THR	ALA	LEU	VAL	LYS	ALA		
	3.95	*GLU*	PHE	ALA	ALA	LEU	VAL	LYS	ALA		

Figure 6. The amino acid sequences of carp parvalbumins with isoelectric points of 4.47, 4.25, and 3.95 (Coffee *et al*.,1974). Residues in italics indicate ligands to the calcium.

Table 2

The Amino Acid Compositions of Three Isozymes of Carp Parvalbumin

pI	4.47	4.25	3.95
ALA	18	20	20
ARG	1	1	1
ASN	3	3	3
ASP	13	14	13
CYS	1	1	1
GLN	2	2	2
GLU	6	6	6
GLX	0	0	2
GLY	9	8	9
HIS	1	1	0
ILE	5	5	6
LEU	9	9	9
LYS	13	13	11
MET	0	0	0
PHE	10	10	9
PRO	0	0	1
SER	5	5	6
THR	7	5	4
TRY	0	0	0
TYR	0	0	1
VAL	5	5	4

compositions of all three isozymes.

Homologous sequences to carp parvalbumin (Kretsinger, 1976) have been found in the following proteins: rabbit skeletal parvalbumin (Enfield *et al*., 1975; Capony *et al*., 1976), rabbit skeletal DTNB and alkali light chains (Collins, 1974; Collins, 1976; Frank & Weeds, 1974; Weeds & McLachlan, 1974), rabbit skeletal troponin C (Collins *et al*., 1973,1977), bovine cardiac troponin C (van Eerd & Takahashi, 1976), bovine brain calmodulin (Vanaman *et al*., 1977; Watterson *et al*., 1980), rat testis calmodulin (Dedman *et al*., 1978), bovine intestinal calcium binding protein (Fullmer & Wasserman, 1977), porcine intestinal calcium binding protein (Hofmann *et al*., 1979), and other calcium binding proteins. A comparison of putative calcium binding site sequences of selected calcium binding proteins (Barker *et al*., 1978) is presented in Figures 7 and 8. The number of times in a given protein the twelve residue loop sequence repeats, and the number of substitutions therein, can be correlated with the number of metals bound to the protein and their binding strengths respectively (Weeds *et al*., 1977). These findings have lead to the proposal that homologous structures, at least at the level of the calcium binding sites, exist for all these proteins.

	X		Y		Z		-Y		-X			-Z
MCBP-AB[1]	LYS	ALA	ALA	ASP	SER	---	PHE	---	ASP	HIS	LYS	ALA
MCBP-CD[1]	ASP	GLN	ASP	LYS	SER	GLY	PHE	ILE	GLU	GLU	ASP	GLU
MCBP-EF[1]	ASP	SER	ASP	GLY	ASP	GLY	LYS	ILE	GLY	VAL	ASP	GLU
RPARV-1[2]	ASP	LYS	ASP	LYS	SER	GLY	PHE	ILE	GLU	GLU	GLU	GLU
RPARV-2[2]	ASP	LYS	ASP	GLY	ASP	GLY	LYS	ILE	GLY	ALA	ASP	GLU
DTNB-1[3]	ASP	GLN	ASN	ARG	ASN	GLY	ILE	ILE	ASP	LYS	GLU	ASP
DTNB-2[3]	LYS	GLU	ALA	---	SER	GLY	PRO	ILE	ASN	PHE	THR	VAL
DTNB-3[3]	ASP	PRO	GLU	GLY	LYS	GLY	THR	ILE	LYS	LYS	GLN	PHE
DTNB-4[3]	PRO	PRO	ASP	VAL	GLY	GLY	ASN	VAL	ASP	TYR	LYS	ASN
ALC-1[4]	ASP	ARG	THR	GLY	ASP	SER	LYS	ILE	THR	LEU	SER	GLN
ALC-2[4]	ASP	GLU	GLN	MET	ASN	ALA	LYS	LYS	ILE	GLU	PHE	GLU
ALC-3[4]	ASP	LYS	GLU	GLY	ASP	THR	VAL	GLY	MET	GLY	ALA	GLU
ALC-4[4]	GLN	GLU	ASP	SER	ASN	GLY	CYS	ILE	ASN	TYR	GLU	ALA

Figure 7. A comparison of putative calcium binding site sequences of different calcium binding proteins (Barker *et al*., 1978). X,Y,Z,-X,-Y, and -Z indicate the residues supposedly involved in calcium coordination.

---

[1] Residues 19-29,51-62, and 90-100 respectively from carp parvalbumin, pI=4.25 (Coffee & Bradshaw *et al*., 1973). The symbol --- indicates the absence of a residue.

[2] Residues 51-62, and 90-101 respectively from rabbit skeletal parvalbumin (Enfield *et al*., 1975; Capony *et al*., 1976).

[3] Residues 37-48, 70-80, 108-119, and 144-155 respectively from rabbit muscle DTNB light chains (Collins, 1976). The symbol --- indicates the absence of a residue.

[4] Residues 59-70, 96-108, 136-147, and 171-182 respectively from rabbit myosin A1 (and A2) light chains (Frank & Weeds, 1974). The insertion of ALA 101 between ASN 100 and LYS 102 has been omitted for clarity.

	X		Y		Z		-Y		-X			-Z
MCBP-CD[1]	ASP	GLN	ASP	LYS	SER	GLY	PHE	ILE	GLU	GLU	ASP	GLU
MCBP-EF[1]	ASP	SER	ASP	GLY	ASP	GLY	LYS	ILE	GLY	VAL	ASP	GLU
SkTNC-4[2]	ASP	LYS	ASN	ASN	ASP	GLY	ARG	ILE	ASP	PHE	ASP	GLU
SkTNC-3[2]	ASP	ARG	ASN	ALA	ASP	GLY	TYR	ILE	ASP	ALA	GLU	GLU
SkTNC-2[2]	ASP	GLU	ASP	GLY	SER	GLY	THR	ILE	ASP	PHE	GLU	GLU
SkTNC-1[2]	ASP	ALA	ASP	GLY	GLY	GLY	ASP	ILE	SER	VAL	LYS	GLU
CDRP-1[3]	ASP	LYS	ASP	GLY	ASN	GLY	THR	ILE	THR	THR	LYS	GLU
CDRP-2[3]	ASP	ALA	ASP	GLY	ASN	GLY	THR	ILE	ASP	PHE	PRO	GLU
CDRP-3[3]	ASP	LYS	ASP	GLY	ASN	GLY	TYR	ILE	SER	ALA	ALA	GLU
CDRP-4[3]	ASN	ILE	ASP	GLY	ASP	GLY	GLU	VAL	ASN	TYR	GLU	GLU
PIG-1[4]	ALA	LYS	GLU	GLY	ASP	ASN	GLN	LEU	SER	LYS	GLU	GLU
PIG-2[4]	ASP	LYS	ASN	GLY	ASN	GLY	GLU	VAL	SER	PHE	GLU	GLU

Figure 8. A comparison of putative calcium binding site sequences of different calcium binding proteins (Barker *et al*., 1978). X,Y,Z,-X,-Y, and -Z indicate the residues supposedly involved in calcium coordination.

---

[1] Residues 51-62, and 90-101 respectively from carp parvalbumin, pI=4.25 (Coffee & Bradshaw, 1973).

[2] Residues 139-150, 103-114, 63-74, and 27-38 respectively from rabbit skeletal muscle troponin C (Collins *et al*., 1973; Collins, 1974; Collins *et al*., 1977).

[3] Residues 20-31,56-67,93-104, and 129-140 respectively from bovine brain calcium dependent regulatory protein (Vanaman *et al*., 1977; Watterson *et al*., 1980).

[4] Residues 18-30, and 57-68 respectively from pig intestine calcium binding protein. The insertion of PRO 23, between ASP 22 and ASN 24 is omitted for clarity (Hofmann *et al*., 1979).

B. Lanthanides as Structural NMR Probes

The lanthanides, a group of fifteen elements ranging from lanthanum to lutetium, form trivalent ions in aqueous solution. These ions have ionic radii (Shannon, 1976) which are comparable to the 0.99 Å radius of Ca^{2+} (Table 3); thus they have been used extensively as analogs of calcium in biochemical (Darnall & Birnbaum, 1970), optical (for a review, see Martin & Richardson, 1979) and magnetic resonance studies (for reviews, see LaMar *et al.*, 1973; Dobson & Levine, 1976; Morris & Dwek, 1977). The 4f electrons, which characterize this group, are not valence electrons, but are inner core electrons, which results in a similar chemistry for each member of the series (Boudreaux & Mulay, 1976; Hüfner, 1978).

The lanthanides have been used extensively as NMR probes. The observed chemical shifts of nuclei in a lanthanide substituted molecule may result from diamagnetic and paramagnetic contributions. The diamagnetic shift arises from the binding of the tripositive ion. The substitution of the diamagnetic lanthanide La^{3+} or Lu^{3+} is used to determine the diamagnetic shifts in the NMR spectrum. For protons, the effects are usually minimal. Fluctuations in the local magnetic field of paramagnetic species can result in perturbations in the observed chemical shifts and relaxation times of neighboring nuclei. The paramagnetic contributions consist of two sources: contact and dipolar interactions.

The electron delocalization of spin density to the

Table 3

Properties of the Rare Earths

Atomic No.	Name	Symbol	Ionic Radius[1]
57	Lanthanum	La	1.03
58	Cerium	Ce	1.01
59	Praseodymium	Pr	0.99
60	Neodymium	Nd	0.98
61	Promethium	Pm	0.97
62	Samarium	Sm	0.96
63	Europium	Eu	0.95
64	Gadolinium	Gd	0.94
65	Terbium	Tb	0.92
66	Dysprosium	Dy	0.91
67	Holmium	Ho	0.90
68	Erbium	Er	0.89
69	Thulium	Tm	0.88
70	Ytterbium	Yb	0.87
71	Lutetium	Lu	0.86

[1] These ionic radii (in Å) refer to the six coordinated lanthanides (Shannon, 1976).

nucleus results in the 'through bond' effect called the contact (or scalar) interaction; the effect is transmitted through the electrons of chemical bonds. The geometric dependence of the contact shift is not known *a priori*. For lanthanides, there is little overlap of metal orbitals with ligand orbitals; thus the effect is small for this class of ions. By comparison, the contact shift is important for the transition ions, whose d valence electrons are often involved in metal-ligand orbital overlaps.

The dipolar (or pseudocontact) shift results from the 'through space' interaction between the magnetic moment of the unpaired electrons of the metal and any interacting nuclei. The effect is dependent on both the distance and angle between the metal and the nucleus. Since there is a known geometrical dependence in the dipolar shift, a number of workers have attempted to extract geometrical information from these dipolar shifts. The dipolar shift is given by (Bleaney, 1972):

$$\delta_p = A1 \left\langle \frac{3\cos^2\Theta - 1}{r^3} \right\rangle + A2 \left\langle \frac{\sin^2\Theta \cos 2\phi}{r^3} \right\rangle \qquad (1.1)$$

which may be expressed as

$$= A1 \cdot G1 + A2 \cdot G2 \qquad (1.2)$$

where A1 and A2 are constants related to elements of the magnetic susceptibility tensor of the metal, and r, θ, and ϕ are spherical polar coordinates of the nucleus relative to the principal axis system of the metal. This equation is identical to earlier expressions for the pseudocontact shift (McConnell & Robertson, 1958); however, anisotropies in the magnetic susceptibility tensor replace those values for anisotropies in the g tensor.

The lanthanides have been used as NMR probes of the structure of organic molecules. Hinckley (1969) first reported the use of lanthanide tris beta diketonates as shift reagents in organic solvents, to simplify the spectral analysis of cholesterol. (This area has been reviewed by Reuben, 1973a). The use of lanthanides as "shift reagents" often results in the resolution of previously overlapping peaks. In these earlier studies, equation 1.1 was simplified by assuming axial symmetry for the arrangement of the ligands about the metal. If the constant A2 in equation 1.1 is equal to 0, if A2 << A1, or if G2 << G1 (with A1 approximately equal to A2 for all geometries), then the second term is negligible, and the assumption of axial symmetry is made; the resulting equation contains the two unknowns of one distance (r) and one angle (θ).

In 1971, the first studies on the use of lanthanide tripositive ions in the determination of the structure of mononucleotides in aqueous solution was reported (Barry *et al.*, 1971; Geraldes & Williams, 1978a; Geraldes, 1979). More recently, the work has been extended to cyclic mononucleotides (Geraldes & Williams, 1978b), dinucleotides

(Geraldes & Williams, 1979), trinucleotides (Tanswell *et al.*, 1975), and ribonucleotides (Dobson *et al.*, 1978). Their analysis for flexible molecules results in the determination of a series of geometries of the nucleotide which are compatible with the observed lanthanide induced NMR shifts.

The Oxford Enzyme Group first proposed that perturbations induced by lanthanide ions could be used to probe the structure of a protein (Dwek *et al.*, 1971; Campbell *et al.*, 1973a, 1973b; Campbell *et al.*, 1975a, 1975b). The early studies (Dwek *et al.*, 1971; Campbell *et al.*, 1973a) were based upon the binding of the broadening probe Gd^{3+} to a site on the enzyme lysozyme. Gd^{3+} induces no dipolar shifts because of its isotropic $4f^7$ electron configuration; however it does induce nuclear relaxation which manifests itself in the form of broadening of resonances of nearby nuclei. There is an r^6 dependence in this interaction (Chapter 5). When Gd^{3+} is added to lysozyme, it binds to a site on the protein, thereby broadening certain resonances. By comparing the affected resonances and the calculated distances with the X-ray crystallographic structure of the protein, assignments were made.

In addition to the broadening studies, NMR shifts of lysozyme induced by lanthanides other than Gd^{3+} were used to determine geometrical information (Campbell *et al.*, 1975b). The validity of the axial symmetry assumption was tested by an analysis of the observed lanthanide shift ratios.

However, further investigations by another group (Agresti *et al.*, 1977) indicate considerable non-axial symmetry contributions; this group also determined the metal position in the protein, the magnitude of the principal elements of the magnetic susceptibility tensor of the metal, and the direction of the magnetic susceptibility tensor.

Marinetti (1975) and Marinetti *et al.* (1975, 1976, 1977) have demonstrated that these techniques can be extended to proteins that do not normally bind metals. By chemical modification, specific metal binding sites on the bovine pancreatic trypsin inhibitor were introduced to probe its protein conformation.

C. Objectives of this Project

In this thesis, I shall present an NMR methodology whose final goal is to compare the structures of calcium binding proteins in solution; the technique then can be used to test the structural hypothesis, outlined above, that calcium binding proteins have homologous structures. As part of this methodology, I have studied the structure of the metal binding site of carp parvalbumin by analyzing the ^1H NMR lanthanide induced shifts of the lanthanide substituted protein. The method is based upon the fact that the interaction of parvalbumin 4.25 with selected lanthanides such as ytterbium results in a series of highly resolved ^1H NMR resonances shifted as far downfield as 32 ppm and as far upfield as -19 ppm. These shifted resonances are sensitive monitors of the behavior and geometry of the metal binding sites in solution as seen in equation 1.1. The long term approach is to study carp parvalbumin initially and to use its known X-ray structure to determine the unknown parameters of the NMR experiment which are required before the shifts and broadenings can be interpreted in terms of the protein structure. With these parameters and a knowledge of the amino acid substitutions for a different calcium binding protein, the calculated and observed spectra may be analyzed as a probe of its structure.

The immediate goal of this thesis is to study the ytterbium induced ^{1}H NMR shifts of parvalbumin in order to 1) ascertain the three dimensional structure of the metal binding site in solution, and 2) to compare this solution structure with the structure determined by X-ray crystallographic techniques.

With this aim, I have completed a number of major areas of this project. I shall present an overview of this work in Chapter 2 and a description of the materials and methods used in Chapter 3. I have studied the stoichiometry of the binding of ytterbium to parvalbumin (Chapter 4). By analyzing the linewidths of the shifted resonances (Chapter 5), I have determined the individual metal to proton distances. In Chapter 6, I shall describe how the temperature dependence of the shifts are used to determine the diamagnetic shift positions. Chapter 7 details the assignment of observed NMR resonances of parvalbumin to specific protein nuclei. Chapter 8 is a summary of the data known to date. In Chapter 9, I shall describe how the principal elements and orientation of the magnetic susceptibility tensor are determined and how these parameters are used to analyze the shifts in terms of the three dimensional structure of the protein. Finally, in Chapter 10, I shall discuss the conclusions, implications, and the future of this study.

II. An Overview of the NMR Methodology

A. Introduction

As described in Chapter 1, the major goal of this project is to 1) ascertain the three dimensional structure of the parvalbumin metal binding site and 2) to compare this structure with the X-ray crystallographic structure. In this chapter, I shall briefly discuss the major areas of study as an overview of the NMR methodology I have developed.

B. Diamagnetic Spectrum

The 270 MHz ^{1}H NMR spectrum of calcium saturated parvalbumin is presented in Figure 9. The observed chemical shifts of the non-exchangeable carbon bound resonances span the expected region of approximately 8 ppm to 0 ppm. In addition, a series of potentially exchangeable backbone NH resonances are observed in the region of 10.5 to 8.5 ppm. The upfield shifted resonance at -0.48 ppm has been attributed to Val 106 (Parello *et al.*, 1974).

C. Paramagnetic Spectrum

Paramagnetic ions such as ytterbium (Yb^{3+}) shift the NMR resonances of nuclei in the vicinity of the metal ion (Figure 10) to positions outside the envelope of the diamagnetic spectrum. The chemical shifts of these resonances have a precise geometrical dependence on the position of the nucleus with respect to the principal axes

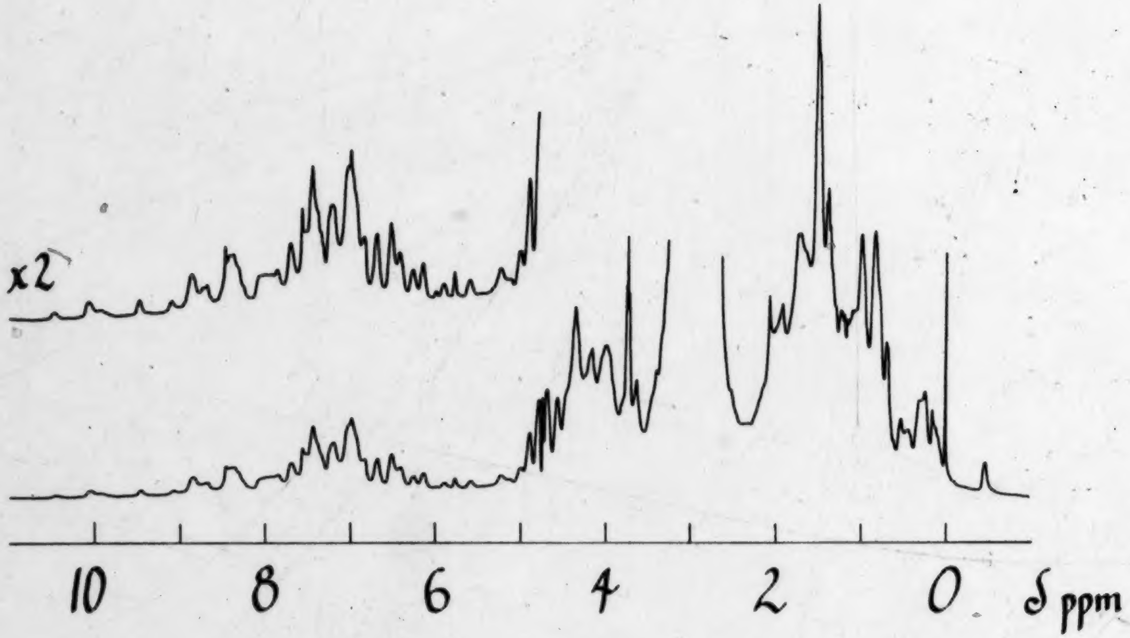

Figure 9. The diamagnetic ^{1}H NMR spectrum of calcium saturated parvalbumin. The 0.69 mM protein sample was prepared in 15 mM Pipes, 0.15 M KCl, 10 mM DTT, 0.5 mM DSS, pH 6.68. A 0.8 s acquisition time and a spectral width of ± 2500 Hz were used for data accumulation. The insert is a vertical expansion (2X) of the aromatic region.

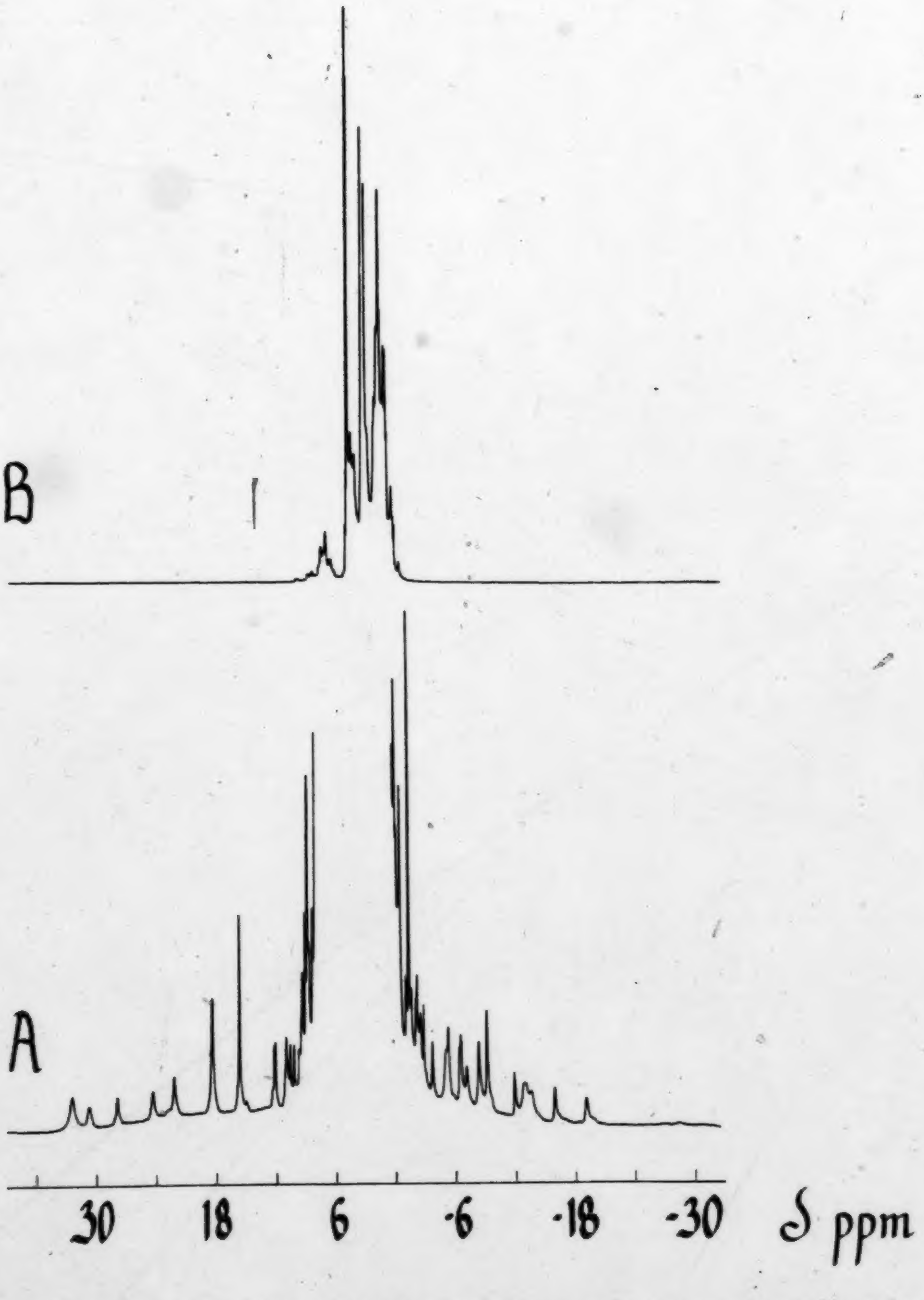

Figure 10. The 270 MHz ^1H NMR spectrum of carp parvalbumin in the presence of calcium and in the presence of ytterbium.
A. 1.0 mM parvalbumin in 15 mM Pipes, 0.15 M KCl, 0.5 mM DSS, 10 mM DTT, in D2O, pH 6.65, temperature=302°K, at a total Yb^{3+} to total protein ratio of 0.96.
B. 1.1 mM calcium saturated parvalbumin in 15 mM Pipes, 0.15 M KCl, 0.5 mM DSS in D2O, pH 6.65.

of the magnetic susceptibility tensor. The aim is to analyze this geometric dependence to determine the three dimensional structure of the protein in solution. Exquisite spectra with chemical shifts which range from 33 ppm to -19 ppm are observed directly for the parvalbumin ytterbium complex.

D. Paramagnetic Shifts and Diamagnetic Positions

The observed chemical shift positions (δ_{OBS}) of the resonances which are in the NMR slow exchange limit (see below) shown in Figure 10B consist of three contributions:

$$\delta_{OBS} = \delta_d + \delta_p + \delta_c \tag{2.1}$$

where δ_{OBS} is the observed chemical shift position, δ_d , the diamagnetic shift position, δ_p , the paramagnetic shift, and δ_c , the contact shift. For this study, the contact contributions are neglected (this point is discussed further in Chapter 5); thus the observed shift position consists of a paramagnetic shift from the diamagnetic position. The determination of the paramagnetic shift requires a knowledge of the diamagnetic positions. In Chapter 6, I discuss how the temperature dependence of the observed positions is used to determine the diamagnetic shift positions.

The introduction of the lanthanides with a +3 charge (versus the +2 charge of calcium) may influence the protein structure and the diamagnetic positions of the protein NMR spectra. As an indication of the effects, the ^{1}H NMR spectra of the parvalbumin complex with diamagnetic lutetium (Lu^{3+}) and with diamagnetic Ca^{2+} ions are presented in Figures 11 and 12. Although the spectrum of the parvalbumin with diamagnetic Ca^{2+} is not identical to the spectrum with the diamagnetic lanthanide ion Lu^{3+}, the differences in the diamagnetic positions are minimal. Since the diamagnetic positions are experimentally determined (in the presence of a lanthanide (Chapter 6)), these observed differences are not directly relevant to the determination of the protein structure. Also the very large observed chemical shift positions in the presence of the paramagnetic ions are far greater than any of these minor diamagnetic effects.

E. The Binding of Ytterbium to Parvalbumin

Yb^{3+} shifts the NMR resonances of protein nuclei in the vicinity of the metal. To establish the location of the metal and to determine the stoichiometry of binding of ytterbium to parvalbumin (Chapter 4), I have analyzed the ytterbium titrations of parvalbumin. The substitution of Yb^{3+} for one or both of the calcium ions of parvalbumin induces a series of shifted resonances to appear in the ^1H NMR spectrum far outside the spectrum of the Ca^{2+} form of the protein. In general terms, when Yb^{3+} is added to Ca^{2+} saturated parvalbumin at a total Yb^{3+} to total protein ratio of 1/1, a series of shifted resonances appear, corresponding to nuclei in the vicinity of the first site filled. At higher ratios in the range of 1/1 to 2/1, a new set of

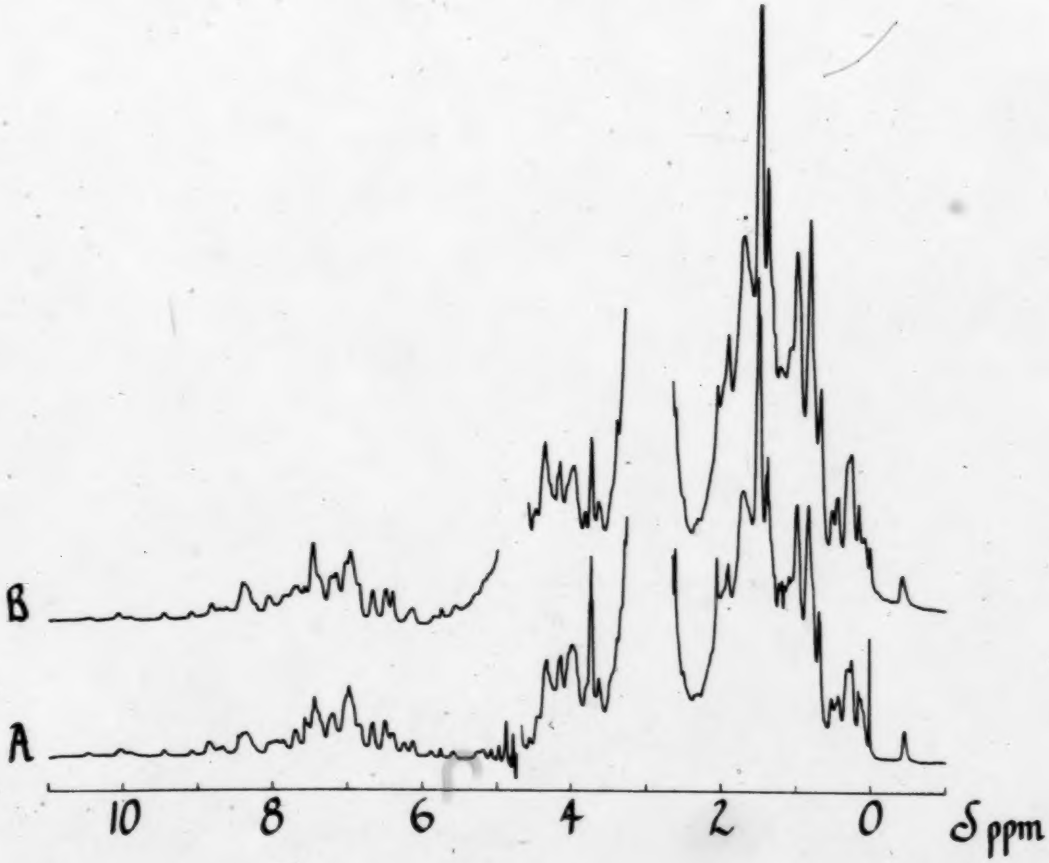

Figure 11. A comparison between the 270 MHz ^{1}H NMR spectra of the lutetium parvalbumin complex and the calcium parvalbumin complex.
A. 0.79 mM calcium saturated parvalbumin in 15 mM Pipes, 0.15 M KCl, 10 mM DTT, 0.5 mM DSS, in D2O, pH 6.64.
B. 0.76 mM parvalbumin in 15 mM Pipes, 0.15 M KCl, 10 mM DTT, 0.5 mM DSS, in D2O, pH 6.64, at a total Lu^{3+} to total protein ratio of 1.04.

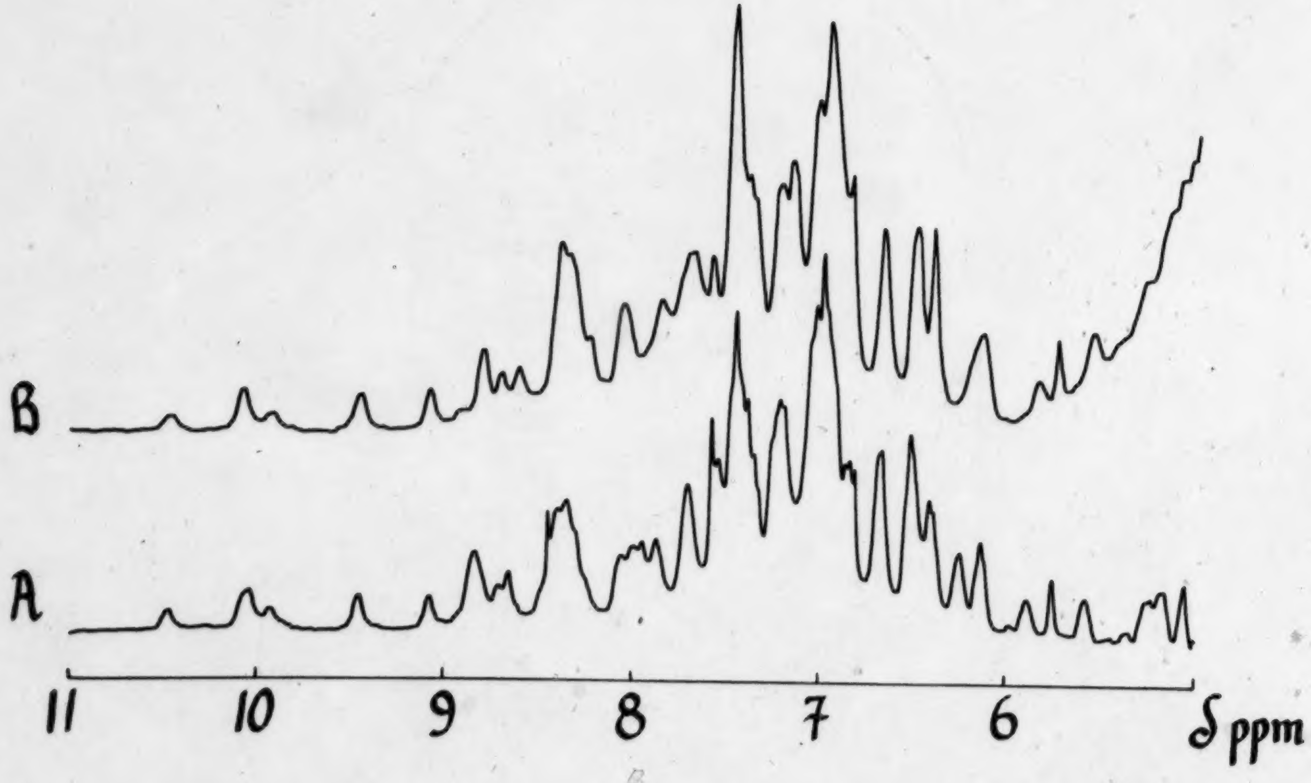

Figure 12. A comparison between the aromatic regions of the 270 MHz ^1H NMR spectra of the lutetium parvalbumin complex and the calcium parvalbumin complex. This figure consists of expansions of spectra presented in Figure 11.

resonances appears corresponding to nuclei in the vicinity of the second site filled. These results indicate that Yb^{3+} sequentially replaces the two Ca^{2+} ions of parvalbumin. They also indicate that at low metal to protein ratios, only a single, unique site of parvalbumin is occupied by Yb^{3+}. By analogy to previously published studies, I conclude that Yb^{3+} replaces first the calcium bound to the EF site of the protein. Thus, I shall focus on the structure of this EF binding site of carp parvalbumin in solution.

I have also determined the relative affinities of the CD and EF sites for ytterbium with respect to calcium. The dissociation constants are approximately equal; this result is verified by Yb^{3+} titrations of apo parvalbumin.

F. Metal to Proton Distances

The linebroadening of the shifted resonances has been measured at 200, 270, 400, and 600 MHz and the spin lattice relaxation times have been measured at 270 MHz. The analysis of the relaxation rates based upon the theories of Vega and Fiat (Vega & Fiat, 1976) and Gueron (Gueron, 1975) indicates that the susceptibility relaxation mechanism is the major source to the observed linebroadening. From this contribution, I have evaluated metal to proton distances of nuclei in the EF metal binding site. Thus two dimensional information relating the protons to the metal is determined.

G. Magnetic Susceptibility Tensor

By analyzing the paramagnetic shifts of three assigned resonances, the C-2 and C-4 protons of histidine 26 and the amino terminal acetyl protons (Chapter 6), as well as a number of methyl groups, I have been able to determine the principal elements and orientation of the magnetic susceptibility tensor of the bound metal (Chapter 9). These parameters are necessary, because they contain the angular information required to analyze the observed shifts in terms of the three dimensional structure of the protein metal binding site. With their determination, I am able to view the coordination geometry of the metal binding site.

H. General Conclusions

A significant number of the calculated paramagnetic shifts based upon the X-ray crystallographic structure are far larger than any of the observed paramagnetic shifts. Thus, there is a disagreement between the structure determined from the NMR and X-ray crystallographic methodologies (Chapter 9; Chapter 10). The differences may possibly result from actual differences between the solution structure and crystallographic structure, errors in the X-ray based proton coordinates, the effects of internal motions of the protein on the NMR results, and the increased sensitivity of the NMR method to small deviations in the positions of nuclei very close to the metal ion. On the basis of the analysis presented here, I feel that the most probable cause of this disagreement lies in errors in the X-ray crystallographic structure of atoms nearby the metal. In the future, I hope to be able to refine the X-ray based proton coordinates using the geometrical information contained in the lanthanide induced shifted resonances. In addition, the application of the proposed NMR methodology to other calcium binding proteins such as the remaining carp parvalbumin isozymes, troponin C, myosin light chains, and calmodulin will also be possible.

I. Advantages and Disadvantages

Up to this point of this thesis, lanthanide induced ^{1}H NMR shifts had been used to probe the structure of lysozyme (Campbell *et al.*, 1973a, 1973b; Campbell *et al.*, 1975a, 1975b; Agresti *et al.*, 1977) and the bovine pancreatic trypsin inhibitor (Marinetti, 1975; Marinetti *et al*. 1975, 1976, 1977; Perkins & Wüthrich, 1978). Neither of these proteins have high affinity specific metal binding sites; the metal binding ligands being two carboxyls in the active site of lysozyme and nitrotyrosyl side chains of the chemically modified trypsin inhibitor.

In these previous experiments, the weak metal ion binding has lead to NMR spectra (of mixtures of metal and protein) which are in the NMR fast exchange limit. Figure 13 is presented as an illustration of the NMR fast exchange limit. A single resonance at 4 ppm is observed in the absence of metal ions (Figure 13A). If the metal binding is

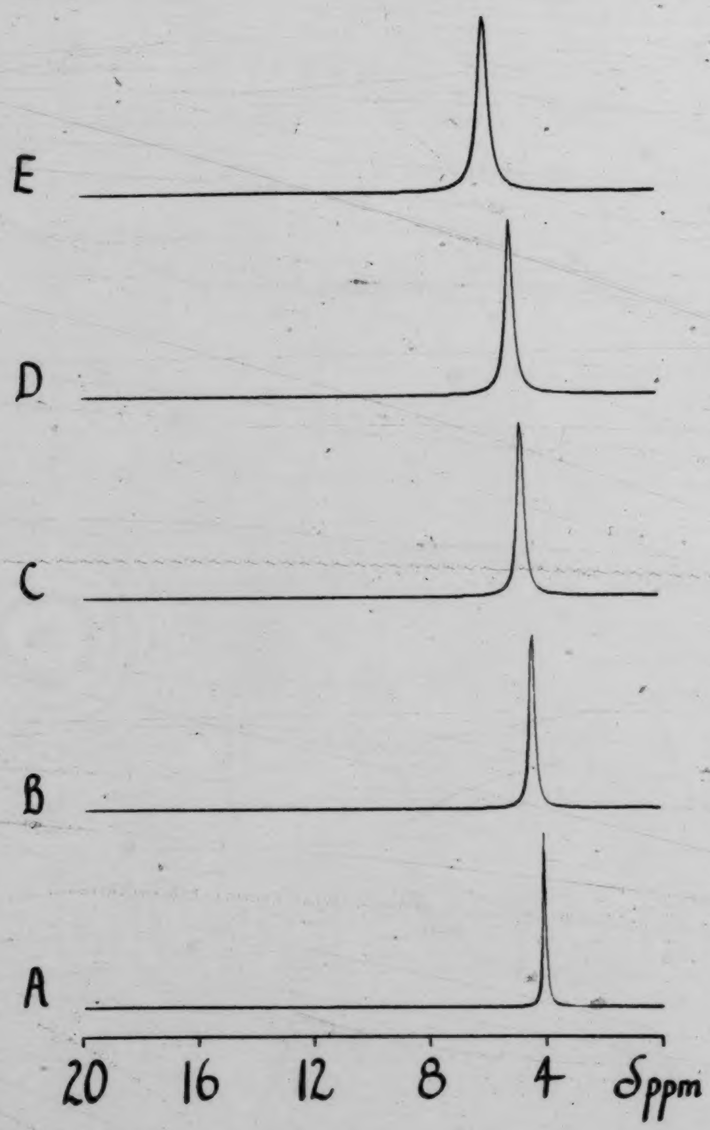

Figure 13. Theoretical spectra illustrating the NMR fast exchange limit. A single resonance at 4 ppm is observed in the absence of metal ions (A). If the metal binding is weak (dissociation constant = 1×10^{-2} M; off rate constant = 2×10^{5} s^{-1}); then the resulting spectra (B to E) consisting of a single resonance are in the fast exchange limit. See text for a further discussion. The initial ligand concentration is 1.0 mM; the metal concentrations of spectra B to E are 0.33, 0.66, 1.0, and 2.0 mM, respectively. Spectra B to E are scaled to A with the following factors, 1.81, 2.29, 2.70, and 3.70, respectively. These calculated spectra were generated by a program written by Lewis Kay.

weak (a dissociation constant of 1×10^{-2} M and an off rate constant of 2×10^{5} s^{-1} were assumed in the calculation), then the resulting spectra (Figures 13B to 13E) are in the fast exchange limit. The following parameters were used in the calculation. The initial ligand concentration is 1.0 mM. The metal concentrations in spectra 13B to 13E are 0.33, 0.66, 1.0, and 2.0 mM, respectively. A free chemical shift position of 4 ppm and a bound chemical shift of 16 ppm are assumed. The chemical shift of the single observed resonance is the sum of the bound chemical shift position (in the presence of metal ions) and the free chemical shift position (in the absence of metal ions), weighted by their respective populations. This has the advantage that the influence of the paramagnetic metal ion can be progressively followed for assigned resonances; however, it has the disadvantage that shifts, linewidths, or relaxation rates characterizing the protein-metal complex can only be obtained by a fitting procedure involving an extrapolation to the fully bound form. Data must be acquired at high concentrations of metal ion where non-specific binding can influence the results. For example, in Figure 13E, the observed chemical shift position of the single resonance (6 ppm) is only 2 ppm from the free chemical shift position (4 ppm), even though an excess of metal ions (metal to ligand ratio is equal to 2/1) has been added. Additional metal must be added to approach the fully bound chemical shift position of 16 ppm.

The biggest difference in the application described herein to the calcium binding protein parvalbumin, is that the metal binding is tight and specific. This has a dramatic influence on the form of the NMR experiment. When the metal binding is tight and specific as in the case with parvalbumin, the resulting NMR spectra are in the NMR slow exchange limit; in this limit, the spectrum of the metal protein complex is directly observed. Figure 14 is presented as an illustration of the NMR slow exchange limit. A single resonance at 4 ppm is observed in the absence of metal ions (Figure 14A). If the metal binding is tight and specific (a dissociation constant of 1×10^{-6} and an off rate constant of 10 s^{-1} were assumed in the calculation), then the resulting spectra (Figures 14B to 14E) are in the NMR slow exchange limit. The following parameters were used in the calculation. The initial ligand concentration is 1.0 mM. The metal concentrations in spectra 14B to 14E are 0.33, 0.66, 1.0, and 2.0 mM, respectively. A free chemical shift position of 4 ppm and a bound chemical shift position of 16 ppm are assumed. The spectra in the presence of metal ions (Figure 14B) consists of two resonances, one corresponding to the ligand nuclei in the absence of metal ions (4 ppm) and one, to nuclei in the presence of metal ions (16 ppm). Thus the resonance corresponding to the ligand metal complex is directly observed. As the concentration of the metal is increased, a decrease in the free resonance and an increase in the bound resonance are observed (Figure 14C). At a metal to ligand ratio of 1/1 (Figure 14D), a single

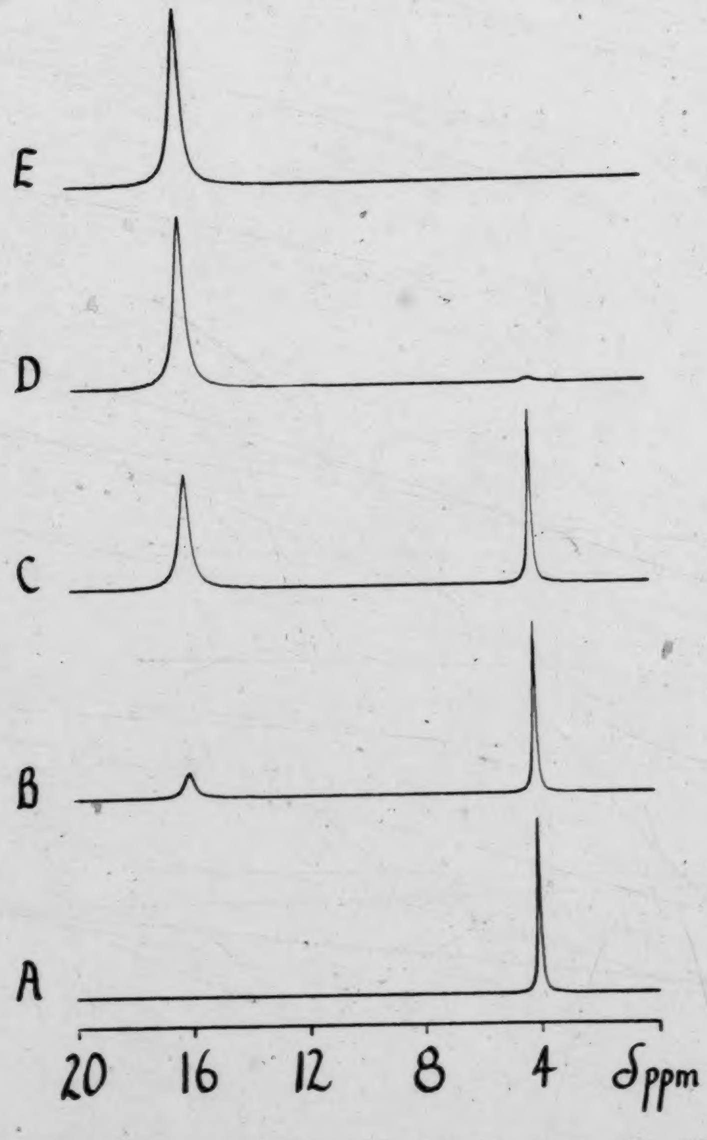

Figure 14. Theoretical spectra illustrating the NMR slow exchange limit. A single resonance at 4 ppm is observed in the absence of metal ions (A). If the metal binding is strong (dissociation constant = 1×10^{-6} M; off rate constant = 10 s^{-1}), then the resulting spectra (B to E) consisting of two resonances are in the slow exchange limit. See text for a further discussion. The initial ligand concentrations is 1.0 mM; the metal concentrations of spectra B to E are 0.33, 0.66, 1.0, and 2.0 mM, respectively. Spectra B to E have been scaled to A with the following factors, 1.53, 3.50, 3.57, and 3.44, respectively. These calculated spectra were generated by a program written by Lewis Kay.

resonance corresponding to the fully bound ligand nuclei is observed; no resonances corresponding to nuclei of the free ligand are observed. The main advantage in the slow exchange limit is that the chemical shift positions and relaxation times of the protein metal complex can be directly and accurately determined. However, the main disadvantage is in the assignment of the observed resonances.

The experiments described above are not limited to lanthanide ions. A parallel set of experiments have been performed on the binding of transition ion Co^{2+} to lysozyme (McDonald & Phillips, 1969; Lenkinski *et al.*, 1978) which is in the NMR fast exchange limit, and the binding of Co^{2+} to concanavalin A (Carver *et al.*, 1977) which is in the NMR slow exchange limit.

Previously determined lanthanide induced NMR shifts and relaxation times have not been accurately enough determined, as a consequence of the above, to prove more than a general consistency between the X-ray and the solution structure (Campbell *et al.*, 1975b; Agresti *et al.*, 1977; Marinetti *et al.*, 1976, 1977). The NMR measurements presented here provide structural detail at a potential resolution much higher than that presently obtainable from X-ray crystallographic studies because of the high order dependence on distance involved in the NMR experiment. The strategy, interpretation, and analysis of the lanthanide induced shift data and their implication with respect to the

X-ray structure are presented in this thesis.

III. Experimental Methods

This chapter focuses on the procedures used to purify and to characterize the protein parvalbumin. In addition, the general experimental methods used in this study are discussed. More detailed information relevant to specific experiments is included in the individual chapters.

A. Protein Purification

Parvalbumin was isolated by the method of Pechere and co-workers (Pechere *et al.*, 1971a). (A more efficient purification procedure which exploits the heat stability of the protein has been recently reported (Haiech *et al.*, 1979a).) The myogen of lower vertebrates contains several acidic components of low molecular weight. Usually two to four highly homologous but distinct proteins are found in a single fish. In carp, four separate components have been isolated. Isoelectric focusing (Pechere *et al.*, 1971a) of these low molecular weight proteins from carp myogen indicates the presence of four isozymes of parvalbumin with isoelectric points of 4.47, 4.37, 4.25, and 3.95. Since the X-ray crystallographic structure of parvalbumin component 'B' with pI of 4.25 had been determined (Kretsinger & Nockolds, 1973), the aim of the protein purification was the isolation of this particular isozyme for these studies. Carp (*Cyprinus Carpio*) were obtained from the Billingsgate Fish Company of Calgary.

1. Extraction

All procedures were performed between 0° and 4°C. 462 g of skinfree fillets of white carp muscle was homogenized with 690 ml of sucrose solution (0.3 M sucrose, 0.01 M triethanolamine, 0.003 M disodium EDTA (ethylenediamine tetraacetic acid)). After the mixture was stirred for 15 min, it was centrifuged for 30 min at 8000 rpm at 13,200 x g. The supernatant was filtered through glass wool, then placed into previously boiled Fisher 8-667E dialysis tubing. The material was dialyzed against 8 changes of 16 l of cold doubly distilled deionized water over a period of 3 days. The precipitate was removed by centrifugation at 8000 rpm for 30 min at 13,200 x g. The supernatant was collected through glass wool. Of the 860 ml of supernatant, 695 ml was frozen. The remaining 165 ml was subjected to ammonium sulfate fractionation.

2. Ammonium Sulfate Fractionation

72.6 g of Schwarz Ultrapure Ammonium Sulfate was added to the 165 ml of supernatant at 0°C to bring the solution to 70% saturation in ammonium sulfate. 1.0 M NaOH was added to maintain neutral pH. After 30 min of gentle stirring, the suspension was centrifuged for 30 min at 6000 rpm at 5860 x g. Once again, the supernatant was collected through glass wool. To the 156 ml of pink supernatant was added 34.32 g of solid ammonium sulfate at 0°C to bring the supernatant to 100% saturation. This was stirred for 2 hr; the pH was maintained at 6.95. The precipitate was separated by centrifugation at 5500 rpm for 30 min at 4920 x g. 31 ml of cold water was added to dissolve the salmon colored precipitate. It was then dialyzed against 2 changes of 500 ml of 15 mM piperazine buffer at pH 5.70.

3. Gel Exclusion Chromatography

A Pharmacia (5 x 85 cm) column was packed with approximately 137 g of Sephadex G-75 which had been preswollen in 15 mM piperazine buffer at pH 5.70. A flow rate of 80 ml/hr was maintained throughout this fractionation. After the column had equilibrated the dissolved proteins were applied to the column. 10 ml fractions were collected by a Gilson fraction collector. The absorbance at 254 nm of these fractions were recorded by a Gilson Model 260 Biochemical UV Monitor. The profile of these absorbance readings is shown in Figure 15. The high molecular weight proteins were discarded. Fractions 100-120, which contained the lower molecular weight proteins were pooled together.

4. Ion Exchange Chromatography

180 g of Whatman DE-52 cellulose was prepared according to the manufacturer's suggestions. After removing fines, the cellulose was equilibrated in 15 mM piperazine buffer at pH 5.70. A 2.5 x 45 cm column was packed with this material. A flow rate of 31 ml/hr was maintained throughout this fractionation. 200 ml of sample were applied to the column before a linear gradient of 1.4 l, 0.015 M - 0.14 M NaCl was begun. The absorbances of the 9 ml fractions were monitored

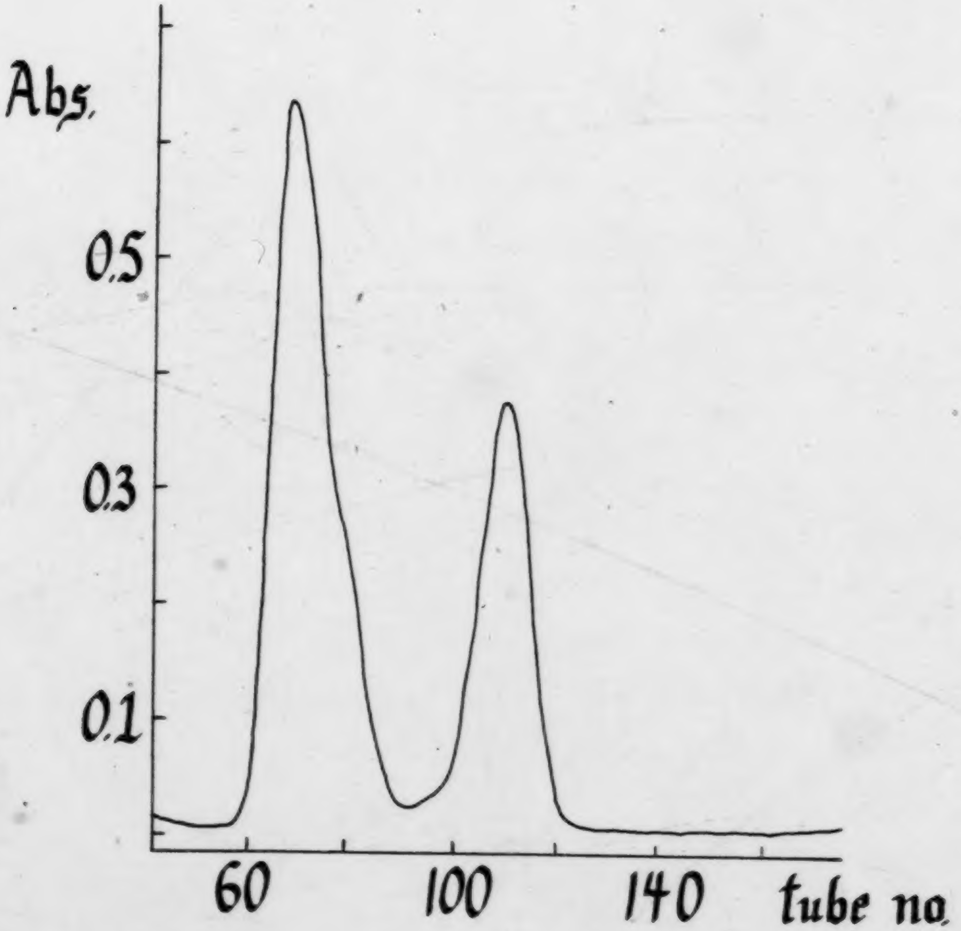

Figure 15. Sephadex G-75 chromatography (column 5 x 85 cm) of ammonium sulfate fractionated carp myogen. The elution rate was 80 ml/hr; 10 ml fractions were collected. Ultraviolet absorption was recorded at 254 nm with the aid of a Gilson Model 260 Biochemical UV monitor.

at 254 nm. A profile is shown in Figure 16. Three fractions were clearly separated: fractions 86-95, fractions 110-120, and fractions 130-140. These three fractions represent isozymes of the protein. The appropriate fractions were pooled and exhaustively dialyzed against water. Spectrapore 23 x 100 mm #1 tubing was used for these dialyses. After 3 changes of 16 l, the solutions were lyophilized. The final yields were: 31 mg from fractions 86-95, 57 mg from fractions 110-120, and 32 mg from fractions 130-140. This observed elution profile was similar to a previously published profile (Pechere *et al.*,1971a). On this basis, a comparison was made, and fractions 110-120 was tentatively assigned as the isozyme with an isoelectric point of 4.25. The source for this peak's asymmetry is not clear. Fractions 86-95 and 130-140 were tentatively assigned as the isozymes with isoelectric points 4.37 and 3.95 respectively. The isozyme with an isoelectric point of 4.47 was not successfully fractionated. After a number of general procedures are described, evidence to support the assignment of fractions 110-120 as parvalbumin component 'B' with isoelectric point of 4.25 will be presented.

B. General Methods

The general methods used in this study are discussed in this section.

1. *Polyacrylamide gel electrophoresis*

Slab polyacrylamide gel (8% w/v) electrophoresis was

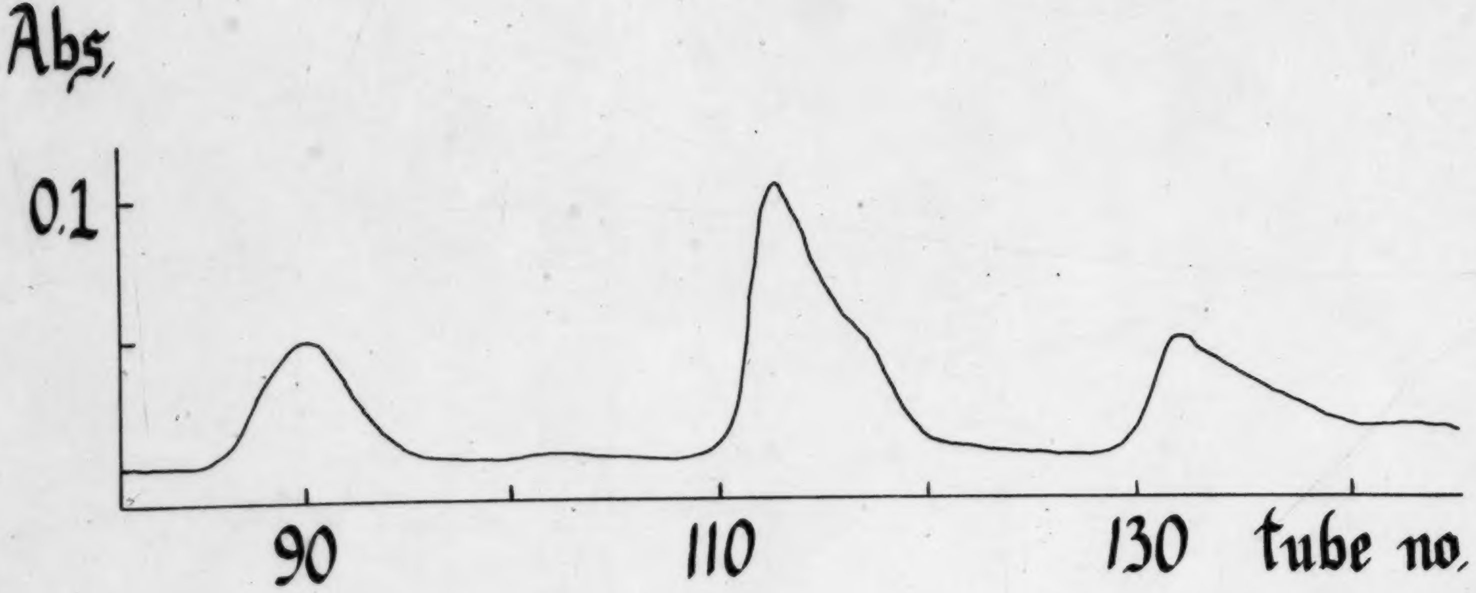

Figure 16. DE-52 cellulose chromatography (column 2.5 x 45 cm) of the low molecular weight proteins of carp myogen. The elution rate was 31 ml/hr; 9 ml fractions were collected. Ultraviolet absorption was recorded at 254 nm with the aid of a Gilson Model 26 Biochemical UV monitor.

performed in 100 mm sodium phosphate buffer, 0.1% (w/v) SDS (sodium dodecyl sulfate), 6 M urea, pH 7.0. Protein samples (1 mg/ml) were prepared by dissolving the protein in 50 mM phosphate, 1% (w/v) SDS, 6 M urea, ph 7.0. 10 microliters of beta-mercaptoethanol were added to each sample before they were incubated at 60°C for 30 minutes. One drop of 0.5% (w/v) bromophenol blue marker in 0.1 M phosphate was added to each sample before application to the gel. At the end of the run, the gel was destained for 2 hr in 10% (v/v) acetic acid, 10% (v/v) methanol. The gel was then stained fo 30 min in 0.25% (w/v) Coomassie Brilliant Blue R250 in 10% (v/v) acetic acid, 10% (v/v) methanol. The gel was then destained in 10% (v/v) acetic acid, 10% (v/v) methanol.

2. NMR Procedures

NMR Sample Preparation. Bio-rad D2O was made metal-free by extraction with 0.001% Mallinckrodt analytical grade dithizone in carbon tetrachloride, followed by extraction of dissolved dithizone and aeration with nitrogen to remove the excess solvent (Vogel, 1961). The standard buffer used for NMR samples consisted of 15 mM Pipes (piperazine-N, N'-bis(2-ethanesulfonic acid)), 0.15 M KCl, 10 mM DTT (dithiothreitol), and 0.5 mM DSS (sodium 2,2-dimethyl-2-silapentane-5-sulfonate), pH 6.88. The NMR samples were prepared by dissolving the protein in the standard buffer in a Fisher 1 ml polystyrene centrifuge tube. Microliter aliquots of 0.5 M NaOD or 0.5 M DCl in D2O were added to adjust the pH, which was measured with an Ingold microelectrode (Model 6030-04) attached to a Radiometer 26 pH meter. All pH measurements quoted are those observed and are not corrected for the deuterium isotope effect. The samples were centrifuged at maximum speed for 5 min on a Fisher Model 59 centrifuge, before they were dispensed into an NMR tube. Argon was blown on top of the solution to maintain an inert atmosphere.

Data Collection. ^{1}H NMR spectra were obtained on a Bruker HSX-270 spectrometer operating in the Fourier transform mode with quadrature detection. Typical instrumental settings for the 270 MHz spectra shown in this chapter were acquisition time 0.8192 s, sweep width +/- 2500 Hz, spectral size 8192 data points, and 1 Hz line broadening. HDO decoupling was employed. The sample temperature was 301°K. All chemical shifts quoted are measured with respect to the principal resonance of DSS as an internal standard.

3. *Protein Concentration Determination*

Amino acid analyses were performed on a Durrum model D500 analyzer. A known volume of protein solution was dispensed into a fired pyrex test tube which contained 200 microliters of distilled water. 10 microliters of 3.9 mM norleucine was also added to determine any loss of material during these procedures. After the contents of the tubes were lyophilized, 200 microliters of constant boiling HCl with 0.1% phenol was added. The tubes were then evacuated, sealed and incubated at 110°C for 24 hr. The hydrolysate was dried over NaOH pellets in a vacuum dessicator. The exact protein concentration was determined by an analysis of the alanine and leucine content present. All concentration measurements were made in triplicate.

4. Lanthanide Solution Preparation

Solution Preparation. Ytterbium solutions were prepared by first drying Specpure Johnson-Matthey ytterbium oxide at 110°C for 2 hr. The oxide was weighed directly into a tared 50 ml round bottom flask. Concentrated HCl was added to dissolve the oxide, thus forming the chloride. The following cycle was incorporated to remove excess solvent. The solution was rotavaporated to dryness. Distilled water was then added and again the resulting solution was rotavaporated to dryness. After this was repeated several times, a comparable cycle was initiated to exchange the H_2O solvent with dithizoned D_2O. The final stock solution of ytterbium chloride in D_2O was maintained at pH 4 to prevent hydroxide formation. Similar methods were used to prepare other lanthanide solutions.

Concentration Determination. EDTA in the form of the free acid was purchased from the Sigma Chemical Company. Xylenol orange was obtained from the J. T. Baker Chemical Company. Solutions of EDTA, used as a primary standard, were prepared according to analytical chemical techniques (Flaschka, 1964; Schwarzenbach & Flaschka, 1969). The concentration of lanthanide was determined by titration with EDTA, using xylenol orange as an indicator (Korbl & Pribil, 1956). Samples consisted of 2 ml of 0.1 M Mes (2-(2-morpholino)ethanesulfonic acid) buffer, pH 6.0, 1 drop of 0.05% (w/v) xylenol orange in water, and a known volume of stock lanthanide solution. EDTA was delivered from a pre-calibrated microburet model SB2 (Micro-Metric Instrument Company, Cleveland, Ohio) fitted with a 1000 microliter gas tight Hamilton syringe until the rose to yellow endpoint was observed.

C. Protein Characterization

In this section, evidence to support the assignment of the isolated protein as the appropriate isozyme of carp parvalbumin is presented.

1. Polyacrylamide gel electrophoresis

SDS urea polyacrylamide gels were used to assess the purity of the protein during various stages of the preparation (Figure 17). Slot D depicts the muscle extract. Slots A, B, and C represent tubes 70, 84, and 110 respectively from the G 75 column chromatogram (Figure 15). This demonstrates the progressive purification of the protein. Slots E, F, and G represent fractions 86-95, 110-120, and 130-140 respectively from the DE-52 column profile (Figure 16). A small amount of contaminating protein is present. Slots H, I, and J demonstrate the purity of a second preparation of parvalbumin (pI=4.25). These three slots represent three different concentrations of applied protein.

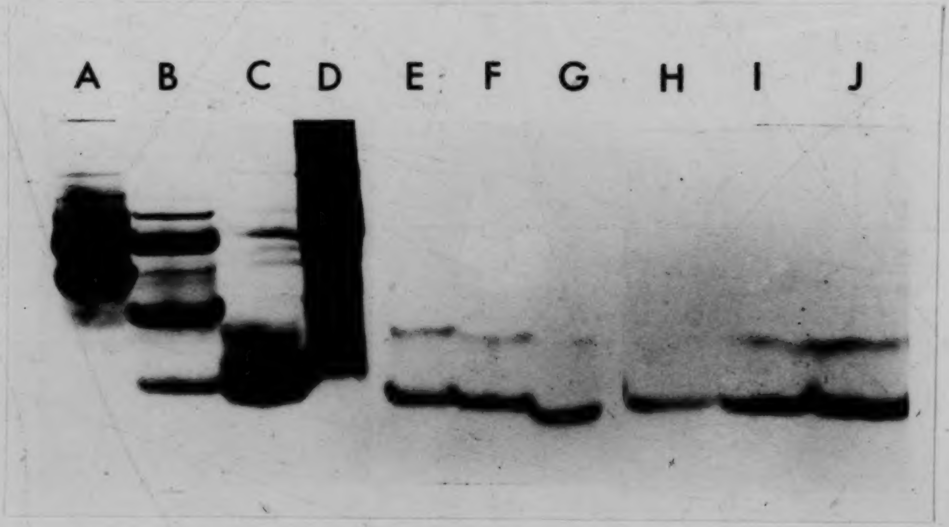

Figure 17. The isolation of parvalbumin: polyacrylamide gel electrophoresis in SDS urea. D, dialyzed extract; A, B, C, tubes 70, 84, and 110 respectively from the G 75 fractionation; E, F, G, tubes representing fractions 86-95, 110-120, and 130-140 respectively from DE-52 cellulose chromatography; H, I, J, samples from a second preparation of parvalbumin (pI=4.25), representing 3 different concentrations of applied protein.

2. Amino Acid Analysis

Table 2 indicates that parvalbumin (pI=4.47) contains 0 Met, 0 Pro, and 0 Tyr, that parvalbumin (pI=4.25) contains 0 Met, 0 Pro, and 0 Tyr, and that parvalbumin (pI=3.95) contains 0 Met, 1 Pro, and 1 Tyr. The amino acid analysis of parvalbumin isolated from fractions 110-120 (Figure 16) indicates the absence of methionine, proline, and tyrosine. By comparing the methionine, proline, and tyrosine content of the observed analyses, one can only state that fractions 110-120 do not represent the parvalbumin with isoelectric point of 3.95. Further experiments are necessary in order to make a final assignment.

3. Ultraviolet Absorption Spectroscopy

A UV spectrum recorded on a Cary 14 recording UV spectrophotometer of the isozyme with isoelectric point 4.25 isolated from the second protein preparation is shown in Figure 18. This sample was taken directly from the appropriate fractionation tube. The spectrum is very similar to that observed for hake parvalbumin (Parello & Pechere, 1971). Figure 18 confirms the absence of both tyrosine and tryptophan in this isozyme; in addition, the absorption at 259 nm corroborates the high phenylalanine content of this isozyme. This however does not establish a final assignment for the protein.

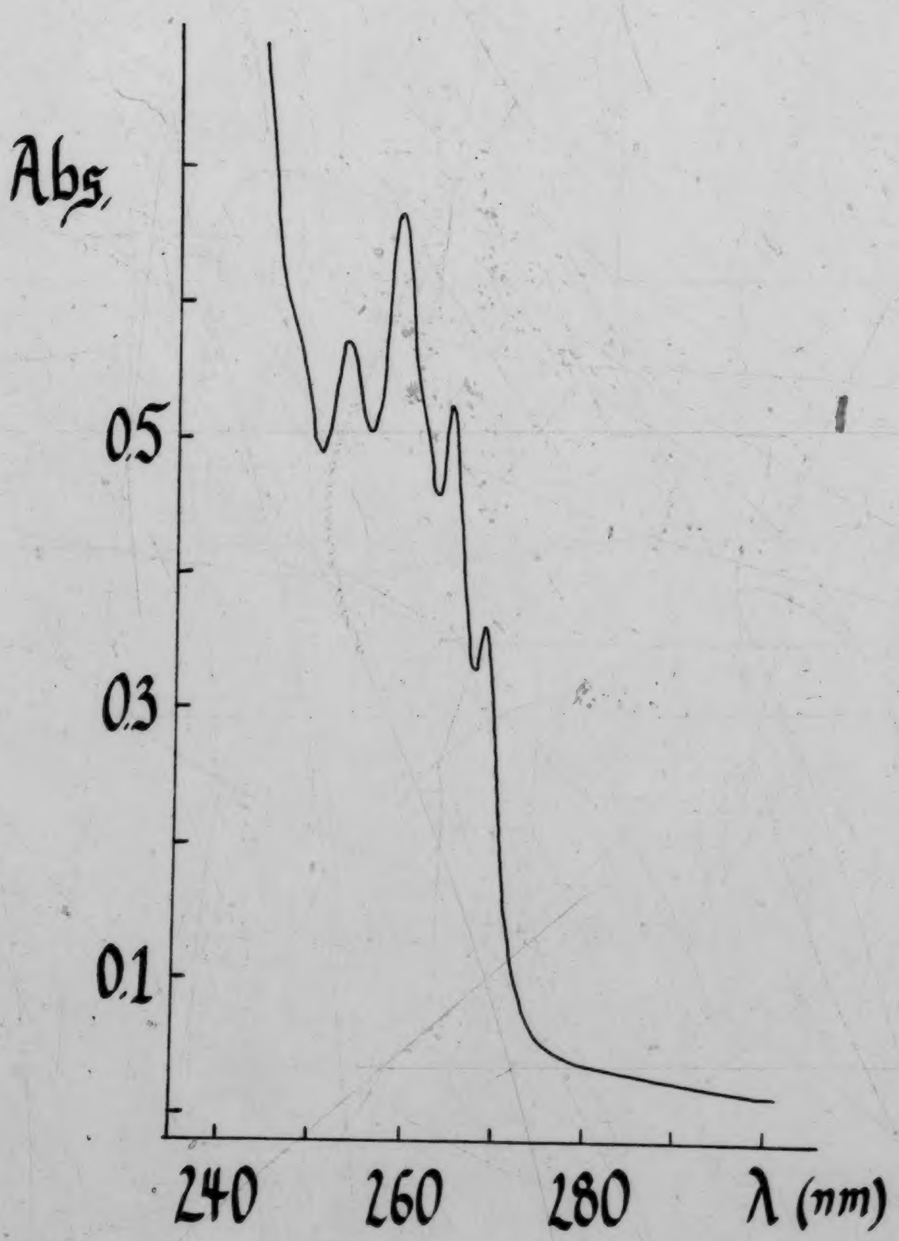

Figure 18. The ultraviolet absorption of parvalbumin, pI=4.25. The sample was taken directly from the appropriate fractionation tube after DE-52 cellulose chromatography. This spectrum was recorded on a Cary 14 UV spectrophotometer.

4. Nuclear Magnetic Resonance Spectroscopy

^1H NMR was also used to characterize the isozymes. The 270 MHz ^1H NMR spectra of fractions 86-95, 110-120, and 130-140 are shown in Figures 19 to 22. A similarity between Figure 20 and a previously published spectrum of the parvalbumin with pI of 4.25 (Parello *et al*., 1974) supports the assignment of fractions 110-120 as the appropriate isozyme with pI of 4.25.

A common feature of these spectra is the presence of non-exchanged NH resonances with observed chemical shifts 8 to 11 ppm downfield from DSS. Although similarities exist among these three spectra (Figures 19-21), an expansion of their aromatic regions (Figure 22) demonstrates the distinct identities for each of the three isozymes.

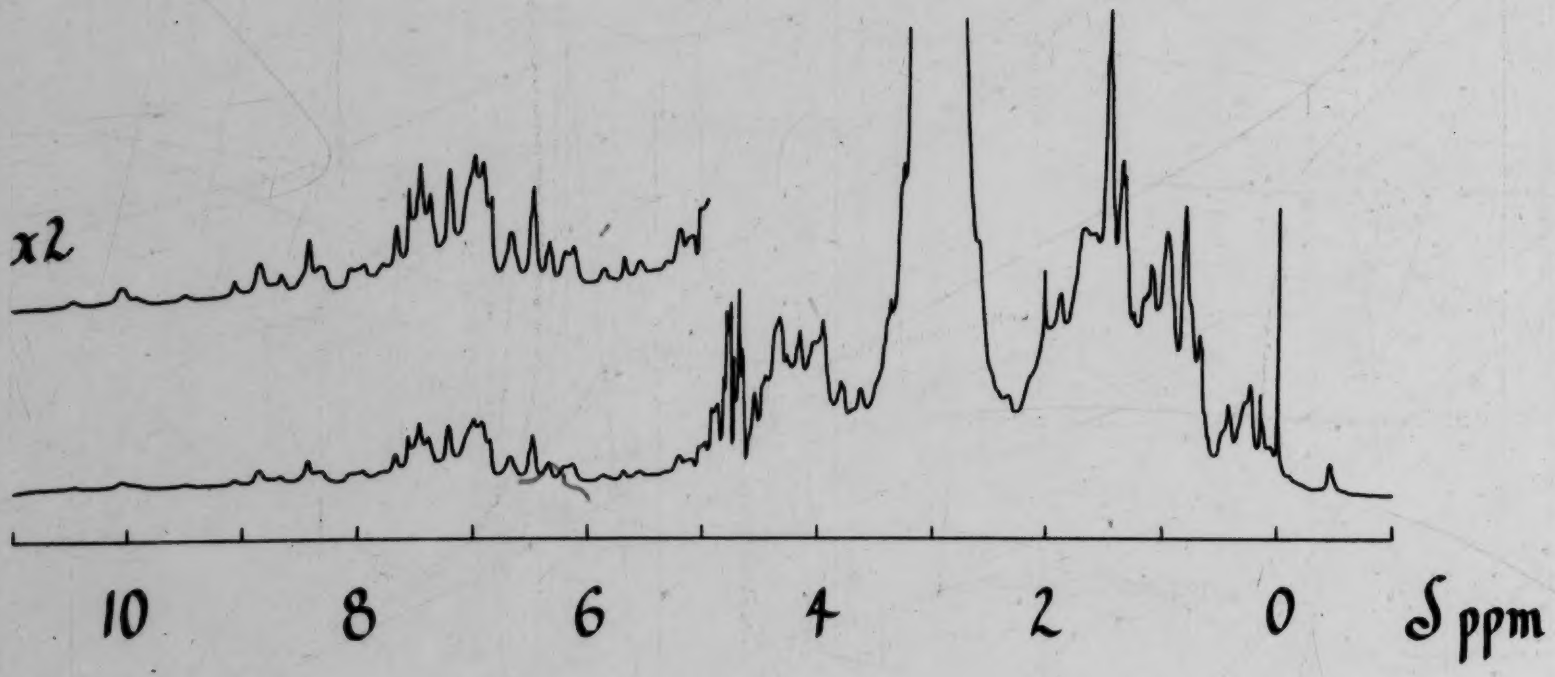

Figure 19. The 270 MHz ^{1}H NMR spectrum of parvalbumin obtained from tubes 86-95 in the DE-52 cellulose fractionation of the low molecular weight proteins of carp myogen (Figure 16). The sample contained 5 mg/ml of protein in 15 mM Pipes, 0.15 M KCl, 0.5 mM DSS in D2O, pH 6.83.

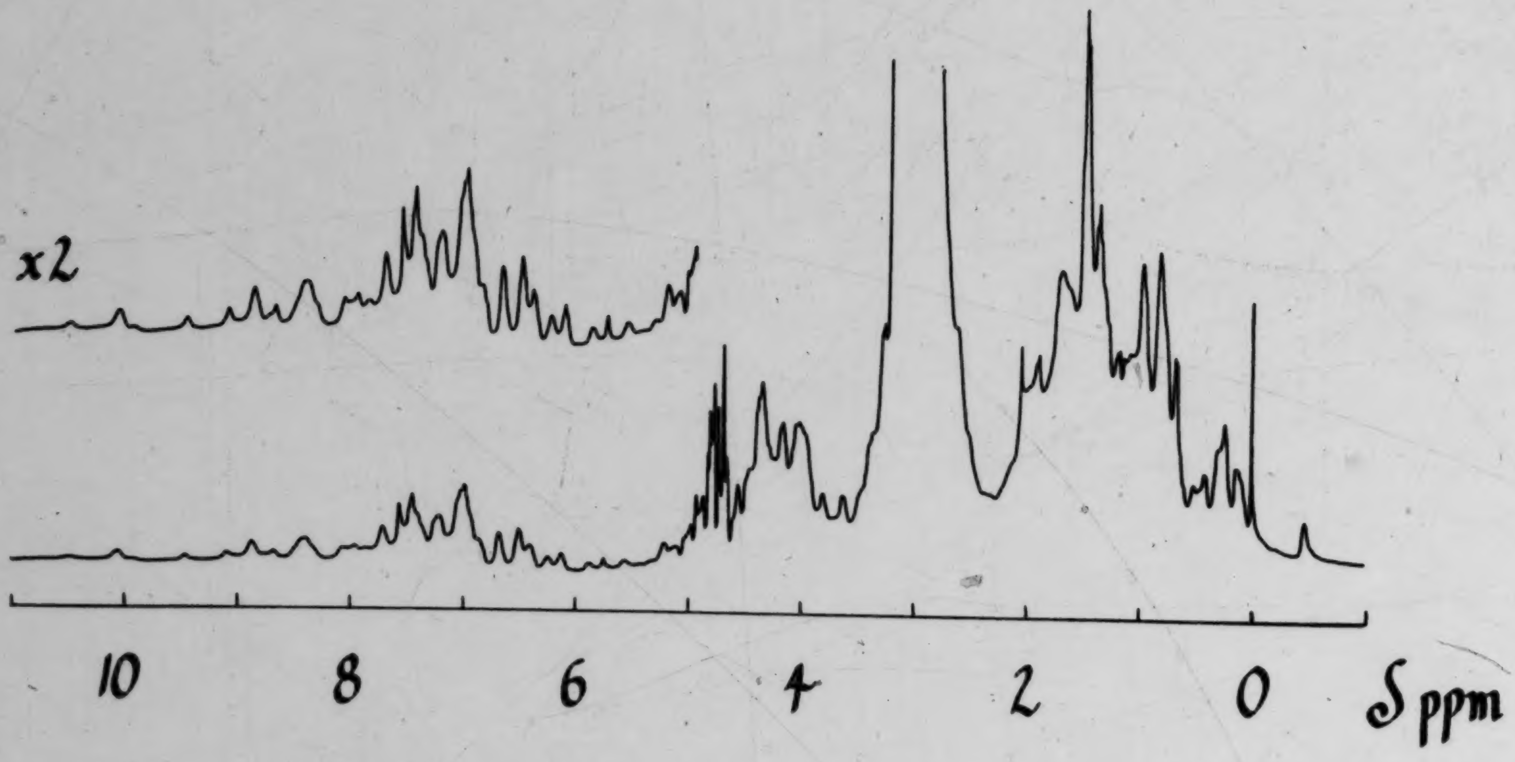

Figure 20. The 270 MHz ¹H NMR spectrum of parvalbumin obtained from tubes 110-120 in the DE-52 cellulose fractionation of the low molecular weight proteins of carp myogen (Figure 16). The sample contained 5 mg/ml of protein in 15 mM Pipes, 0.15 M KCl, 0.5 mM DSS in D2O, pH 6.83.

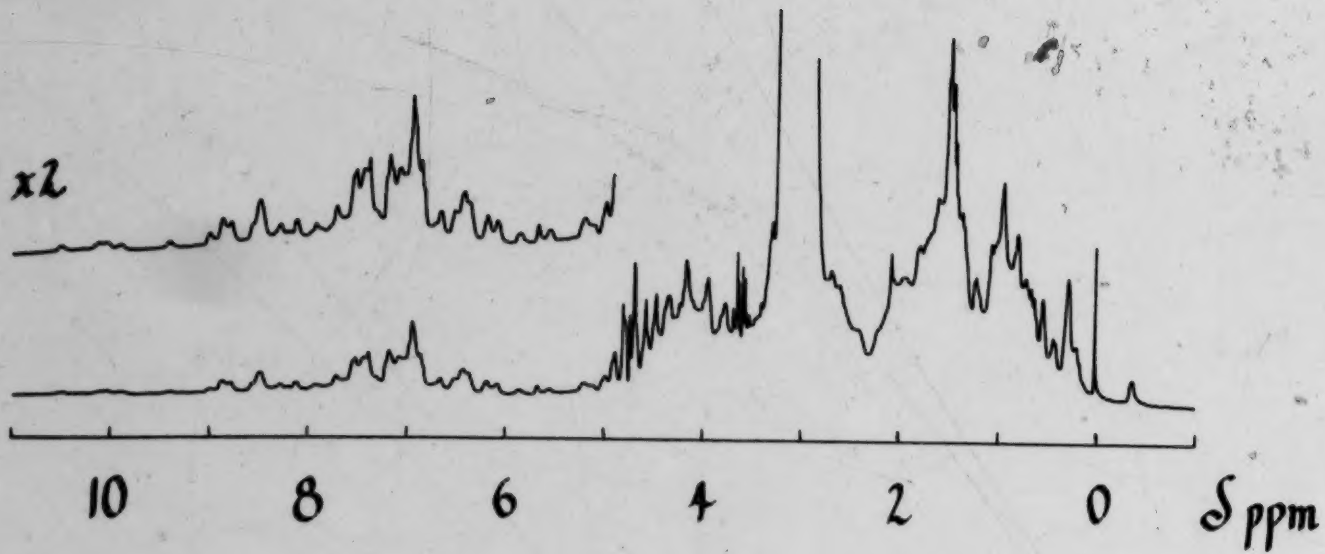

Figure 21. The 270 MHz ^{1}H NMR spectrum of parvalbumin obtained from tubes 130-140 in the DE-52 cellulose fractionation of the low molecular weight proteins of carp myogen (Figure 16). The sample contained 10.8 mg/ml of protein in 15 mM Pipes, 0.15 M KCl, 0.5 mM DSS in D2O, pH 6.85.

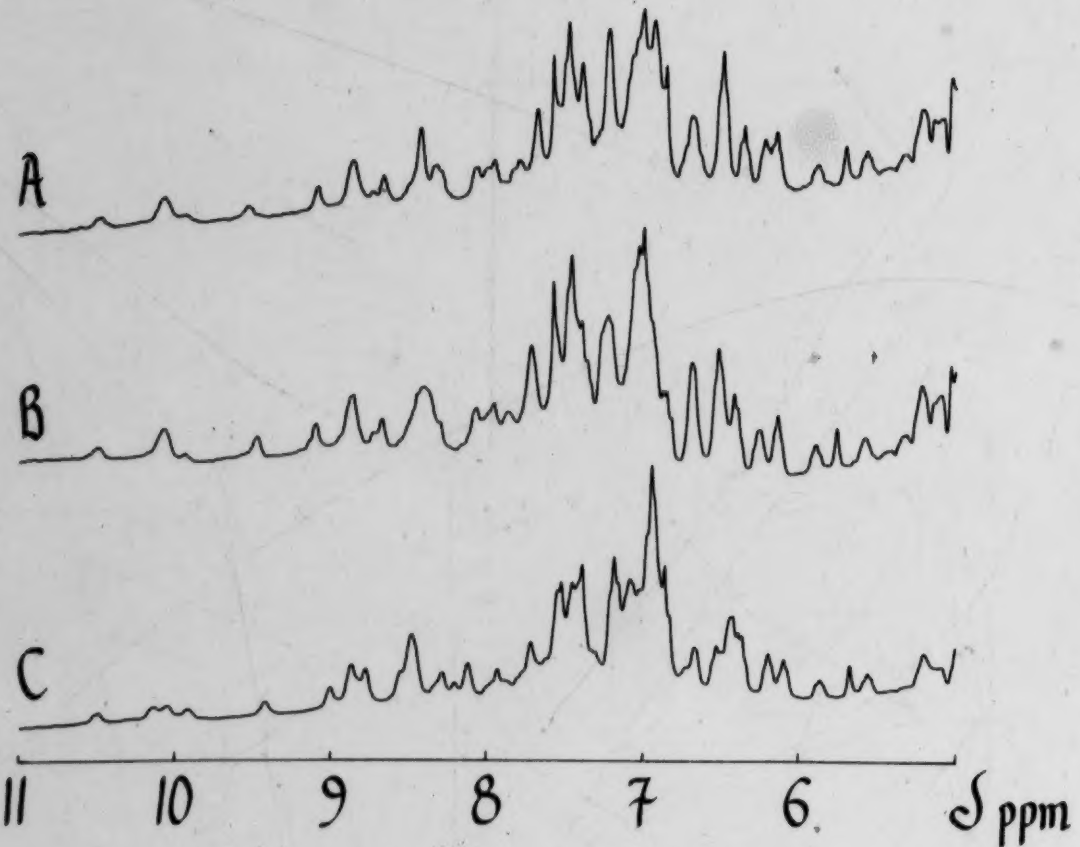

Figure 22. A comparison of the aromatic regions of the 270 MHz ^1H NMR spectra of the three isozymes of parvalbumin isolated by DE-52 cellulose chromatography. A. fractions 86-95, B. fractions 110-120, C. fractions 130-140. This Figure consists of expansions of spectra presented in Figures 19-21.

5. *X-ray Crystallography*

Kretsinger and co-workers have attempted to isolate and to crystallize the various parvalbumin isozymes (Kretsinger *et al*., 1971). They observed that 3 of the carp isozymes crystallize with 3 different unit cell dimensions. Crystallization of protein tentatively assigned as the isozyme with isoelectric point of 4.25 was attempted to establish the identity of this protein. Crystals of parvalbumin were obtained by the technique of equilibrium dialysis (Zeppezauer *et al*., 1968). 250 microliters of water and 10 microliters of 0.4 M Pipes buffer were added to dissolve 12 mg of protein. The solution was filtered through a 0.45 micron Millipore filter, and then dispensed into zeppezauer tubes. These tubes were placed into test tubes, containing 2 ml of 2.5 M ammonium sulfate, 0.01 M K_2HPO_4, pH 6.5, and 100 microliters of 0.4 M Pipes buffer. Crystals were obtained within 3 days.

Precession photographs, for example in Figure 23, were obtained on a Nonius precession camera with CuK alpha radiation from an Elliot rotating anode generator operating at 40 kV and 40 mA and a 6 hr exposure time. The unit cell dimensions observed for these crystals in addition to published unit cell dimensions of three parvalbumin isozymes are presented in Table 4. The similarity between the observed unit cell dimensions and those of the parvalbumin with an isoelectric point of 4.25 is evident. The appropriate isozyme of parvalbumin has been isolated.

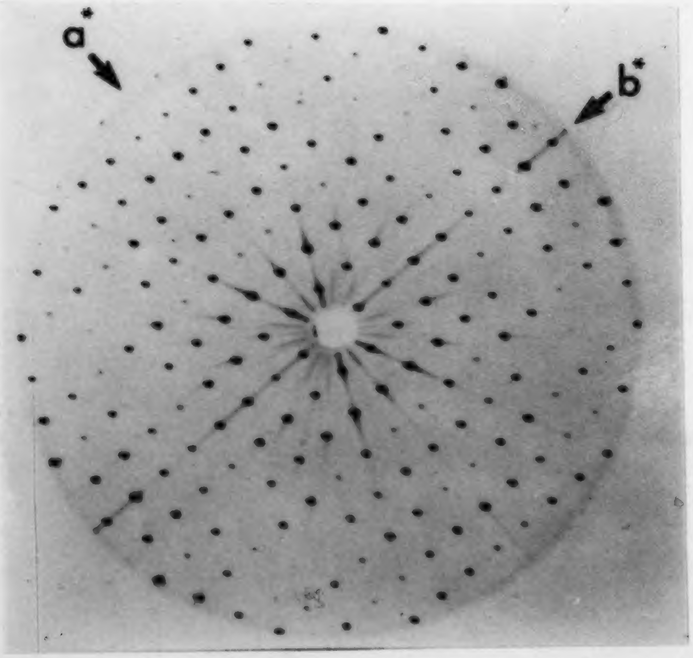

Figure 23. Precession photograph of a carp parvalbumin crystal, depicting the hko diffraction plane to the limit of 2 angstrom resolution. This photograph was taken using nickel filtered CuK alpha radiation, 40 kV, 40 mA, and a 6 hr exposure time.

Table 4

A Comparison of the Observed and Published Unit Cell Dimensions of Carp Parvalbumin Crystals[1]

	Observed	Published[1]		
pI	--	3.95	4.25	4.47
Sp.Gp.	C2	P2	C2	P1?
a(Å)	28.2	60.9	28.7	25.0
b(Å)	60.7	59.2	61.1	82.0
c(Å)	54.2	59.4	54.5	39.0
α(°)	90.0	90.0	90.0	95.0
β(°)	95.0	109.8	94.6	82.0
γ(°)	90.0	90.0	90.0	82.0

[1] Kretsinger *et al*., 1971.

IV. The Binding of Ytterbium to Parvalbumin

A. Introduction

The substitution of the paramagnetic lanthanide ion ytterbium for the calcium ions bound to the CD and EF sites of carp parvalbumin results in a series of ^1H NMR resonances which are shifted far outside of the envelope of the ^1H NMR spectrum of the diamagnetic form of the protein. In this chapter, I shall focus on the analysis of the stoichiometry of the binding of Yb^{3+} to carp parvalbumin (pI=4.25).

Titrations of Ca^{2+} saturated parvalbumin with ytterbium demonstrate that there is a sequential replacement of the two protein bound calcium ions. Analysis of the data results in the determination of the relative affinities for ytterbium with respect to calcium for each of the two sites (CD and EF). The affinities of these two sites for ytterbium can then be calculated from the previously measured calcium affinities.

A problem is that conflicting results exist for the binding of Ca^{2+} to parvalbumin, both qualitatively and quantitatively. The early studies of Benzonana and co-workers (Benzonana *et al.*, 1972) suggested that the two calcium binding sites of hake and frog parvalbumin have equal dissociation constants for calcium of 1×10^{-7} M. However, these studies were performed in the presence of competing Mg^{2+} ions, and later studies indicate the dissociation constants to be approximately two orders of magnitude smaller (Potter *et al*., 1977a). In addition, several reports suggest that the binding of calcium is cooperative (Benzonana *et al*., 1972; Cave *et al*., 1979b); whereas others contradict this hypothesis (Donato & Martin, 1974; Nelson *et al*., 1977; Sowadski *et al*., 1978). Recently Haiech and co-workers (Haiech *et al*., 1979b) have reported that the two calcium binding sites of hake parvalbumin have different affinities for calcium. Here I shall demonstrate that the cooperativity versus independent sites question is not relevant under the given experimental protocol, that the experimental results support the conclusions of Haiech *et al*., (1979b), and that the calculated ytterbium dissociation constants for the CD and EF calcium binding of carp parvalbumin are $K^{CD}_{Yb^{3+}} = (4\text{-}7) \times 10^{-10}$ M and $K^{EF}_{Yb^{3+}} = (2\text{-}6) \times 10^{-10}$ M. The approximate equality of these constants is verified by Yb^{3+} titrations of apo parvalbumin. The results are compared with literature results for the binding of other lanthanides (Sowadski *et al*., 1978; Cave *et al*., 1979c).

B. Experimental Procedures

NMR Procedures ^1H NMR spectra were obtained on a Bruker HXS-270 spectrometer operating in the Fourier transform mode with quadrature detection. Typical instrumental settings for the spectra were acquisition time 0.2 s, sweep width ± 10 kHz, spectrum size 8192 data points and linebroadening 5 Hz.

No HDO homonuclear decoupling was employed. The sample temperature was 302°K. The chemical shifts were measured relative to the principal resonance of DSS (sodium 2,2-dimethyl-2-silapentane-5-sulfonate) as an internal standard. The standard filters on the HXS-270 spectrometer were replaced with Bessel filters (Ithaco, model 4302). Spectra were taken with a filter width set equal to twice the spectral width which results in minimum baseline distortion. The data were accumulated with NMR recycle times long relative to the spin lattice relaxation times (Lee & Sykes, 1980c); therefore the observed areas represent true intensities. The areas of the resonances were calculated as the product of the linewidth times the maximum line intensity which is proportional to the area for a Lorentzian lineshape.

Sample Preparation Stock ytterbium solutions were prepared from dried Johnson-Matthey ultrapure oxides as discussed earlier (Birnbaum & Sykes, 1978; Chapter 3). The concentrations of Yb^{3+} were determined by titration with EDTA in pH 6 MES (2-(N-morpholino)-ethanesulfonic acid) buffer using xylenol orange as an indicator (Korbl & Pribil, 1956).

Carp parvalbumin (pI=4.25) was isolated by the method of Pechere and co-workers (Pechere *et al.*, 1971; Chapter 3). The protein so isolated was Ca^{2+} saturated as evidenced by comparison with the ^1H NMR spectrum of apo and Ca^{2+} saturated parvalbumin and by crystallization of the protein, since the apo form does not crystallize (Kretsinger & Nockolds, 1973).

The NMR samples for the Ca^{2+} saturated protein titrations were prepared by dissolving the lyophilized protein in D2O buffer, 15 mM Pipes, 0.15 M KCl, 10 mM DTT, 0.5 mM DSS, pH 6.6. pH measurements were made with an Ingold electrode (Model 6030-04) attached to a Beckman Expandomatic SS-2 or Radiometer 26 pH meter. The pH values quoted are those observed and are not corrected for the deuterium isotope effect on the glass electrode. Protein concentrations were determined by amino acid analysis after 24 hr of acid hydrolysis at 110°C. The Yb^{3+} titrations were performed by addition of 5 microliter aliquots of Yb^{3+}, prepared at the same pH as the protein sample, pH 6.6. The addition of Yb^{3+} did not affect the final pH of the resulting protein solution.

Demetallized parvalbumin was prepared in the following manner. 11.3 mg of parvalbumin was dissolved in 1 ml of 15 mM Pipes buffer, pH 7.0, containing 50 mM EDTA. The solution was gently stirred for 1.5 hr, and then desalted on a Sephadex G-25 column (1 x 24 cm). The protein fraction was then dialyzed extensively against doubly distilled water and lyophilized. The lyophilized protein was dissolved in Chelex-treated and dithizoned 15 mM Pipes, 0.15 M KCl, 15 mM DTT, 0.5 mM DSS, in D2O, pH 6.64. The protein was then shown to be apo, within the limits of NMR ($\gtrsim$ 90%), by comparison of its ^{1}H NMR spectrum with that of the protein in the presence of EDTA. The absence of NH resonances, in particular, in the ^{1}H NMR spectrum indicates a partially unfolded state of the protein, resulting from the loss of bound calcium ions. This phenomenon has been reported elsewhere for another carp isozyme (Birdsall *et al.*, 1979).

Analysis of the Ytterbium Titration Data The possible species present during the titration of calcium saturated parvalbumin with ytterbium are shown in Figure 24, wherein parvalbumin is represented as two squares ($\boxed{}\boxed{}$) with the left hand square taken to represent the CD site and the right hand square, the EF site. The dissociation constants are written as K^{i}_{mn} where i = CD or EF, and n, m = 0, C or Y for apo, Ca^{2+}, or Yb^{3+} respectively. The superscript indicates to which site the binding is referred, whereas the double subscript indicates the final product of the binding. Thus the dissociation constant K^{CD}_{CY} refers to the reaction

$$\boxed{}\boxed{Y} + C \rightleftharpoons \boxed{C}\boxed{Y} \qquad (4.1)$$

It is assumed that while the binding to a given site may depend upon whether or not there is a metal in the other site, it does not depend upon which metal (Ca^{2+} or Yb^{3+}) is present in the other site. Thus, for example $K^{EF}_{CY} = K^{EF}_{YY}$. With the concentrations of metals and proteins used (in the mM range) for the titration of the Ca^{2+} saturated parvalbumin, and with the extremely small dissociation constants (~ 10^{-9} M for Ca^{2+} and ~10^{-11} M for Yb^{3+}), there

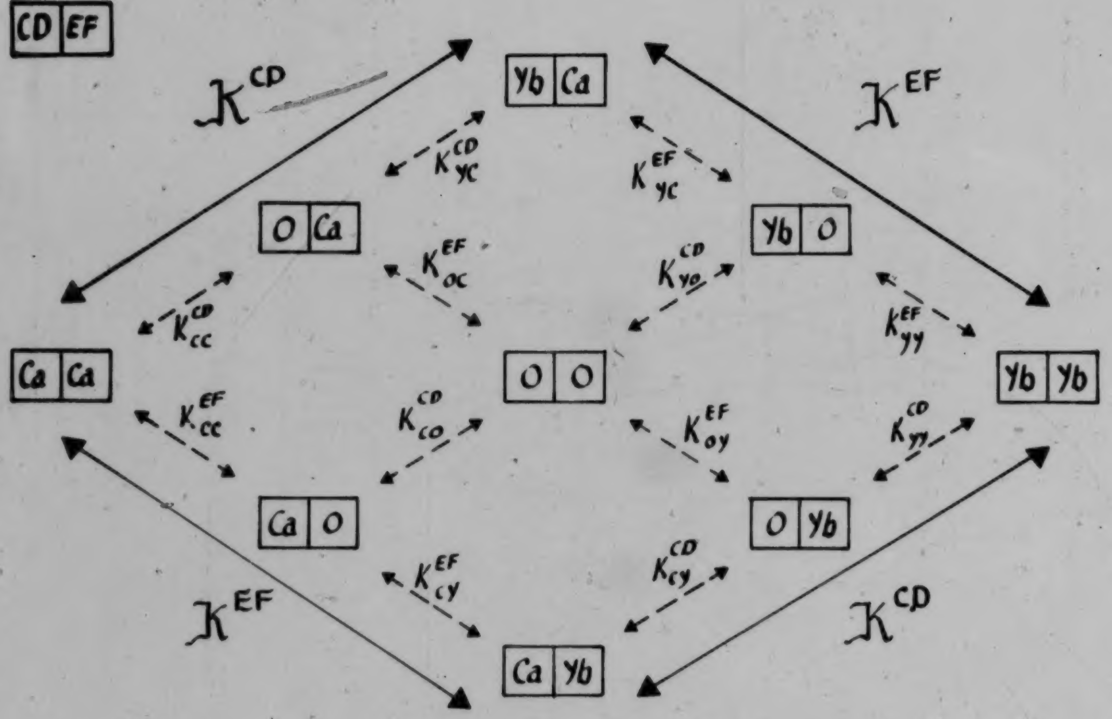
CD EF
Yb Ca
O Ca
Yb O
Ca Ca
O O
Yb Yb
Ca O
O Yb
Ca Yb
$\mathcal{K}^{CD}$
$\mathcal{K}^{EF}$
$\mathcal{K}^{EF}$
$\mathcal{K}^{CD}$
K^{CD}_{yc}
K^{EF}_{yc}
K^{EF}_{oc}
K^{CD}_{yo}
K^{CD}_{cc}
K^{EF}_{yy}
K^{EF}_{cc}
K^{CD}_{co}
K^{EF}_{oy}
K^{CD}_{yy}
K^{EF}_{cy}
K^{CD}_{cy}

Figure 24. An outline of the mechanism for the binding of ytterbium and calcium to parvalbumin. The two squares represent the two metal binding sites of parvalbumin. the left square represents the CD site; the right, the EF site. Y refers to Yb^{3+}; C, to Ca^{2+}. The superscripts of the association constants refer to the site being filled; the subscript, to the final state of metal occupancy. An open circle indicates no metal present.

will be negligible concentrations of any of the apo or partially apo species. Thus the relevant mechanism may be reduced to the four species connected by the solid lines (Figure 24). The relative concentrations of the four species are a function of only two constants which are the relative affinities of the CD or EF site for Yb^{3+} with respect to Ca^{2+} (K^{CD} and K^{EF}). That is for example

$$K^{EF}_{YC} = \frac{[YO][C]}{[YC]} \qquad K^{EF}_{YY} = \frac{[YO][Y]}{[YY]} \tag{4.2}$$

therefore

$$\frac{[YC][Y]}{[YY][C]} = \frac{K^{EF}_{YY}}{K^{EF}_{YC}} \equiv K^{EF} \tag{4.3}$$

In this limit, any cooperativity even if present, is not observable in the titration of the Ca^{2+} saturated protein.

This simplified scheme was used to analyze the data in Figure 27. The solid lines in Figure 27 were calculated on a NOVA 1220 computer with the only adjustable parameters being K^{CD} and K^{EF}, and the final areas of each of the three peaks analyzed. Thus any two curves in Figure 27 determine the third within an arbitrary scaling parameter related to the relative areas of the peaks.

C. Results

When a paramagnetic trivalent lanthanide (excluding the isotropic Gd^{3+}) is added to a protein metal ion binding site, it will cause shifting and broadening of the NMR resonances of nearby nuclei. Since the rates of dissociation of the lanthanide ion from the protein are in the NMR slow exchange limit on the NMR chemical shift timescale (Lee & Sykes, 1980a,b,c,d; Chapter 2), the resulting shifted and broadened resonances will be observed separate from the resonances of the diamagnetic protein. When Yb^{3+} is added to Ca^{2+} saturated parvalbumin, the sequential appearance and disappearance of several sets of shifted peaks are observed (Figures 25 and 26). Up to a ratio of total metal to total protein (Yb^{3+}/P) of ~1/1, one set of peaks appears (Figure 25) exemplified by the resonance indicated by a triangle (▲) in Figure 25. As the second calcium is replaced at higher (Yb^{3+}/P) ratios, some of the first set of peaks such as the one indicated by a triangle are not affected. However, other resonances disappear (shifted elsewhere, see resonance labelled with a square (■)) and are replaced by a new set of peaks. In addition, some peaks appear only after binding of the first metal; such as the resonance labelled with a circle (●). These results indicate immediately that Yb^{3+} sequentially replaces the two Ca^{2+} ions of parvalbumin.

The areas of three shifted resonances, selected to represent the various possible modes of behavior during titration as described above, were corrected for dilution

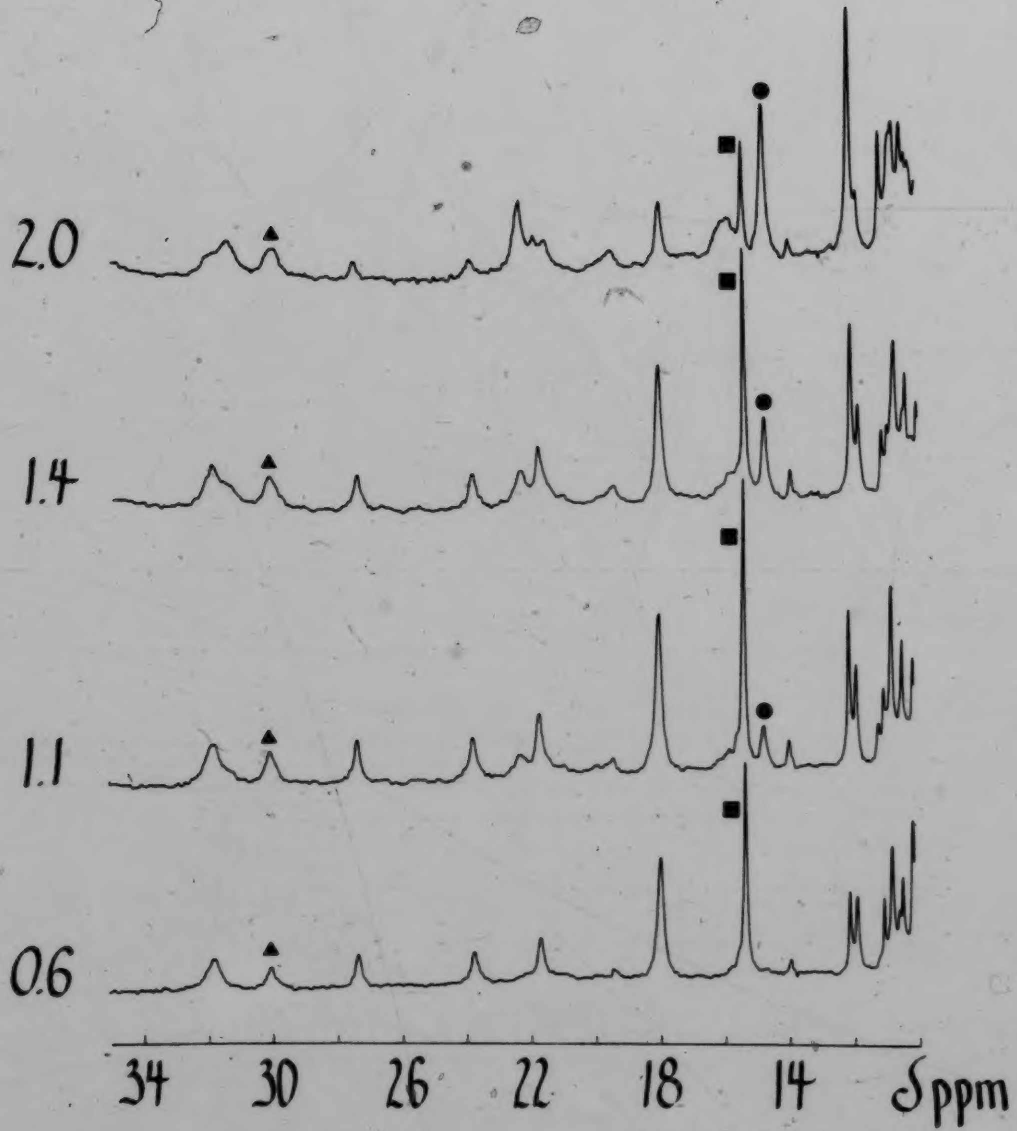

Figure 25. The downfield portion of the ^1H NMR spectrum of carp parvalbumin as a function of total Yb^{3+} to total protein ratio. The 0.84 mM protein sample was prepared in 15 mM Pipes, 0.15 M KCl, 10 mM DTT, 0.5 mM DSS in D2O, pH 6.63 at total Yb^{3+} to total protein ratios of 0.6, 1.1, 1.4, and 2.0. The ambient temperature was 302°K. The symbols ●, ■, and ▲ indicate peaks plotted in Figure 27.

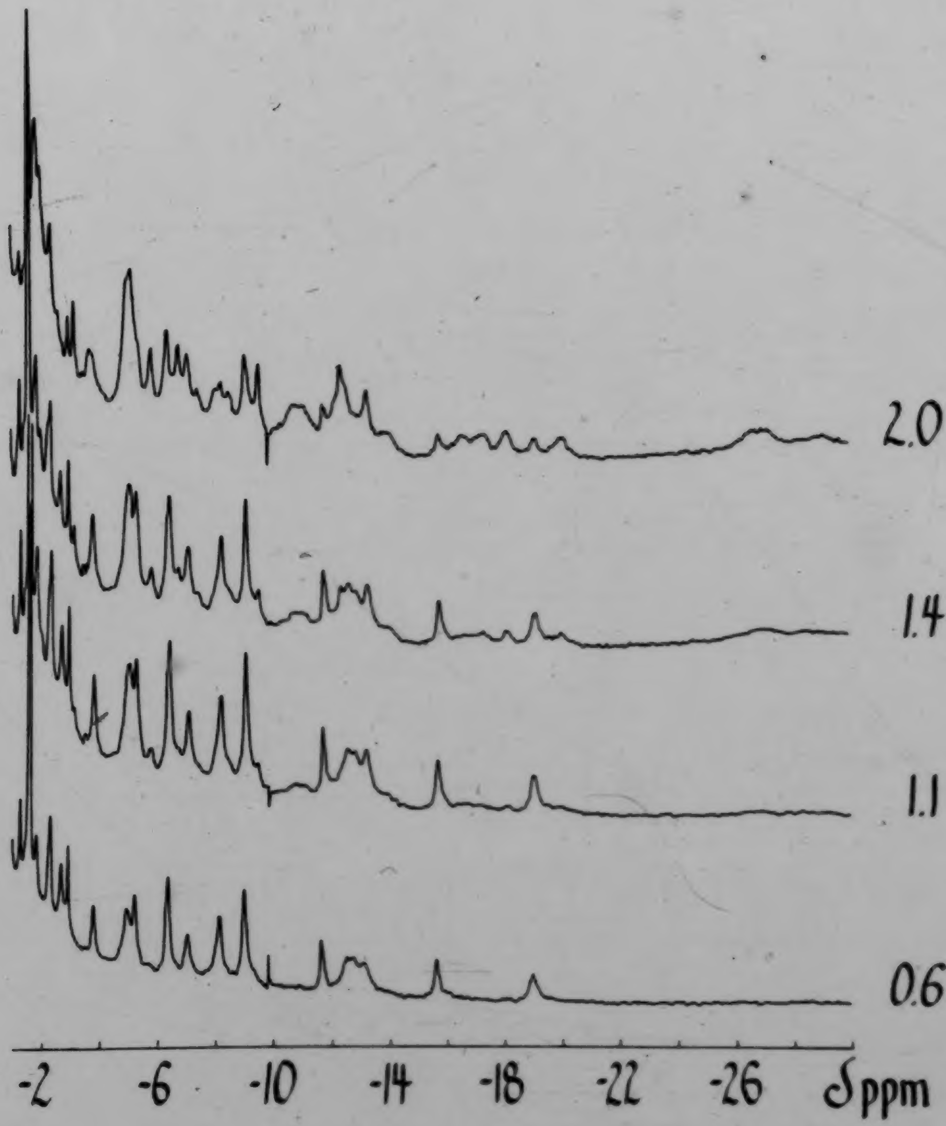

Figure 26. The upfield portion of the ^1H NMR spectrum of carp parvalbumin as a function of total Yb^{3+} to total protein ratio. The 0.84 mM protein sample was prepared in 15 mM Pipes, 0.15 M KCl, 10 mM DTT, 0.5 mM DSS in D2O, pH 6.63 at total Yb^{3+} to total protein ratios of 0.6, 1.1, 1.4, and 2.0. The ambient temperature was 302°K.

effects, and plotted as a function of total Yb^{3+} to total protein concentration (Figure 27 and Table 5). The solid lines in Figure 27 represent the fit to the mechanism proposed in Figure 24, as described in the Experimental Procedures section. The relative dissociation constants of each site for Yb^{3+} with respect to Ca^{2+} obtained from the fitting procedure were $K^{CD} = 0.13$, and $K^{EF} = 0.01$ (see Discussion for the assignment to CD and EF sites). Area measurements were also determined as part of the fitting procedure. The calculated areas of the resonances with observed chemical shifts of 14.55 and 15.17 ppm were 983 ± 57 and 804 ± 24 respectively, whereas the area of the resonance with an observed chemical shift of 29.80 ppm is 304 ± 13.

The titration of the partially apo parvalbumin with Yb^{3+} yielded the same final spectrum at a ratio of Yb^{3+}/P 2-3 as the titration of the Ca^{2+} saturated protein. However, some of the intermediate resonances observed were different, and the order of appearance of the resonances plotted in Figure 27 were different. In Figure 28 and Table 6 the appearance of the resonance at 29.80 ppm (represented by the filled triangle in the titration of the Ca^{2+} saturated protein) is plotted as a function of Yb^{3+}/P. It is clear that the appearance of this resonance in the titration of the apo protein significantly lags behind its appearance in the titration of the Ca^{2+} saturated protein, plateauing near approximately 2/1 for apo as opposed to near approximately

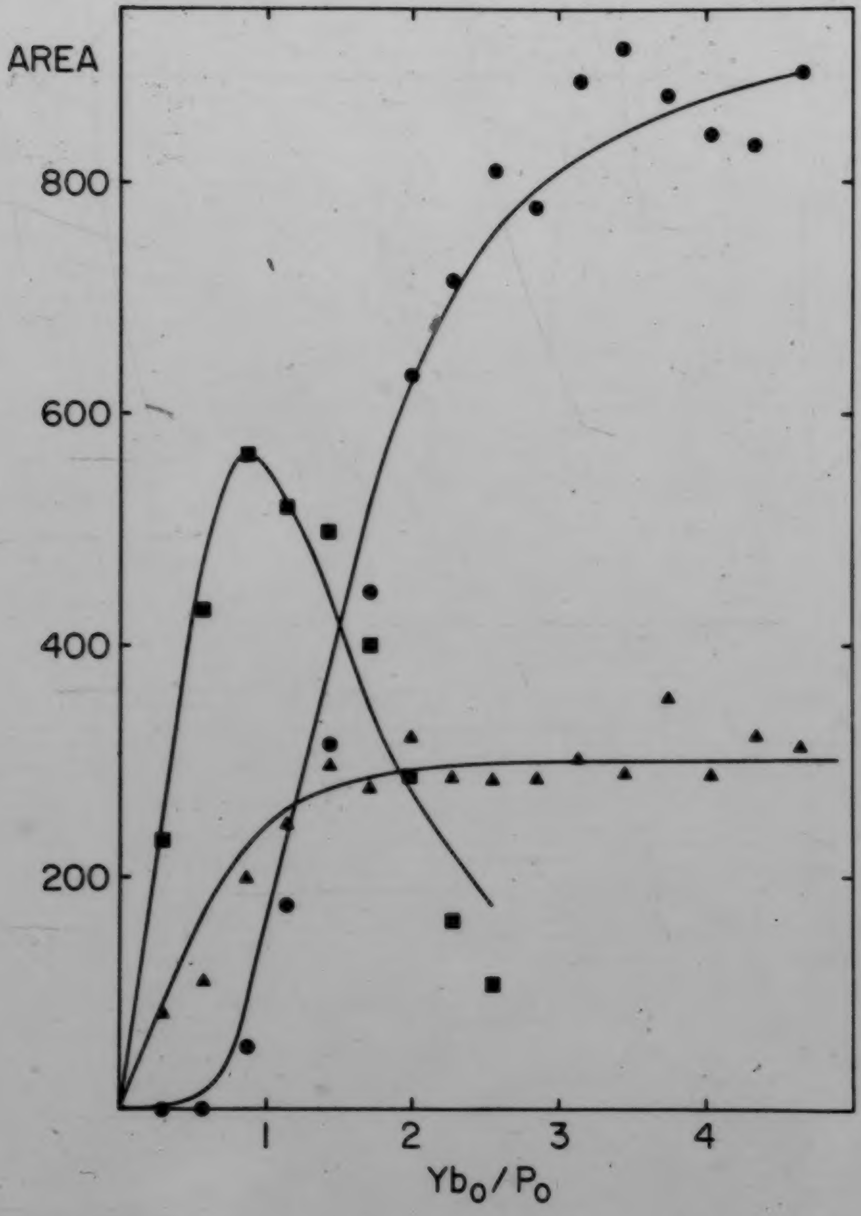

Figure 27. The areas of three representative peaks as a function of (Yb^{3+}/P) ratio in the Yb^{3+} titration of calcium saturated parvalbumin. The resonances represented by ▲ , ■, and ● have observed chemical shift positions of 29.80, 15.17, and 14.55 ppm respectively (see Figure 25).

Table 5

Yb^{3+} Titration of Ca^{2+} Saturated Parvalbumin

Yb^{3+}/P[1]	Area A[2]	Area B[3]	Area C[4]
0.283	83.2	230.8	ND[5]
0.565	109.1	428.0	ND
0.848	197.9	566.7	53.3
1.132	246.4	518.8	176.0
1.414	296.8	499.0	314.3
1.699	276.3	379.6	445.6
1.983	321.2	288.1	633.4
2.269	286.1	162.6	715.8
2.555	284.4	107.7	809.9
2.839	284.9	ND	785.8
3.137	303.4	ND	882.8
3.436	288.0	ND	917.4
3.735	356.9	ND	875.9
4.035	287.5	ND	843.9
4.336	323.6	ND	833.3
4.640	312.5	ND	888.4

---

[1] total ytterbium to total protein ratio.

[2] The areas of the resonances were calculated as the product of the linewidths times the maximum line intensity. A refers to the resonance with an observed chemical shift position of 29.80 ppm (see filled triangles in Figure 27).

[3] B refers to the resonance with an observed chemical shift position of 15.17 ppm (see squares in Figure 27).

[4] C refers to the resonance with an observed chemical shift position of 14.55 ppm (see circles in Figure 27).

[5] ND indicates not determined.

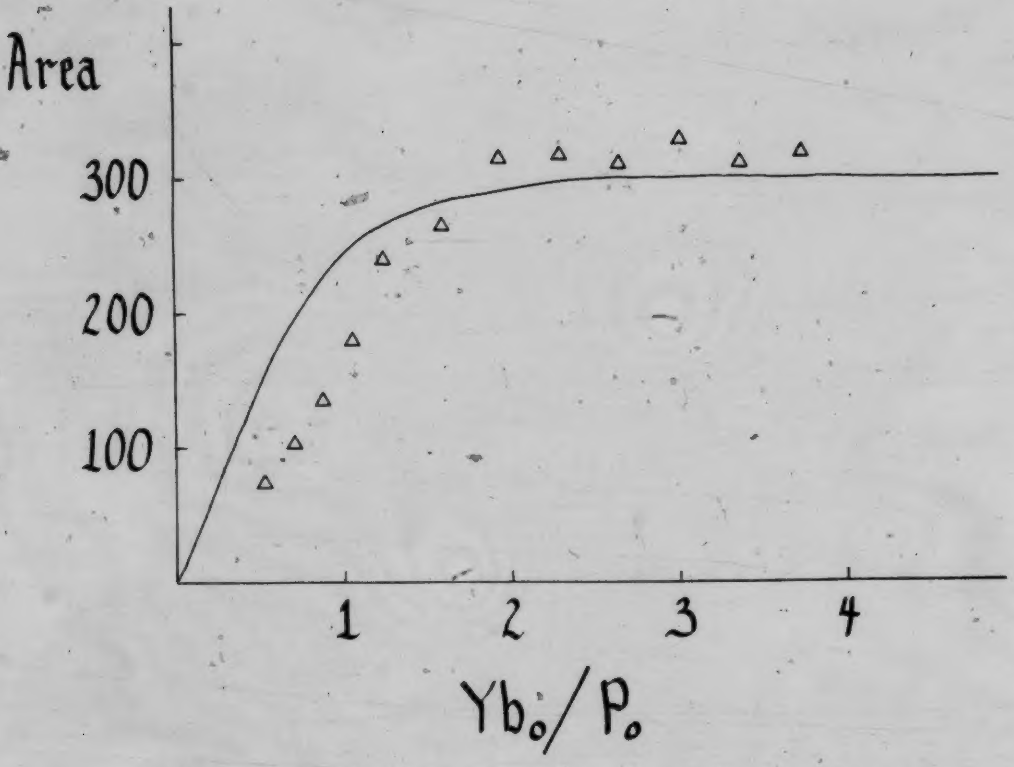

Figure 28. The area of a representative peak as a function of (Yb^{3+}/P) ratio in the Yb^{3+} titration of apo parvalbumin. The open triangles indicate the area of the resonance in the Yb^{3+} titration of apo parvalbumin which corresponds to the resonance in the Yb^{3+} titration of the Ca^{2+} saturated parvalbumin at 29.80 ppm (see resonances indicated by a filled triangle in Figures 25 and 27). The solid line is the fit from Figure 27 to the area of this resonance in the Yb^{3+} titration of Ca^{2+} saturated parvalbumin as a function of the (Yb^{3+}/P) ratio. The concentration of apo parvalbumin was 0.85 mM; all other conditions were identical to those listed in Figure 25.

Table 6

Yb^{3+} Titration of Apo Parvalbumin

Yb^{3+}/P[1]	Area[2]
0.173	ND[3]
0.349	ND
0.523	74.8
0.698	103.6
0.874	134.5
1.051	179.7
1.226	239.8
1.579	265.0
1.932	315.9
2.287	317.2
2.643	310.7
2.999	328.2
3.364	311.8
3.727	318.3

[1] total ytterbium to total protein ratio.

[2] The area of the resonance with an observed chemical shift position of 29.80 ppm was calculated as the product of the half height linewidth times the maximum line intensity.

1/1 for the Ca^{2+} saturated titration.

D. Discussion

The strategy for the complete analysis of the lanthanide induced ^1H NMR chemical shifts of the ytterbium parvalbumin complex in order to determine the structure of the EF metal binding site of carp parvalbumin in solution (Lee & Sykes, 1980a,b,c,d) is outlined in Chapter 2. In this Chapter, I shall focus on the stoichiometry of the binding of ytterbium to parvalbumin. The ^1H NMR studies described herein have enabled me to observe the sequential filling of the two metal binding sites by ytterbium, to characterize the proximity of the shifted resonances to the two metal binding sites, to measure their relative areas, and to determine the relative affinities of the two metal binding sites of parvalbumin for ytterbium. These studies do not however, indicate which metal binding site of parvalbumin is filled first. Three studies do demonstrate that lanthanides preferentially bind to the EF site of calcium saturated parvalbumin. These studies include the X-ray analysis (Sowadski *et al.*, 1978) and optical studies (Donato & Martin, 1974; Horrocks & Sudnick, 1979) on the partially terbium substituted protein. The X-ray crystallographic structure of parvalbumin indicates that the protein contains two metal binding sites. The CD site is surrounded by six protein ligands and is solvent inaccessible, whereas the EF site is surrounded by five protein ligands and one water molecule. Terbium fluorescence of the partially substituted protein (Donato & Martin, 1974; Nelson *et al.*, 1977) is observed upon irradiation at 259 nm. Phe 57 which is the nearest aromatic ring to either Ca^{2+} ion is closer to the EF site. Thus energy transfer is believed to occur between Phe 57 and the Tb^{3+} bound in the EF site of parvalbumin. The laser induced fluorescent decay constants of europium (Eu^{3+}) and terbium (Tb^{3+}) substituted parvalbumin (Horrocks & Sudnick, 1979) indicate that there is only one water molecule bound to the lanthanide at low lanthanide to protein ratios. This evidence also supports the hypothesis that the EF site which contains one water molecule in the first coordination sphere of the metal (Kretsinger & Nockolds, 1973) is the site of initial lanthanide replacement. X-ray crystallographic studies of the parvalbumin (Moews & Kretsinger, 1975b; Sowadski *et al.*, 1978) indicate that the isomorphous replacement of Ca^{2+} by Tb^{3+} in parvalbumin at low Tb^{3+}/P ratios results in the increase of electron density at the EF site; additional increase of electron density at the CD site is only observed upon subsequent increases in the Tb^{3+}/P ratios. Replacement of both Ca^{2+} ions is observed; however, the EF site is initially occupied. Other studies such as the ^{113}Cd NMR investigation of parvalbumin (Drakenberg *et al.*, 1978) also suggest that the lanthanide Gd^{3+} replaces the Cd^{2+} ions bound to the EF site first, before the Cd^{2+} ions in the CD site. By analogy to these reports, I conclude that the Ca^{2+}

bound in the EF site of parvalbumin is initially replaced by ytterbium.

When the Ca^{2+} saturated protein was titrated with Yb^{3+}, the sequential appearance and disappearance of sets of shifted peaks were observed. Up to a total metal to total protein ratio of 1/1, one set of resonances, such as the resonance labelled with a filled triangle, is observed; these resonances correspond to nuclei in the vicinity of the first site filled, the EF site. At higher ratios, some of the first set of peaks such as the peak labelled with a (■) disappear (shift elsewhere) and were replaced by a new set of peaks; these resonances correspond to nuclei in the vicinity of both the EF and CD sites of parvalbumin. In addition, some peaks appeared only after binding of the first metal (see resonance labelled with a (•)); these resonances correspond to nuclei either in the vicinity of the CD site only or in the vicinity of both sites. These results allow for the determination of the approximate proximity of each resonance to each of the two metal binding sites.

By measuring the areas of the shifted resonances, obtained as part of the fitting procedure, I am able to discriminate single protons from methyl groups. For example the resonances labelled with a circle (•) and a square (■) (Figure 25) have calculated areas of 983 ± 57 and 804 ± 24 respectively; the calculated area of the resonance labelled with a filled triangle is 304 ± 13. These data indicate that the latter resonance corresponds to a single proton, whereas the former resonances correspond to methyl groups. These two methyl groups, as well as four other shifted methyl groups, are used extensively in the fitting procedure which relates the observed chemical shifts to the three dimensional structure of the metal binding site (Lee & Sykes, 1980a,b,c,d).

The metal binding properties of parvalbumin have previously been investigated by numerous methods. Parvalbumin contains two high affinity metal binding sites for which both Ca^{2+} and Mg^{2+} compete. In the presence of millimolar concentrations of Mg^{2+}, the dissociation constant of calcium for parvalbumin is 1×10^{-7} M (Benzonana *et al.*, 1972). In the absence of Mg^{2+}, the dissociation constant decreases to 4×10^{-9} M (Potter *et al.*, 1977a). Tables 7 to 10 lists previously published dissociation constants for a variety of parvalbumins.

Evidence to support both the cooperative and non-cooperative binding of Ca^{2+} to parvalbumin has been reported. Cooperative binding was first suggested (Benzonana *et al.*, 1972) by the observation of a small curvature in Scatchard plots of ^{45}Ca binding to calcium free parvalbumins. The NMR observation that the spectrum of the protein with 1 Ca^{2+} bound contains features of the spectra from both the apo protein and the fully calcium bound protein (Parello *et al.*, 1974; Cave *et al.*, 1979b) further supports cooperative binding. However, the selective removal

Table 7

The Calcium Dissociation Constants of Parvalbumin I

Parvalbumin (pI)	Lineage[1]	K_D[2]	K_D[3]
hake[5] (4.36)	beta	1.0×10^{-7}	ND[4]
frog[5] (4.88)	alpha	1.0×10^{-7}	ND
frog[5] (4.50)	beta	1.0×10^{-7}	ND
carp[6] (4.25)	beta	ND	4.0×10^{-9}
carp[7] (4.25)	beta	1.3×10^{-7}	ND
rabbit[8] (ND)	alpha	$<10^{-6}$	ND
rabbit[9] (ND)	ND	4.0×10^{-7}	1.0×10^{-9}

[1] The parvalbumins have been separated into the alpha and beta lineages (Goodman & Pechere, 1977).

[2] All dissociation constants listed are in units of M. All data listed indicate equivalent dissociation constants for the two binding sites, except where two individual constants are entered. This column lists previously published calcium dissociation constants measured in the presence of millimolar concentrations of Mg^{2+}.

[3] This column lists previously published calcium dissociation constants measured in the absence of Mg^{2+}.

[4] ND indicates that the data is not determined or not defined.

[5] Conditions: 30 mM imidazole, 60 mM KCl, 2 mM Mg^{2+}, 1 mM EGTA, ph 6.7. Method: ^{45}Ca-Chelex partition. (Benzonana *et al.*, 1972).

[6] Conditions: 20 mM imidazole, 0.1 M KCl, 0.1 mM EDTA, ph 7.5. Method: equilibrium dialysis. (Potter *et al.*, 1977a).

[7] Conditions: 20 mM imidazole, 0.1 M KCl, 0.1 mM EDTA, 3 mM Mg^{2+}, pH 7.0. Method: equilibrium dialysis. (Potter *et al.*, 1977a).

[8] Conditions: 50 mM imidazole, 4°C, pH 6.7. Method: equilibrium dialysis. (Cox *et al.*, 1977).

[9] Conditions: 25 mM tricine, 80 mM KCl, 1 mM EDTA or EGTA, pH 7.4. Method: equilibrium dialysis. (Cox *et al.*, 1977).

Table 8

The Calcium Dissociation Constants of Parvalbumin II

Parvalbumin (pI)	Lineage[1]	K_D[2]	K_D[3]
whiting[5] (ND[4])	beta	ND	1.4×10^{-6}
			5.0×10^{-7}
rabbit[6] (5.55)	alpha	ND	6.6×10^{-9}
frog[6] (4.88)	alpha	ND	7.8×10^{-9}
frog[6] (4.50)	beta	ND	2.2×10^{-9}
hake[7] (4.36)	beta	ND	$3\text{-}5 \times 10^{-9}$
			$>17 \times 10^{-9}$
chicken[8] (ND)	ND	ND	$\leq 10^{-6}$

[1] The parvalbumins have been separated into the alpha and beta lineages (Goodman & Pechere, 1977).

[2] All dissociation constants listed are in units of M. All data listed indicate equivalent dissociation constants for the two binding sites, except where two individual constants are entered. This column lists previously published calcium dissociation constants measured in the presence of millimolar concentrations of Mg^{2+}.

[3] This column lists previously published calcium dissociation constants measured in the absence of Mg^{2+}.

[4] ND indicates that the data is not determined or not defined.

[5] Conditions: 50 mM tris, 100 mM KCl, 20°C, pH 8.0. Method: fluorescence. (White & Closset, 1979).

[6] Conditions: pH 7.55. Method: UV difference spectroscopy. (Haiech *et al*., 1979b).

[7] Conditions: 0.1 M Hepes, 0.1 M KCl, pH 6.8-8.0. Method: UV difference spectroscopy. (Haiech *et al*., 1979b).

[8] Conditions: 50 mM imidazole, 4°C, pH 6.7. Method: equilibrium dialysis. (Heizmann & Strehler, 1979).

Table 9

The Magnesium Dissociation Constants of Parvalbumin

Parvalbumin (pI)	Lineage[1]	K_D[2]
carp[3] (4.25)	beta	9.1×10^{-5}
rabbit[4] (ND)	alpha	4.3×10^{-6}
carp[5] (4.25)	beta	6.7×10^{-5}
rabbit[6] (5.55)	alpha	1.6×10^{-5}
frog[6] (4.88)	alpha	2.1×10^{-5}
frog[6] (4.50)	beta	2.7×10^{-5}
hake[7] (4.36)	beta	3.0×10^{-5}

[1] The parvalbumins have been separated into the alpha and beta lineages (Goodman & Pechere, 1977).

[2] All dissociation constants listed are in units of M. All data listed indicate equivalent dissociation constants for the two binding sites, except where two individual constants are entered. This column lists previously published magnesium dissociation constants.

[3] Conditions: 20 mM imidazole, 0.1 M KCl, 0.1 mM EDTA, pH 7.5. Method: equilibrium dialysis. (Potter *et al.*, 1977a).

[4] Conditions: 25 mM tricine, 80 mM KCl, 1 mM EDTA (or EGTA), pH 7.4. Method: equilibrium dialysis. (Cox *et al.*, 1977).

[5] Conditions: not defined. Method: not defined. (Potter *et al.*, 1978).

[6] Conditions: pH 7.55. Method: UV difference spectroscopy. (Haiech *et al.*, 1979b).

[7] Conditions: 0.1 M Hepes, 0.1 M KCl, pH 6.8-8.0. Method: UV difference spectroscopy. (Haiech *et al.*, 1979b).

Table 10

Additional Dissociation Constants of Parvalbumin

Parvalbumin (pI)	Lineage[1]	$K_{[D]}$[2]
carp[3] (4.25)	beta	$K_{Gd}/K_{Cd} = 1/8$
carp[4] (4.25)	beta	$K_{Tb}^{CD} = 6.3 \times 10^{-7}$ (6)
carp[4] (4.25)	beta	$K_{Tb}^{EF} = 1.6 \times 10^{-7}$ (6)
carp[5] (4.25)	beta	$K_{Gd} = 5.0 \times 10^{-11}$
carp[5] (4.25)	beta	$K_{Mn} = 6.0 \times 10^{-4}$

---

[1] The parvalbumins have been separated into the alpha and beta lineages (Goodman & Pechere, 1977).

[2] All dissociation constants listed are in units of M. This column lists previously published metal dissociaton constants.

[3] Conditions: not defined. Method: ^{113}Cd NMR. (Drakenberg *et al*., 1978). The dissociation constant ratio (K_{Gd}/K_{Cd}) for the EF site is 1/8 times the ratio for the CD site.

[4] Conditions: 0.1 M KCl - piperazine, pH 6.5. Method: fluorescence spectroscopy. (Sowadski *et al*., 1978).

[5] Conditions: 50 mM cacodylate, 25°C, pH 6.0. Method: proton relaxation enhancement. (Cave *et al*., 1979c).

[6] A dissociation constant of 2×10^{-7} M (Benzonana *et al*., 1972) was assumed by Sowadski *et al*., (1978). However, this constant refers to the case where Mg^{2+} is present. Data in this table suggest that there is a decrease by two orders of magnitude in the dissociation constant when Mg^{2+} is present. Since no Mg^{2+} was apparently present during their experiments, the published data of Sowadski *et al*., (1978) should be corrected by a factor of approximately 10^{-2}.

of one calcium from calcium saturated parvalbumin (Donato & Martin, 1974) is inconsistent with strong positive cooperativity.

In the titration of the calcium saturated form of parvalbumin with Yb^{3+}, I am unable to address the question of cooperativity. Under the conditions of high metal and protein concentrations, there will never be any of the apo or partially apo species present. Therefore, I can only determine the relative affinities of each of the two metal binding sites for ytterbium with respect to Ca^{2+}.

Haiech and co-workers (Haiech *et al.*, 1979b) have demonstrated that the CD and EF sites have different affinities for calcium. The two dissociation constants of hake parvalbumin are $(3-5) \times 10^{-9}$ M and $(17-60) \times 10^{-9}$ M. I assume these same values for the homologous protein carp parvalbumin, another member of the beta lineage of parvalbumin (Goodman & Pechere, 1977). EGTA will remove one Ca^{2+} preferentially from carp parvalbumin (Nelson *et al.*, 1977). If the calcium has the higher affinity for the CD site (Donato & Martin, 1974), then the calculated ytterbium dissociation constants (using the determined values of $K^{CD} = 0.13$, $K^{EF} = 0.01$) are: $K^{CD}_{Yb^{3+}} = (4-7) \times 10^{-10}$ M and $K^{EF}_{Yb^{3+}} = (2-6) \times 10^{-10}$ M. This indicates that the sequential Yb^{3+} replacement of the two Ca^{2+} ions from Ca^{2+} saturated parvalbumin is controlled by the Ca^{2+} affinities and implies that the binding of Yb^{3+} to the two sites of parvalbumin, starting from the apo form, will be approximately equal.

This is supported by the data for the resonance at 29.80 ppm in Figure 28. As shown above, this resonance is near to the EF site, but is unaffected by metals in the CD site. Its area is thus a measure of the sum of the concentrations of species CY + YY in the Ca^{2+} saturated titration, or OY + YY in the apo titration. In the apo titration, the area of this resonance increases linearly up to a Yb^{3+}/P ratio of approximately 2-3 (Figure 28). This is consistent with equal affinities of the CD and EF sites for Yb^{3+} in the absence of Ca^{2+}.

The high affinities of the CD and EF site of parvalbumin for Yb^{3+} ($K \approx 5 \times 10^{-10}$ M) is consistent with previously published results for Tb^{3+} and Gd^{3+}. Sowadski and co-workers (Sowadski *et al.*, 1978) calculate Tb^{3+} affinities of $K^{CD}_{Tb^{3+}} = 6.3 \times 10^{-7}$ and $K^{EF}_{Tb^{3+}} = 1.6 \times 10^{-9}$ M from the fluorescence data of Nelson *et al.* (1977) using the same model described herein. They assumed, however, Ca^{2+} dissociation constants from Benzonana *et al.*, (1972) of 2×10^{-7} which were determined in the presence of 2 mM Mg^{2+}. Since the data of Nelson *et al.* (1977) were measured in the absence of Mg^{2+}, the calculated constants of Sowadski *et al.*, (1978) are more accurately calculated as $K^{CD}_{Tb^{3+}} \simeq 6 \times 10^{-9}$, $K^{EF}_{Tb^{3+}} \simeq 2 \times 10^{-11}$ M. These numbers bracket the observed constants for Yb^{3+}. Cave *et al.*, (1979c), using proton relaxation enhancement techniques, calculate equal dissociation constants of the CD and EF sites for Gd^{3+} of 5×10^{-11} M, which are approximately one order of magnitude less than the value for Yb^{3+}. They determine, however, as in this study, the relative dissociation constants for Gd^{3+} with respect to Ca^{2+}, which they measure as 0.05 - 0.005 for both sites. They are unable to distinguish between the two sites, and choose an approximate Ca^{2+} dissociation constant of 10^{-9} M.

The interpretation of fluorescence measurements using terbium bound parvalbumin suggests the existence of a third metal binding site in parvalbumin (Nelson *et al.*, 1977); however, X-ray crystallographic studies (Sowadski *et al.*, 1978) indicate the absence of such a third site. The discrepancy may be due to differences between the solution and solid state protein structure. The NMR methods presented herein are extremely sensitive to metal binding, because unique resonances are observed corresponding to each of the metals bound to the protein. The results indicate that up to a total metal to total protein ratio of 4.5, no shifted resonances due to binding at a third site are observed. Shifting and broadening of resonances in the fast exchange limit is possible for weakly bound metals, but under the conditions of the titration, no such effects were observed. A third metal binding site may exist near the EF site, but it apparently only binds metal such as Mn^{2+} or Mg^{2+} (Cave *et al.*, 1979c, 1979a). There are only two specific metal binding sites in parvalbumin to which the lanthanide ytterbium will bind; these two sites are the EF and CD binding sites.

In conclusion, I have shown that the ytterbium induced shifted resonances of carp parvalbumin are sensitive monitors of the specific metal binding sites on the protein in solution. I have used these resonances to determine the lanthanide binding affinities for each of the two sites in the presence and absence of Ca^{2+} The data indicate that the sequential Yb^{3+} replacement of the CD and EF Ca^{2+} ions of parvalbumin (EF displaced first) is the result of differences in Ca^{2+} affinities between the two sites rather than differences in Yb^{3+} affinities.

V. The Analysis of the Linebroadening

A. Introduction

In the previous chapter, I described how the lanthanide induced shifted resonances of ytterbium substituted parvalbumin can be used to monitor the binding of the metal to the protein. At low total Yb^{3+} to total protein ratios, the substitution of Yb^{3+} for the calcium ion bound in the EF binding site of carp parvalbumin results in a series of shifted resonances far outside the envelope of the ^{1}H NMR spectrum of the diamagnetic form of the protein. In this chapter, the linebroadening is discussed; the linewidths of the shifted resonances have been measured at 200, 270, 400, and 600 MHz, as well as the spin lattice relaxation rates at 270 MHz. The analysis of the relaxation rates and the frequency dependence of the linebroadening based upon the theories of Vega and Fiat (Vega & Fiat, 1976) and Gueron (Gueron,1975) indicate that the susceptibility relaxation mechanism constitutes a major contribution to the linewidths; the metal to proton distances are then directly calculated from this contribution.

B. Theory

When a paramagnetic trivalent lanthanide ion (excluding the isotropic Gd^{3+}) is added to a protein metal binding site, it will cause shifting and broadening of the NMR resonances of nearby nuclei.

Therefore a given nucleus I in the protein and near the lanthanide ion will experience relaxation from two sources: from other nearby nuclei and from the paramagnetic metal.

The relaxation caused by nearby nuclei is in the form of dipole dipole (DD) interactions.

Dipole Dipole Interactions with Nearby Nuclei Equations 5.1 and 5.2 are the expressions for the spin lattice and spin spin relaxation rates for like nuclei with nuclear spin quantum number I of 1/2 (Abragam, 1961).

$$\frac{1}{T1_{DD}} = \frac{3\gamma_I^4 \hbar^2}{10} \sum\left(\frac{1}{d^6}\right)\left\{\frac{\tau_R}{1+\omega_I^2\tau_R^2} + \frac{4\tau_R}{1+4\omega_I^2\tau_R^2}\right\} \qquad (5.1)$$

$$\frac{1}{T2_{DD}} = \frac{3\gamma_I^4 \hbar^2}{20} \sum\left(\frac{1}{d^6}\right)\left\{3\tau_R + \frac{5\tau_R}{1+\omega_I^2\tau_R^2} + \frac{2\tau_R}{1+4\omega_I^2\tau_R^2}\right\} \qquad (5.2)$$

where γ_I is the gyromagnetic ratio of nucleus I, τ_R is the rotational correlation time of the metal protein complex, ω_I is the resonance frequency of nucleus I, and $\sum(1/d^6)$ represents the weighted summed distance between the proton under observation and nearby protons.

The nuclear relaxation caused by the unpaired 4f electrons of the metal consists of three contributions: scalar (or contact) interactions, dipolar interactions, and the susceptibility mechanism.

Scalar Interactions The first contribution, the scalar (or contact) interaction, is large for nuclei directly bonded to the metal such as ^{13}C and ^{17}O, since it results from electron density at the nucleus under observation (Bloembergen, 1957a; 1957b). This 'through bonds' effect is transmitted through the electrons of chemical bonds. However in this discussion, the contact contribution will be neglected for the following reasons: 1) the 4f electrons are inner core electrons and are not highly delocalized (when compared to the transition metal valence 3d electrons) resulting in small effects, 2) all the protons under consideration are several bonds removed from the metal, 3) of all the lanthanides, ytterbium which is used in this study, contributes the smallest contact interaction (Reuben, 1973b), 4) the ratio of pseudocontact to contact shift is smallest for Yb^{3+} (Reuben, 1973b).

Dipole Dipole Interactions with the Lanthanide Ion

Equations 5.3 and 5.4 indicate the expressions for the spin lattice and spin spin relaxation rates of nuclei being relaxed by the second contribution, dipolar interactions (Solomon, 1955).

$$\frac{1}{T1_S} = \frac{2}{15}\frac{\gamma_I^2 g_L^2 \beta^2 J(J+1)}{r^6}\left\{\frac{3\tau_S}{1+\omega_I^2\tau_S^2} + \frac{7\tau_S}{1+\omega_S^2\tau_C^2}\right\} \qquad (5.3)$$

$$\frac{1}{T2_S} = \frac{1}{15}\frac{\gamma_I^2 g_L^2 \beta^2 J(J+1)}{r^6}\left\{4\tau_S + \frac{3\tau_S}{1+\omega_I^2\tau_S^2} + \frac{13\tau_S}{1+\omega_S^2\tau_S^2}\right\} \qquad (5.4)$$

where τ_{S} is the electron correlation time, ω_{S} is the electron spin frequency (= 657 ω_{I}), β is the Bohr magneton for the electron, and r is the metal to proton distance. To compensate for the use of lanthanides in this study, two changes to the original expressions have been made: the electronic g factor has been replaced by the Lande g factor, and the spin quantum number S has been replaced by the total angular quantum number J[4]. Numerical values for these constants are listed in Table 11. These expressions assume that the transverse and longitudinal electron relaxation times are both equal to τ_{S}, and that τ_{S} is much less than τ_{R}. The following data indicates these assumptions are valid: for Yb^{3+}, τ_{S} is equal to 2.2×10^{-13} s (Lenkinski & Reuben, 1976); for parvalbumin τ_{R} is equal to 12×10^{-9} s (Nelson *et al.*, 1976).

Susceptibility Relaxation The novel element not considered in previous discussions of nuclear spin relaxation caused by paramagnetic metals such as Mn^{2+} and Gd^{3+} is that the time average of the dipolar interaction (on the timescale $\tau_{S} < t < \tau_{R}$) is not zero, but results in an electron spin moment $\underset{\sim}{\mu}$ at the metal. The magnetic moment

---

[4] For the lanthanide 4f electrons, the crystal field effects are relatively small so that the L and S angular momenta are coupled to form total angular momentum J states. The appropriate Hamiltonian (Bleaney, 1972) is:

$$\mathcal{H} = g_L \beta (H \cdot J) + \sum_{k,q} A_k^q \langle r^k \rangle \langle J \| k \| J \rangle O_k^q \qquad (5.5)$$

Table 11

Magnetic Properties of the Rare Earths[1]

Ion	Electron Configuration[2]	S[3]	L[4]	J[5]	Term Symbol[6]	g┌L┐[7]
La	$4f^{0}5s^{2}5p^{6}$	0	0	0	^{1}S┌0┐	0
Ce	$4f^{1}5s^{2}5p^{6}$	1/2	3	5/2	^{2}F┌5/2┐	6/7
Pr	$4f^{2}5s^{2}5p^{6}$	1	5	4	^{3}H┌4┐	4/5
Nd	$4f^{3}5s^{2}5p^{6}$	3/2	6	9/2	^{4}I┌9/2┐	8/11
Pm	$4f^{4}5s^{2}5p^{6}$	2	6	4	^{5}I┌4┐	3/5
Sm	$4f^{5}5s^{2}5p^{6}$	5/2	5	5/2	^{6}H┌5/2┐	2/7
Eu	$4f^{6}5s^{2}5p^{6}$	3	3	0	^{7}F┌0┐	0
Gd	$4f^{7}5s^{2}5p^{6}$	7/2	0	7/2	^{8}S┌7/2┐	2
Tb	$4f^{8}5s^{2}5p^{6}$	3	3	6	^{7}F┌6┐	3/2
Dy	$4f^{9}5s^{2}5p^{6}$	5/2	5	15/2	^{6}H┌15/2┐	4/3
Ho	$4f^{10}5s^{2}5p^{6}$	2	6	8	^{5}I┌8┐	5/4
Er	$4f^{11}5s^{2}5p^{6}$	3/2	6	15/2	^{4}I┌15/2┐	6/5
Tm	$4f^{12}5s^{2}5p^{6}$	1	5	6	^{3}H┌6┐	7/6
Yb	$4f^{13}5s^{2}5p^{6}$	1/2	3	7/2	^{2}F┌7/2┐	8/7
Lu	$4f^{14}5s^{2}5p^{6}$	0	0	0	^{1}S┌0┐	0

[1] (Van Vleck, 1932; Abragam & Bleaney, 1970).

[2] The configurations given refer to the relevant outer electrons of the tripositive ions.

[3] Spin angular momentum quantum number.

[4] Orbit angular momentum quantum number.

[5] Total angular momentum quantum number.

[6] The Russell-Saunders nomenclature of term symbols indicates the ground term. The values of J are given within parentheses.

[7] The Lande g┌L┐ factor.

is given by:

$$\underset{\sim}{\mu} = \underset{\approx}{\chi}\,\underset{\sim}{H} \qquad (5.6)$$

where $\underset{\approx}{\chi}$ is the susceptibility and $\underset{\sim}{H}$ is the applied magnetic field. The dipolar interaction of the nuclear spin with this moment is modulated, not by electron spin relaxation, but by molecular rotational tumbling. This interaction results in the *susceptibility* (Vega & Fiat, 1976) or the *Curie spin* (Gueron, 1975) contributions to the nuclear relaxation. Expressed in a power series of T^{-1}, the susceptibility has as its first term (Bleaney, 1972):

$$\bar{\chi} = \frac{g_L^2 \beta^2 J(J+1)}{3kT} \qquad (5.7)$$

Since this term is isotropic, resulting in the interactions averaging to zero, the contributions to the spin lattice and spin spin relaxation rates are not dependent upon the angular orientation of the nucleus relative to the metal (Vega & Fiat, 1976):

$$\frac{1}{T1_\chi} = \frac{6}{5}\,\frac{\omega_I^2 g_L^4 \beta^4 J^2 (J+1)^2}{r^6 (3kT)^2}\left|\frac{\tau_R}{1+\omega_I^2\tau_R^2}\right| \qquad (5.8)$$

$$\frac{1}{T2_\chi} = \frac{1}{5}\,\frac{\omega_I^2 g_L^4 \beta^4 J^2 (J+1)^2}{r^6 (3kT)^2}\left|4\tau_R + \frac{3\tau_R}{1+\omega_I^2\tau_R^2}\right| \qquad (5.9)$$

where k is the Boltzmann constant and T is the temperature in degrees Kelvin. However, if the interaction does not average to zero, a lanthanide pseudocontact shift is observed, the magnitude of which depends upon the angular orientation of the nucleus relative to the metal, and the lanthanide pseudocontact shift. The following correction term in the form of a multiplicative factor

$$1 - \frac{r^3 \delta}{\bar{\chi}} \tag{5.10}$$

can be applied to equations 5.8 and 5.9 (Vega & Fiat, 1976), where δ is the lanthanide induced shift of the observed resonance and $\bar{\chi}$ is the trace of the susceptibility tensor.

C. Experimental Procedures

Sample Preparation The NMR samples were prepared according to the procedures outlined in Chapter 3. Again the pH of the sample was checked to confirm that the addition of Yb^{3+} did not affect the resulting pH. In addition, spin lattice relaxation times were measured with the standard $T - \pi - \tau - \pi/2$ - acquisition pulse sequence with $T > 5T1$ and a variable time delay of τ.

Spin spin relaxation rates were measured from the half height widths ($\Delta\nu$) of the observed shifted resonances with $1/T2 = \pi\Delta\nu$. These rates were corrected by subtracting the linebroadening used during Fourier transformation. No correction was attempted to account for possible multiplet structure of some of the resonances from unresolved spin-spin coupling. The observed linebroadening is much greater than the possible coupling constants so that all non-overlapping shifted resonances appeared completely Lorentzian and any necessary corrections would be small.

Spin lattice relaxation rates (1/T1) were determined using the non-linear least squares fit of the data to the following equation:

$$M_z = M_o\left[1-\left(1-\cos\alpha\right)e^{-t/T1}\right] \tag{5.11}$$

with the equilibrium magnetization M_{o}, the flip angle alpha, and the spin lattice time T1 as parameters. The value of alpha was uniform across the spectrum.

NMR data acquisition at 600 MHz Experiments at 600 MHz were performed to verify the field dependence of the linewidths of shifted resonances. Corrections to the observed linewidths were necessary, because the ambient temperature of the probe was 293°K, and variable temperature work was not easily possible (see Discussion).

D. Results

The substitution of Yb^{3+} for one or both of the calcium ions of parvalbumin results in a series of shifted resonances to appear in the ^1H NMR spectrum far outside of the calcium form of the protein as illustrated in Figure 29

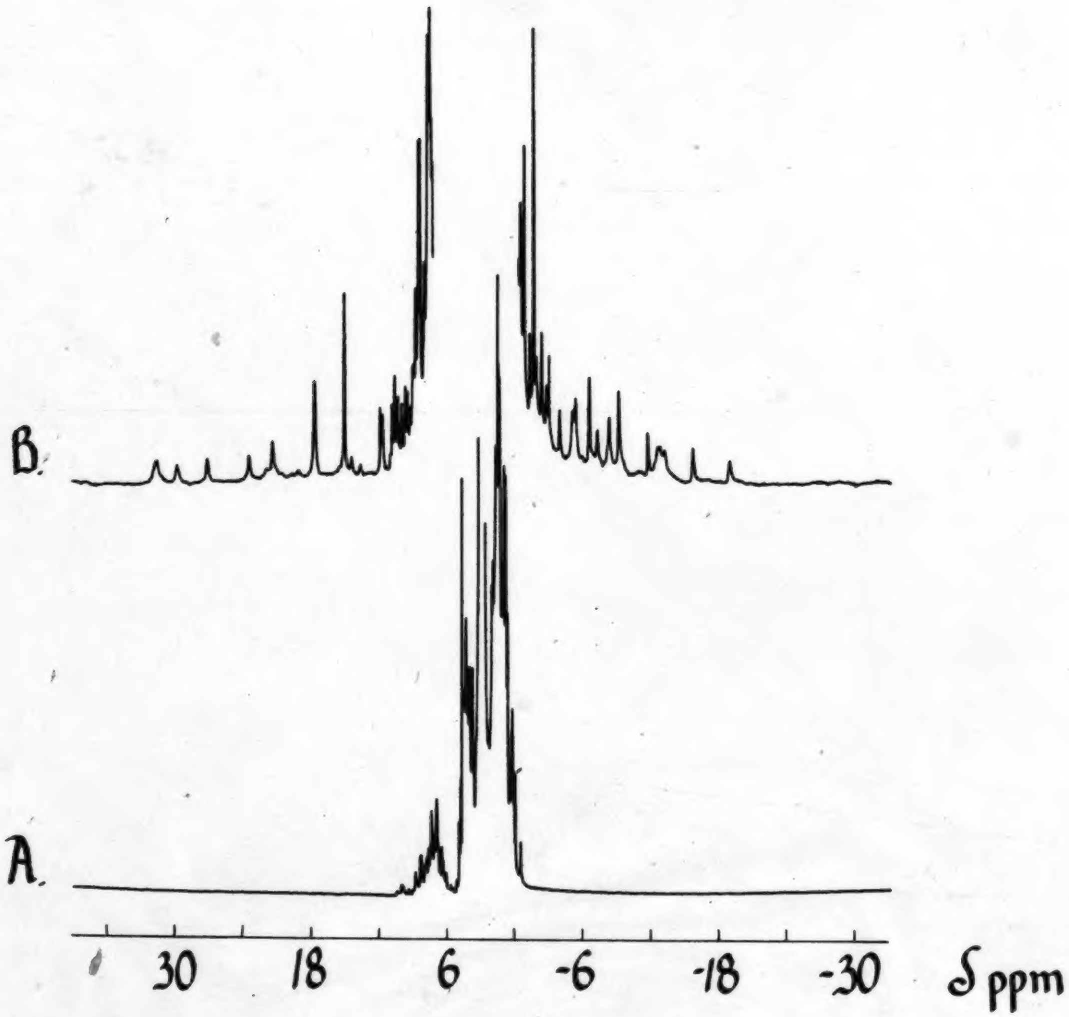

Figure 29. The 270 MHz ^{1}H NMR spectrum of carp parvalbumin in the presence of calcium and in the presence of ytterbium. A. 0.68 mM calcium saturated carp parvalbumin in 15 mM Pipes, 0.15 M KCl, 0.5 mM DSS, 10 mM DTT in D2O, pH=6.65, temperature= 302°K.
B. 0.64 mM carp parvalbumin in 15 mM Pipes, 0.15 M KCl, 0.5 mM DSS, 10 mM DTT, in D2O, pH=6.6, temperature=302°K, at a total Yb^{3+} to total protein ratio of 0.80. The vertical scale for Figure B is 8 times that of Figure A.

(Chapter 4; Lee & Sykes, 1980a,b). As discussed in Chapter 4, Figure 29B represents the spectrum of the parvalbumin Yb^{3+} complex in which Yb^{3+} is bound in the EF site. The shifted resonances are shown in expansion in Figures 30 and 31 with the nomenclature which is used throughout this thesis. Because the shifted peaks all move differently as a function of temperature, overlapping peaks can be resolved. Only those resonances which appear as single resolved resonances at 302°K are discussed in this Chapter.

The corrected linewidths of the resonances at three ^1H NMR frequencies, 200, 270, and 400 MHz, are listed in Table 12. A typical plot of the observed spin spin relaxation rates (1/T2) of the resonances numbered 5 and 8 at 23.57 and 15.17 ppm, respectively, as a function of ω_I^2, the square of the resonance frequency in units of radians s^{-1} is presented in Figure 32. The subsequent separation of the linewidths into two contributions, one field independent ($1/T2_{DD}$) and one field dependent ($1/T2_X$), evaluated at 270 MHz, is presented in Table 13. Also tabulated in Table 13 are the calculated metal to proton distances for each peak with estimated error limits (see Discussion). Metal to proton distances of selected downfield shifted resonances are shown in Figure 33. The observed T1's at 270 MHz for each peak are listed in Table 14 along with an estimated $T1_S$ corrected for the diamagnetic contribution to the spin lattice relaxation (see Discussion), and the ratio of the estimated $T1_S$ to the measured $T2_X$. Experiments performed

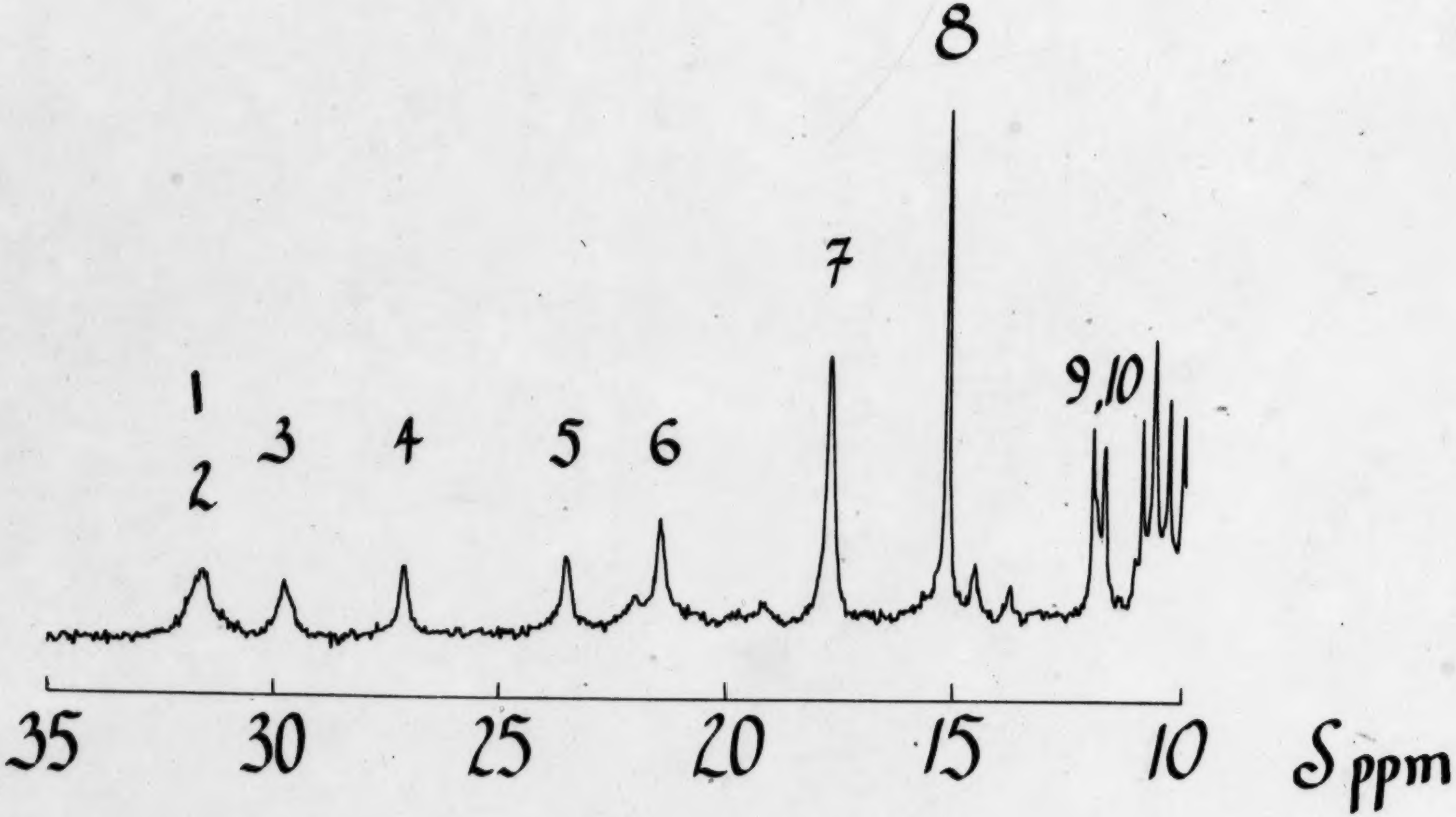

Figure 30. The downfield region of the 270 MHz ^{1}H NMR spectrum of ytterbium substituted parvalbumin. Conditions are the same as indicated in the legend for Figure 29. Indicated is the peak nomenclature: the chemical shifts are measured relative to the principal resonance of DSS.

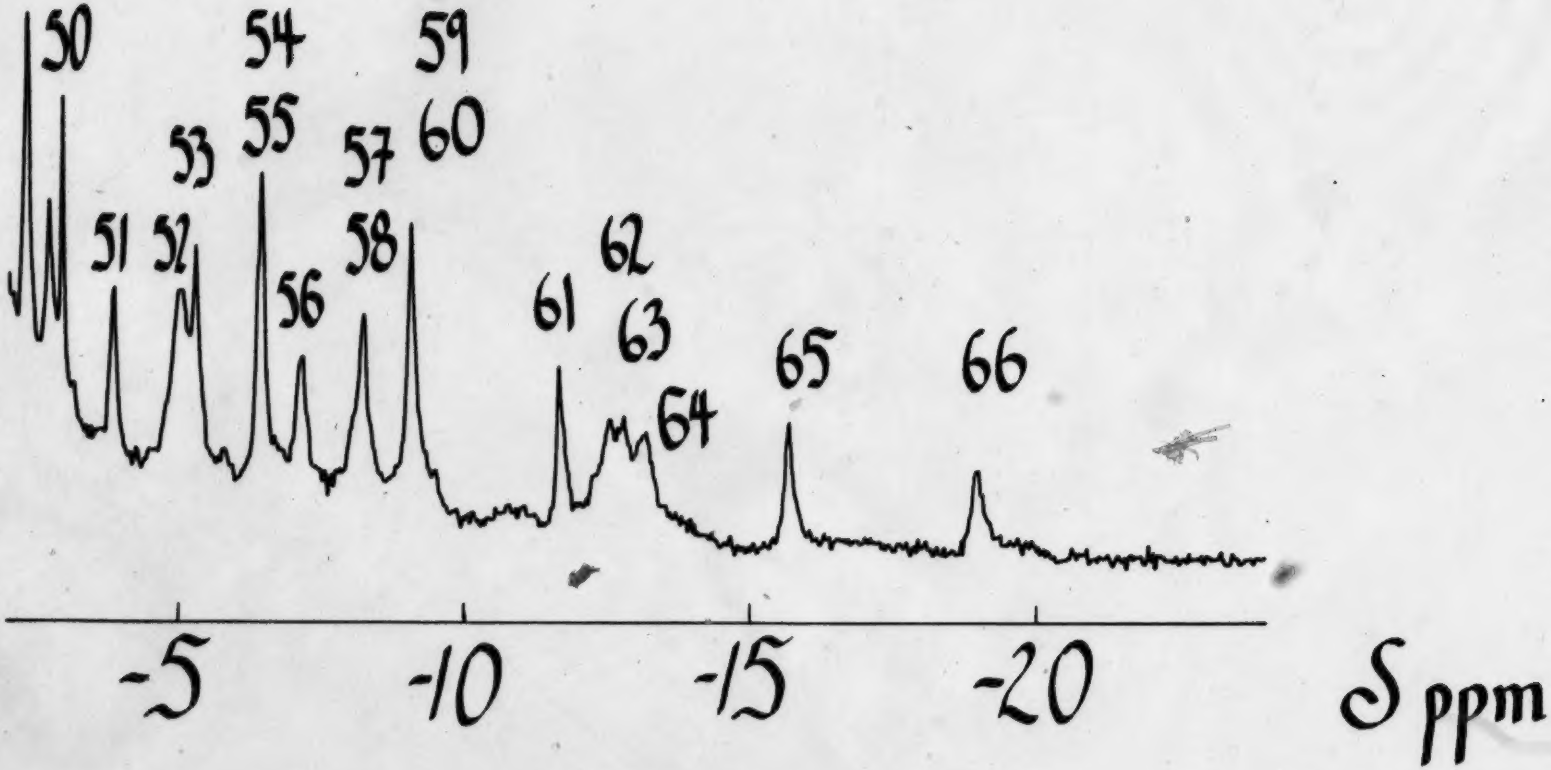

Figure 31. The upfield region of the 270 MHz ^{1}H NMR spectrum of ytterbium substituted parvalbumin. Conditions are the same as indicated in the legend for Figure 29. Indicated is the peak nomenclature; the chemical shifts are measured relative to the principal resonance of DSS.

Table 12

The Observed Spin Spin Relaxation Rates of the Ytterbium Shifted Parvalbumin Resonances as a Function of ^{1}H NMR Resonance Frequency

	Observed[1]	1/T2, s^{-1}		
Resonance[1]	Shift(ppm)	200 MHz	270 MHz	400 MHz
3	29.80	278	303	500
4	27.16	179	213	400
5	23.57	217	263	385
6	21.50	185	256	323
7	17.79	161	189	323
8	15.17	85	94	125
10	11.75	101	120	125
51	-3.84	114	103	152
56	-7.11	161	179	323
61	-11.63	127	137	200
65	-15.65	175	179	278
66	-18.90	170	213	455

[1] Nomenclature and chemical shift positions correspond to data
presented in Figures 30 and 31.

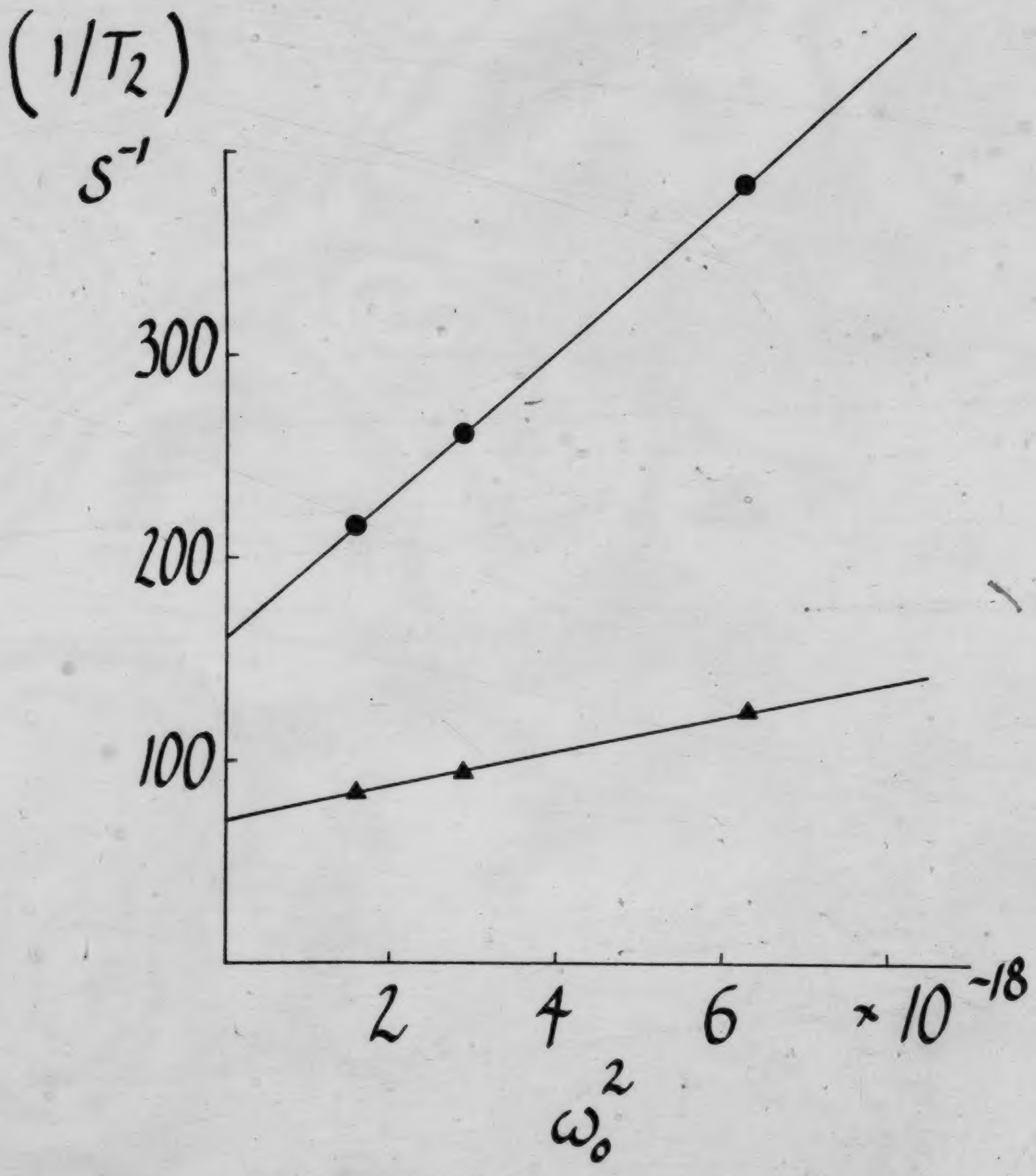

Figure 32. Plot of the observed spin spin relaxation rates (1/T2) versus the square of the resonance frequency $(\omega_{I})^2 = (\omega_{O})^2$ in units of radians s^{-1}. The filled circles indicate data observed for resonance 5 with an observed chemical shift of 23.57 ppm; the filled triangles (▲) indicate data observed for resonance 8 with an observed chemical shift of 15.17 ppm. Linewidths were measured at 200, 270, and 400 MHz.

Table 13

Relative Contributions of Various Mechanisms to Spin Spin Relaxation of Shifted ^{1}H NMR Resonances in Ytterbium Substituted Parvalbumin Determined from ^{1}H NMR Resonance Frequency Dependence of the Observed Linewidths

Resonance[1]	$1/T2_{DD}$[2]	$1/T2_{X}$[3]	r, Å[4]
3	184	141	5.8 -0.1/+0.1
4	91	139	5.9 -0.1/+0.1
5	161	102	6.2 -0.2/+0.2
6	157	78	6.5 -0.2/+0.3
7	98	101	6.2 -0.2/+0.2
8	71	24	7.9 -0.7/+1.8
10	100	12	8.8 -1.2/+1.4
51	90	26	7.7 -0.6/+1.5
56	93	102	6.2 -0.2/+0.2
61	97	46	7.0 -0.4/+0.6
65	127	67	6.6 -0.2/+0.3
66	56	179	5.6 -0.1/+0.1

[2] $1/T2_{DD}$, measured in s^{-1}, was determined by a linear least squares fit to the data presented in Table 12. These values are equal to the best fit y intercepts of plots such as Figure 53.

[3] $1/T2_{X}$, measured in s^{-1}, was determined by linear least squares methods. A best fit $1/T2_{OBS}$ was calculated. From this value, $1/T2_{DD}$ was subtracted to yield $1/T2_{X}$.

[4] r, the metal to proton distance was calculated using data in column 3 and equation 5.19 (see Discussion).

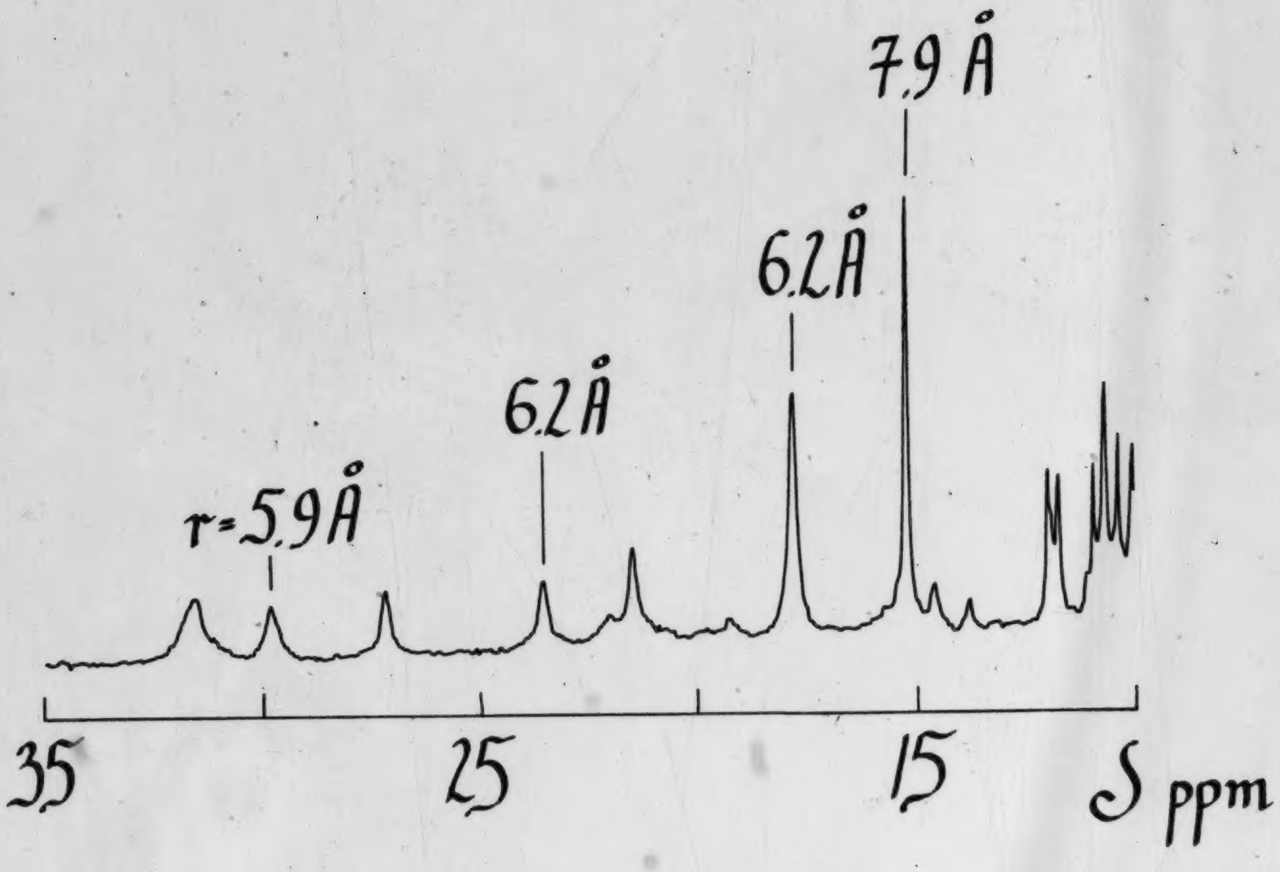

Figure 33. Representative metal to proton distances calculated from the field dependent contributions to the linewidths.

Table 14

Measured Spin Lattice Relaxation Times for Ytterbium Shifted ^{1}H NMR Resonances of Parvalbumin

Resonance[1]	T1[2]	$T1_{\ulcorner S\urcorner}$[3]	$1/T2_{\ulcorner X\urcorner}$	$T1_{\ulcorner S\urcorner}/T2_{\ulcorner X\urcorner}$
3	.032	.033-.035	141	4.7- 4.9
4	.054	.057-.063	139	7.9- 8.8
5	.046	.048-.052	102	4.9- 5.3
6	.043	.045-.048	78	3.5- 3.7
7	.046	.048-.052	101	4.8- 5.3
8	.145	.167-.233	24	4.0- 5.6
10	>0.3[4]		12	
51	.240	.306-.637	26	8.0-16.6
56	.138	.157-.215	102	16.0-21.9
61	.252	.326-.730	46	15.0-33.6
65	.164	.192-.286	67	12.9-19.2
66	.098	.108-.132	179	19.3-23.6

---

[1] nomenclature corresponds to data presented in Figures 30 and 31.

[2] These observed T1's (in s) were measured at 270 MHz by inversion recovery pulse sequences.

[3] $T1_{\ulcorner S\urcorner}$ indicates spin lattice relaxation times which are corrected for proton proton dipole dipole relaxation contributions. These contributions were observed to be in the range of 0.9 sec^{-1} for aromatic protons and 2.6 sec^{-1} for methylene protons, at 270 MHz.

[4] Delay time used in T1 measurement was not sufficient to accurately determine a long T1.

at 600 MHz confirm both the field dependence (Figure 34; Table 15) and the determination of the metal to proton distances (Table 16).

E. Discussion

The strategy for the complete analysis of the lanthanide induced ^{1}H NMR chemical shifts of the ytterbium parvalbumin complex in order to determine the three dimensional structure of the EF binding domain in solution is outlined in Chapter 2. As part of the overall approach, I shall present in this chapter, the analysis of the linewidths and spin lattice relaxation rates to determine metal to proton distances.

Lanthanide induced ^{1}H NMR shifts have been used previously to probe the structure of lysozyme (Campbell *et al.*, 1973a, 1973b, 1975a, 1975b; Agresti *et al.*, 1977) and the bovine pancreatic trypsin inhibitor (Marinetti *et al.*, 1975, 1976, 1977; Perkins & Wüthrich, 1978). Neither of these proteins have high affinity specific metal binding sites; In this application, parvalbumin has high affinity metal binding sites; this results in NMR spectra in the slow exchange limit (Figure 29B; Chapter 2). The advantage here is that chemical shifts and relaxation rates of the protein-paramagnetic ion complex may be accurately and directly determined. The main disadvantage is the assignment of resonances.

As detailed in chapter 4, Yb^{3+} sequentially replaces

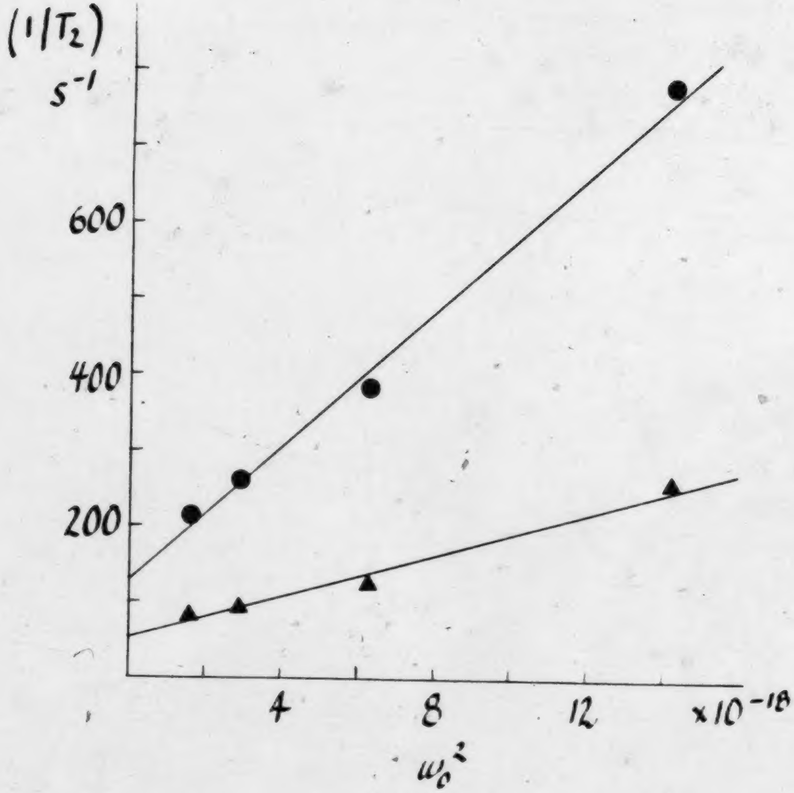

Figure 34. Plot of the observed spin spin relaxation rates (1/T2) versus the square of the resonance frequency $(\omega \ulcorner I \urcorner)^2 = (\omega \ulcorner O \urcorner)^2$, in units of radians s^{-1}. As shown similarly in Figure 32, the filled circles indicate data observed for resonance 5 with an observed chemical shift of 23.57 ppm; the filled triangles indicate data observed for resonance 8 with an observed chemical shift of 15.17 ppm. Linewidths were measured at 200, 270, 400, and 600 MHz.

Table 15

The Observed Spin Spin Relaxation Rates of the Downfield Ytterbium Shifted Parvalbumin Resonances as a Function of ^{1}H NMR Frequency

	Observed[1]	$1/T2, s^{-1}$			
Resonance[1]	Shift(ppm)	200 MHz	270 MHz	400 MHz	600 MHz[2]
4	27.16	179	213	400	741
5	23.57	217	263	385	781
6	21.50	185	256	323	532
7	17.79	161	189	323	596
8	15.17	85	94	125	259

[1] Nomenclature and chemical shift positions correspond to data presented in Figures 30 and 31.
[2] The 600 MHz data have been corrected for differences in temperature as described in the Discussion.

Table 16

Relative Contributions of Various Mechanisms to Spin Spin Relaxation of Shifted ^1H NMR Resonances in Ytterbium Substituted Parvalbumin Determined from the ^1H NMR Frequency Dependence at 200, 270, 400, and 600 MHz of the Observed Linewidths

Peak[1]	$1/T2_{DD}$[2]	$1/T2_{X}$[3]	r, Å[4]	r, Å[5]
4	100	131	5.9 -0.1/+0.2	5.9 -0.1/+0.1
5	130	130	5.9 -0.1/+0.2	6.2 -0.2/+0.2
6	160	76	6.5 -0.2/+0.3	6.5 -0.2/+0.3
7	99	100	6.2 -0.2/+0.2	6.2 -0.2/+0.2
8	53	40	7.2 -0.4/+0.5	7.9 -0.7/+1.8

[1] nomenclature corresponds to data presented in Figures 30 and 31.

[2] $1/T2_{DD}$, measured in s^{-1}, was determined by a linear least squares fit to the data presented in Table 15. These values are equal to the best fit y intercept of plots such as Figure 32.

[3] $1/T2_{X}$, measured in s^{-1}, was determined by linear least squares methods. A best fit $1/T2_{OBS}$ was evaluated to correspond to a calculated value at 270 MHz. From this value, $1/T2_{DD}$ was subtracted to yield $1/T2_{X}$.

[4] r, the metal to proton distance was calculated using data obtained at 200, 270, 400, and 600 MHz (Table 15).

[5] r, the metal to proton distance was calculated using data obtained at 200, 270, and 400 MHz (Table 13).

the two calcium ions of parvalbumin; at Yb^{3+} ratios of 0.80, Yb^{3+} displaces only the calcium bound to the EF site of parvalbumin. Before analyzing the linewidths, it is important to ascertain whether or not there is a significant exchange broadening contribution to the linewidths. In the slow exchange limit, the exchange broadening is equal to K_{off}/π, where K_{off} is the dissociation rate constant for Yb^{3+} from the EF binding site of parvalbumin. This contribution is equivalent for all resonances. However, a wide variation in linewidths is observed; therefore the broadening cannot dominate the observed linewidths except for possibly the narrowest resonances. In Chapter 4, it was demonstrated that the binding of Yb^{3+} to the EF site is stronger than the binding of Ca^{2+} to the site. Fluorescence stopped flow experiments indicate a dissociation rate constant of 0.5 s^{-1} for Ca^{2+} from parvalbumin (Potter *et al.*, 1978). Since the association rate constant is near the diffusion controlled limit (Potter *et al.*, 1978), the tighter binding of Yb^{3+} implies a smaller dissociation rate constant. The exchange linebroadening can therefore be estimated at < 0.1 s^{-1}, which is insignificant for all resonances.

As discussed in the theory section, the three possible sources of nuclear spin relaxation of the shifted resonances are dipolar interactions with other nuclei, with the unpaired electrons on the metal, and with the *Curie spin* moment on the metal. (Contact interactions are neglected as discussed earlier). The relative contributions of the electronic dipolar (S) relaxation and susceptibility (X) relaxation to the nuclear spin spin relaxation rates is given by (Vega & Fiat, 1976):

$$\frac{1/T2_X}{1/T2_S} = \frac{4}{7} \Delta \frac{\tau_R}{\tau_S} \qquad (5.12)$$

in the limit $\omega_I \tau_R > 1$, and where Δ is defined as

$$\Delta = \frac{21}{20} \frac{g_L^2 \beta^2 J(J+1) H_o^2}{(3kT)^2} \qquad (5.13)$$

Similarly the relative contributions of the electronic dipolar (S) and susceptibility (X) mechanism to the spin lattice relaxation rates is given by:

$$\frac{1/T1_X}{1/T1_S} = \frac{6}{7} \frac{1}{\omega_I^2 \tau_R^2} \Delta \frac{\tau_R}{\tau_S} \qquad (5.14)$$

To evaluate equations 5.12 and 5.14, the following constants are substituted: $g_L = 8/7$, $J = 7/2$ for Yb^{3+}, $H_O = 63{,}000$ Gauss, $\omega_I = (2\pi)(270 \times 10^6)$ radians s^{-1}, and T = 300°K. ^{13}C NMR and light scattering studies of carp parvalbumin (Bauer *et al*., 1975; Nelson *et al*., 1976) indicate a rotational correlation time of τ_R of 12×10^{-9} s. The only number whose precise value is unkown is the electron spin relaxation time τ_S, although it is known to be on the order of 10^{-13} to 10^{-12} s. The choice of τ_S 2×10^{-13}, will be shown to be consistent with the value calculated from the experimental results (see below). Using the constants listed above, equations 5.14 and 5.12 are equal to:

$$\frac{1/T1_X}{1/T1_S} \approx 0.06 \qquad (5.15)$$

$$\frac{1/T2_X}{1/T2_S} \approx 16 \qquad (5.16)$$

The susceptibility relaxation mechanism is the primary electronic contribution to spin spin relaxation (Equation 5.16), whereas, the dipolar relaxation mechanism is the main electronic source to spin lattice relaxation (Equation 5.15).

Therefore there are two main contributions to the linewidths: the nuclear dipolar (*DD*) interactions and electronic susceptibility (*X*) interactions are given by Equation 5.17:

$$\frac{1}{T2} = \frac{9}{20}\gamma^4\hbar^2\sum\left(\frac{1}{d^6}\right)\tau_R + \frac{4}{5}\,\frac{\omega_I^2 g_L^4 \beta^4 J^2 (J+1)^2 \tau_R}{(3kT)^2 r^6} \qquad (5.17)$$

where $\sum 1/d^6$ is the weighted summed distance of the observed proton to neighboring protons. In the limit $\omega_I^2\tau_R^2>1$, the first contribution is field independent and the second term is field dependent, being proportional to ω_I^2. Thus these two contributions can be separated by a determination of the dependence of the linewidth on field. The linewidths have been determined at 200, 270, and 400 MHz (Table 12; Figure 32); a ω_I^2 dependence is observed which yields values for both $1/T2_X$ and $1/T2_{DD}$. From the field dependent contribution, metal to proton distances are calculated.

The contributions to the spin lattice relaxation cannot be as easily separated, since the electronic dipolar contributions are not field dependent $(\omega_I \tau_S, \omega_S \tau_S < 1)$ unless τ_S is field dependent, and the nuclear dipolar contributions can be influenced by other considerations such as spin diffusion. The spin lattice relaxation rates (1/T1) have been measured for the calcium saturated protein at 270 MHz and range from 0.9 to 2.6 s^{-1} for various peaks across the spectrum. The estimated range of possible values of $T1_S$ at 270 MHz for each of the shifted peaks is calculated by subtracting the minimum and maximum values of $1/T1_{DD}$ for the diamagnetic protein from the measured relaxation rates. These values are listed in Table 14.

Thus the possible range of $T1_S$ are measured as well as $1/T2_X$ and $1/T2_{DD}$ for each peak. At 270 MHz, expressions for $1/T1_S$ and $1/T2_X$ are equivalent to:

$$1/T1_S = \frac{1.69 \times 10^{-30}}{r^6}\,\tau_S \qquad (5.18)$$

$$1/T2_{X} = \frac{5.60 \times 10^{-42}}{r^{6}}\left(1 - \frac{r^{3}\delta}{\bar{X}}\right) \qquad (5.19)$$

The correction term from equation 5.10 shown in equation 5.19 is expected to be small. In addition, it is approximately constant (except for a change of sign in δ) because $\bar{X}$ is dominated by the first term of an expansion in 1/T (equation 5.7) which is isotropic and δ is proportional to $1/r^{3}$ (omitting angular factors for the moment)(Bleaney, 1972). This predicts that the ratio of $T1_{S}/T2_{X}$ should be approximately constant, although possibly different for the low field and high field shifted peaks; Table 14 lists this ratio for the shifted resonances. The values of the correction factor $r^{3}\delta/\bar{X}$ may be estimated from a peak such as resonance number 4 for which the paramagnetic shift is 20.10 ppm (Lee & Sykes, 1980b; Chapter 6), r is equal to 5.9 Å (neglecting the angular factor), and $\bar{X}$ the trace of the susceptibility tensor (Equation 5.7) is equal to 1.43 x 10^{-26} cm³. Thus $r^{3}\delta/\bar{X}$ is approximately equal to 0.28. The individual distances in Table 13 do not take this correction factor into account, since it could vary slightly from peak to peak, because of the dependence of the shift on the angular orientation of the particular nucleus relative to the metal. If the correction factor were taken into account, it would translate into an error in the distance of approximately 4%, which is less than the error from other sources. The value of the electron relaxation time, calculated from the ratio of $T1_{S}/T2_{X}$ for peak 4 neglecting the correction factor is 4.0×10^{-13} s; this value is comparable to 2.2×10^{-13} s, which was determined by Lenkinski and Reuben (Lenkinski & Reuben, 1976).

The distances calculated from the measured value of $1/T2_{X}$ at 270 MHz and equation 5.17, neglecting the correction factor as discussed above are presented in Table 13. The shifted resonances represent nuclei fairly close to the metal ion. For example, the two protons bonded to the beta carbon of Asp 90, which directly chelates the metal, are 5.6 Å and 4.7 Å removed (Chapter 9). The errors in the calculated distances were measured by considering the probable measurement errors at 270 MHz in comparison with the experimentally deduced value of $1/T2_{X}$ at 270 MHz. The error in the calculated distance gets larger as the distance gets longer; this observation has been reported elsewhere (Rowan *et al.*, 1974). Note that the upper and lower limits in the distances are not equivalent, because of the inverse sixth power relationship between errors in the observed linewidths and errors in the calculated distances. The magnitude of the susceptibility contribution to the linebroadening could be increased by choosing a different lanthanide (Lee & Sykes, 1980a; see below); such an experiment could lead to decreased errors in the measured distances.

However, ytterbium is the lanthanide of choice in this study, for the ratio of pseudocontact to contact shift is the largest for ytterbium (Reuben, 1973b). Of all the lanthanides, ytterbium contributes the smallest contact contribution (Reuben, 1973b). In addition, the ratio of the pseudocontact shift to the susceptibility linebroadening is relatively large (see below), resulting in a relatively high resolution spectrum for the parvalbumin ytterbium complex.

The observed field dependence of the linewidths has been extended to 600 MHz. The linewidths were corrected for differences in temperature (293°K at 600 MHz vs. 300°K at 270 MHz) in the following manner. The rotational correlation time τ_R is proportional to the viscosity and inversely proportional to the temperature T ($\tau_R \alpha \eta /T$); the spin spin relaxation rate 1/T2 is proportional to the rotational correlation time and inversely proportional to the temperature squared (equation 5.9) ($1/T2 \alpha \tau_R /T^2$). Thus the spin spin relaxation rate is proportional to the viscosity and inversely proportional to the temperature cubed ($1/T2 \alpha \eta /T^3$). The value of η/T^3 was used as a correction factor to calculate the expected spin spin relaxation rate at 600 MHz at 300°K from the observed spin spin relaxation rate at 600 MHz at 293°K. The solvent viscosity at 293°K is 1.002; at 300°K, 0.7975 (Handbook of Chemistry and Physics, 1970). Metal to proton distances were calculated using the data obtained at 200, 270, 400, and 600 MHz (Table 15). The distances so determined agree well with the distances determined using data obtained at 200, 270, and 400 MHz

(Table 16).

The experimentally determined values for contributions to the linewidths of the shifted resonances from other nuclei $\Delta\nu_{DD} = 1/\pi T2_{DD}$ range from 18 to 59 Hz (Table 13). This range is appropriate for a protein the size of parvalbumin. For comparison, the calculated linewidth of an isolated CH_2 pair (which corresponds to the shortest possible proton proton distance), such as the Asp beta protons, on a protein with a rotational correlation time of 12×10^{-9} s is 28 Hz, below the upper limit of the experimental values.

I conclude with a discussion of the advantages and disadvantages of the various lanthanides for this kind of study. Table 17 lists the relative contributions of the dipolar and susceptibility relaxation mechanisms to T1 and T2 for each of the lanthanides, the quantity $g_L^4 J^2 (J+1)^2$ which indicates the relative magnitude of the susceptibility linebroadening term, the relative dipolar shift, and the ratio of the shift to the susceptibility linebroadening for each lanthanide. Columns 1 and 2 indicate that for all of the lanthanides, the dipolar mechanism dominates T1, but the susceptibility mechanism dominates T2. The resolution is therefore indicated in the last column. Although terbium and dysprosium induce the largest shifts, the resonances can become unobservable due to the concomitant linebroadening. An evaluation of the shifting/broadening ratio indicates that cerium, ytterbium, and praseodymium are the preferred

Table 17

Relative Shifting and Broadening Contributions in Lanthanide Complexes

Metal	$\frac{1/T_{1X}}{1/T_{1S}}$ [1]	$\frac{1/T_{2X}}{1/T_{2S}}$ [2]	D [3]	$g_L^4 J^2(J+1)^2$ [4]	$\frac{D}{g_L^4 J^2(J+1)^2}$ [5]
Ce	0.019	5.14	-6.3	68	-1.79
Pr	0.037	10.29	-11.0	164	-1.29
Nd	0.039	10.63	-4.2	172	-0.46
Pm	0.021	5.83	+2	52	0.73
Tb	0.275	75.77	-86	8926	-0.19
Dy	0.329	90.86	-100	16042	-0.12
Ho	0.327	90.17	-39	12649	-0.06
Er	0.267	73.71	33	10509	0.06
Tm	0.166	45.94	53	3263	0.31
Yb	0.060	16.46	22	424	1.00

[1] Ratios of the two contributions to relaxation rates assuming, tau$_R$ of 12 ns, T_{1e} of 2×10^{-13}, H_O of 63 kg, and a temperature of 300°K.

[2] Ratios of the two contributions to relaxation rates assuming, tau$_R$ of 12 ns, T_{1e} of 2×10^{-13}, H_O of 63 kg, and a temperature of 300°K.

[3] Relative dipolar shift (Bleaney *et al*., 1972) scaled to 100 for Dy^{3+} where a minus sign indicates a downfield shift.

[4] Relative susceptibility broadening.

[5] Shifting/broadening ratio, scaled to 1.0 for Yb^{3+}.

lanthanide ions for these studies. Figure 35 illustrates the ^{1}H NMR spectra for the Pr^{3+}, Yb^{3+}, and the Tb^{3+} complexes with parvalbumin.

In this chapter, I have shown that the analysis of the nuclear spin relaxation of nuclei directly surrounding the lanthanide metal ion bound to the EF site of parvalbumin results in the determination of metal to proton distances.

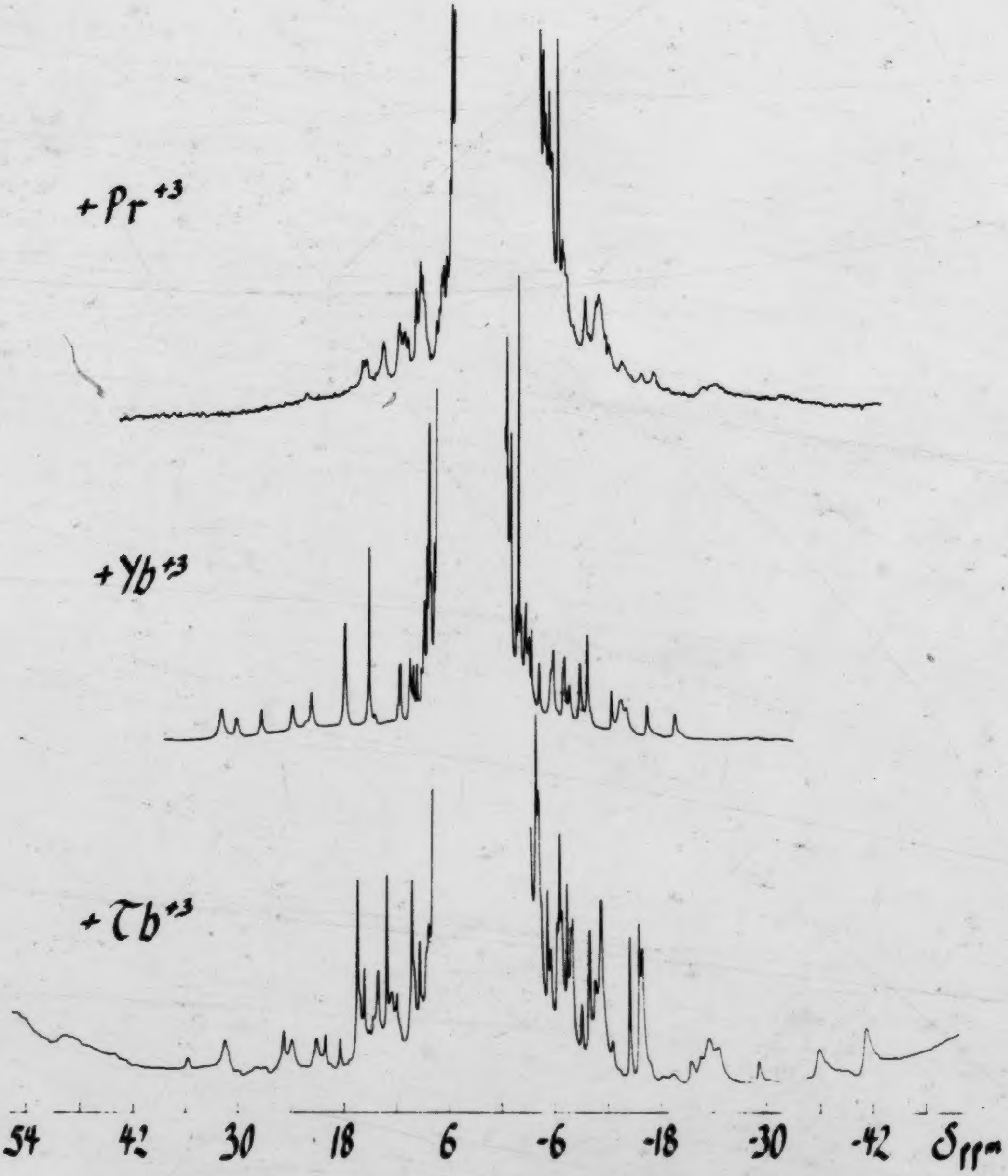

Figure 35. The ^1H NMR spectra of three different parvalbumin lanthanide complexes. This figure compares the spectra of the praseodymium (Pr^{3+}) parvalbumin, the ytterbium (Yb^{3+}) parvalbumin, and the terbium (Tb^{3+}) parvalbumin complexes. The total metal to total protein ratios in each sample is approximately 1/1. The Tb^{3+} parvalbumin spectrum could not be phased properly due to the insufficient spectral width used.

VI. The Temperature Dependence of the Observed Shifts

A. Introduction

The ^{1}H NMR spectrum of the parvalbumin ytterbium complex consists of a series of resonances shifted far outside the envelope of the ^{1}H NMR spectrum of the diamagnetic form of the protein. Although the observed chemical shift positions (δ_{OBS}) are easily and accurately measured, the diamagnetic positions (δ_d) of the observed shifted nuclei (see discussion in Chapter 2) are not readily nor directly evaluated. These diamagnetic positions are required to determine the paramagnetic shifts (δ_p) (equation 6.1)

$$\delta_P = \delta_{OBS} - \delta_d \qquad (6.1)$$

which are to be analyzed in terms of the three dimensional structure of the protein. In this chapter, I shall demonstrate how the temperature dependence of the observed positions are used to sort out overlapping peaks and to determine the diamagnetic positions of the observed resonances.

B. Experimental Procedures

Sample Preparation The protein sample was prepared according to the methods described in Chapter 4. The 0.68 mM protein sample was prepared in 15 mM Pipes, 0.15 M KCl, 10 mM DTT, 0.5 mM DSS, in D2O, pH 6.65, at a total Yb^{3+} to total protein ratio of 0.8.

Data Acquisition The spectra were acquired according to the methods described in Chapter 4. All observed chemical shifts and positions are measured with respect to the principal resonance of DSS. A Bruker variable temperature unit was used to change the sample temperature.

Temperature Calibration The chemical shift difference between the hydroxyl protons and methyl protons of methanol was measured as a function of temperature (Van Geet, 1968; Van Geet, 1970; Raiford *et al.*, 1979). Temperatures were calculated according to the following equation (Van Geet, 1969):

$$T = 406.0 - 0.551\left|\Delta\delta\right| - 63.4\left(\frac{\Delta\delta}{100}\right)^2 \qquad (6.2)$$

where $\Delta\delta$ is the observed chemical shift difference in Hz (scaled to 60 MHz) between the methyl and hydroxyl protons of methanol. The temperatures so calculated were used as calibration curves (Figure 36) to relate the reading on the variable temperature unit to the actual sample temperature.

Determination of the Temperature Dependence The following assumptions are made in the analysis of the

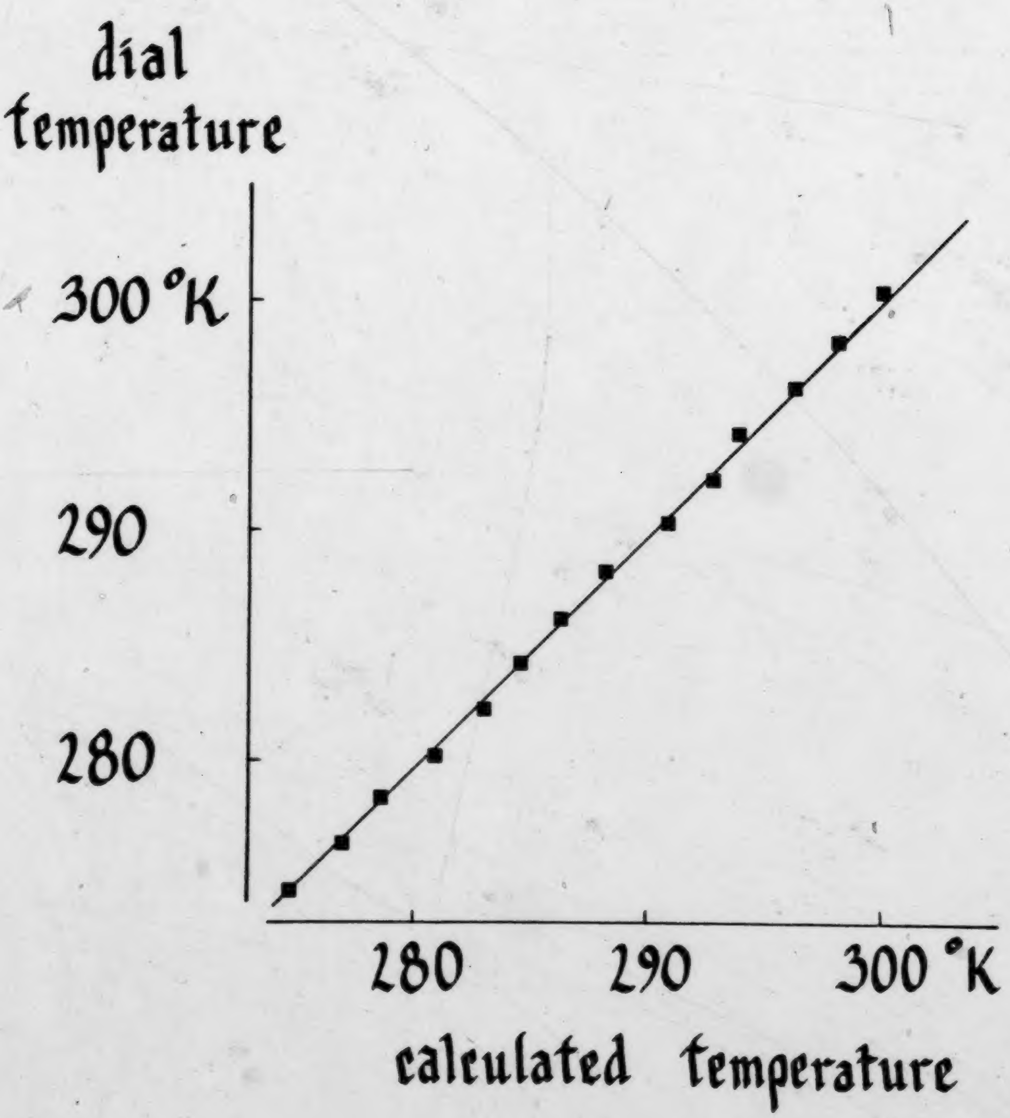

Figure 36. Calibration of the methanol NMR thermometer. The temperatures observed on the Bruker variable temperature unit are plotted vs. the calculated temperatures. These temperatures were based upon the separation of the methyl resonance and OH resonance of methanol and equation 6.2. Details are described in the Experimental Procedures section.

temperature dependence: the geometric factors G1 and G2 (equation 1.1) are temperature independent; the dependencies of A1 and A2 in equation 1.1 are equal. The temperature dependence of the paramagnetic shift is then given in general by (Bleaney, 1972; McGarvey, 1979):

$$\delta_{OBS} - \delta_{D} = \delta_{P} = \frac{A}{T^2} + \frac{B}{T^3} + \frac{C}{T^4} + \ldots \qquad (6.3)$$

where A,B, and C are constants. The contributions of the various terms with increasing powers of 1/T to the temperature dependence were determined by an analysis of the methyl resonance at 15.17 ppm (at 302°K).

Determination of the Diamagnetic Positions The diamagnetic positions for all of the other protons were determined relative to the choice of 1 ppm as the diamagnetic position for the methyl resonance at 15.17 ppm (see below) by assuming that all of the resonances extrapolate with a similar temperature dependence towards $1/T^n = 0$, which implies:

$$\delta^{i}_{OBS} - \delta^{i}_{D} = K\left(\delta^{j}_{OBS} - \delta^{j}_{D}\right) \qquad (6.4)$$

where K is a constant, and i and j are two shifted resonances. The diamagnetic position of peak i is then obtained by plotting the observed shift positions of peak i pairwise versus the observed shift positions of the methyl group at 15.17 ppm. No value of the power dependence (equation 6.3) was assumed in this part of the analysis.

C. Results

The lanthanide induced shifted resonances vary as a function of temperature (Figures 37 and 38). The temperature dependence is useful is sorting out overlapping peaks and confirming the contributions to the area of overlapping peaks (Figure 39) as can be seen by the resonances marked by solid triangles, circles, and squares (Figures 38 and 39).

The observed chemical shift positions as a function of temperature are listed in Tables 18 to 31. The diamagnetic positions and paramagnetic shifts of the resonances are listed in Tables 32 to 34. Figure 40 is an example of the temperature dependence of the resonance with an observed shift of 15.17 ppm indicated by a plot of the log of its paramagnetic shift versus log temperature. A diamagnetic position of 1 ppm is assumed.

D. Discussion

There has been considerable controversy over the form of the temperature dependence of lanthanide induced pseudocontact shifts. The theory proposed by Bleaney (Bleaney, 1972) relates the pseudocontact shift to the isotropic portion of the paramagnetic susceptibility, which involves an expansion of the pseudocontact shift as a power series in T^{-n} with the first non-zero term being the T^{-2} term. Horrocks (Horrocks, 1977), however, has criticized

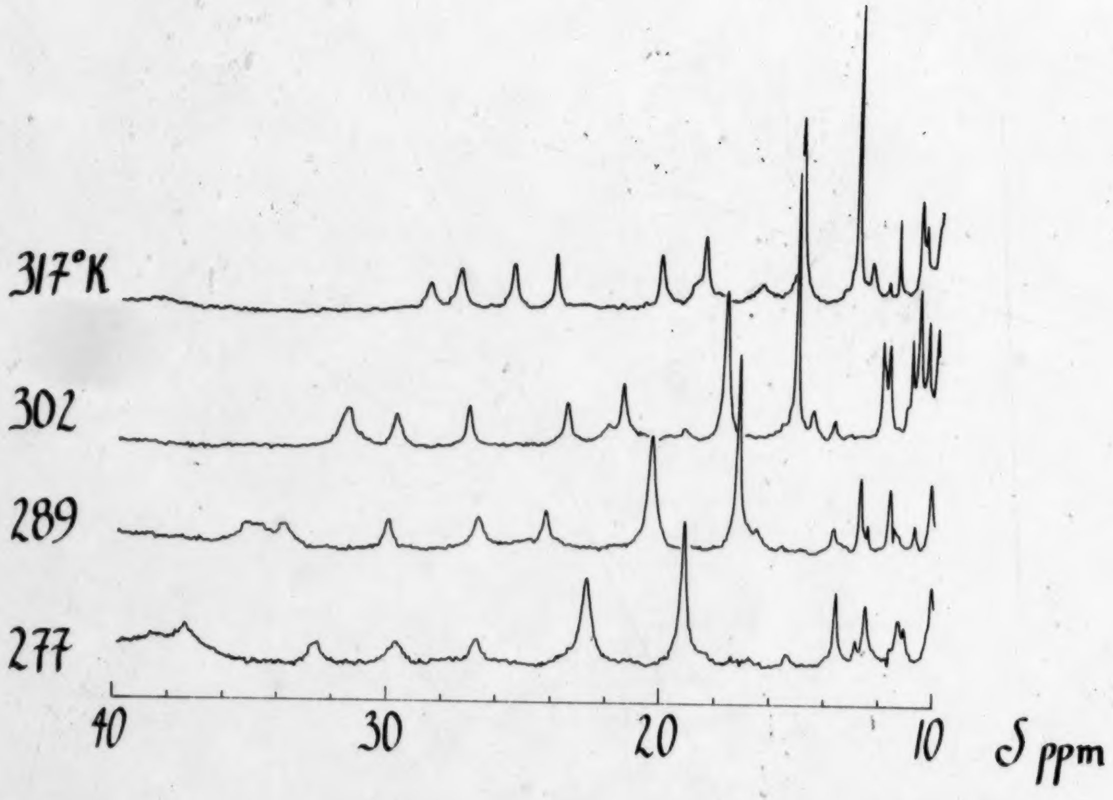

Figure 37. The downfield region of the 270 MHz ^{1}H NMR spectrum of parvalbumin in the presence of Yb^{3+} as a function of temperature. The 0.68 mM protein sample was prepared in 15 mM Pipes, 0.15 M KCl, 10 mM DTT, 0.5 mM DSS in D2O, pH 6.65 at a total (Yb^{3+}/P) ratio of 0.8. The temperatures of these experiments were 277, 289, 302, and 317°K.

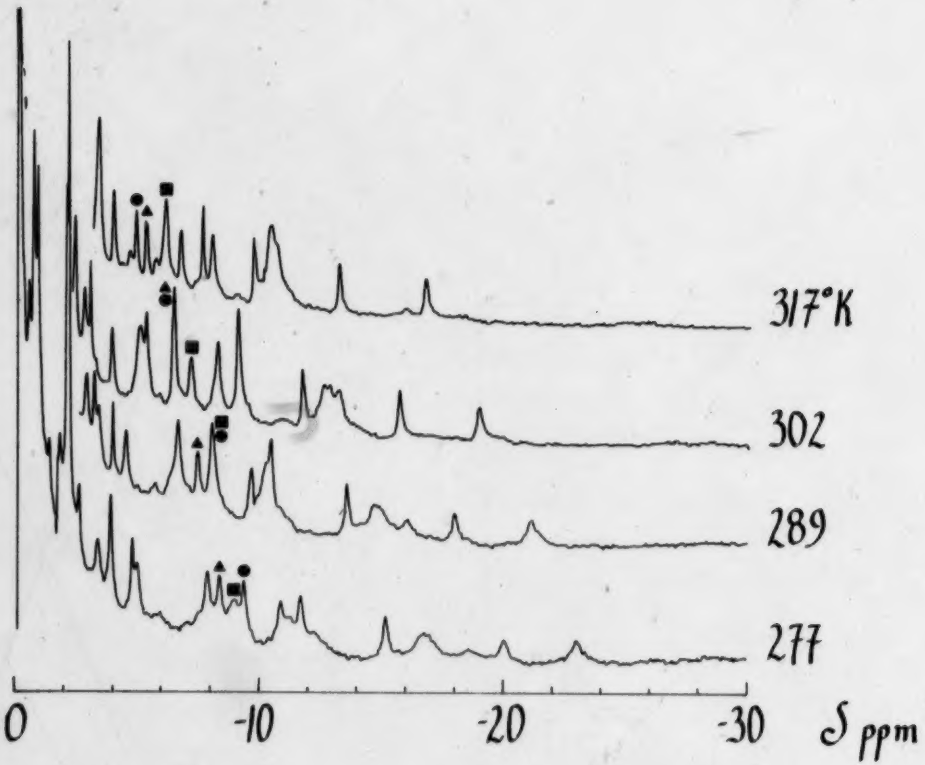

Figure 38. The upfield region of the 270 MHz ^1H NMR spectrum of parvalbumin in the presence of Yb^{3+} as a function of temperature. The 0.68 mM protein sample was prepared in 15 mM Pipes, 0.15 M KCl, 10 mM DTT, 0.5 mM DSS in D2O, pH 6.65 at a total (Yb^{3+}/P) ratio of 0.8. The temperatures of these experiments were 277, 289, 302, and 317°K. The symbols ●, ■, and ▲ indicate resonances which cross over as a function of temperature. The shifts for these resonances are plotted in Figure 39, using the same symbol nomenclature.

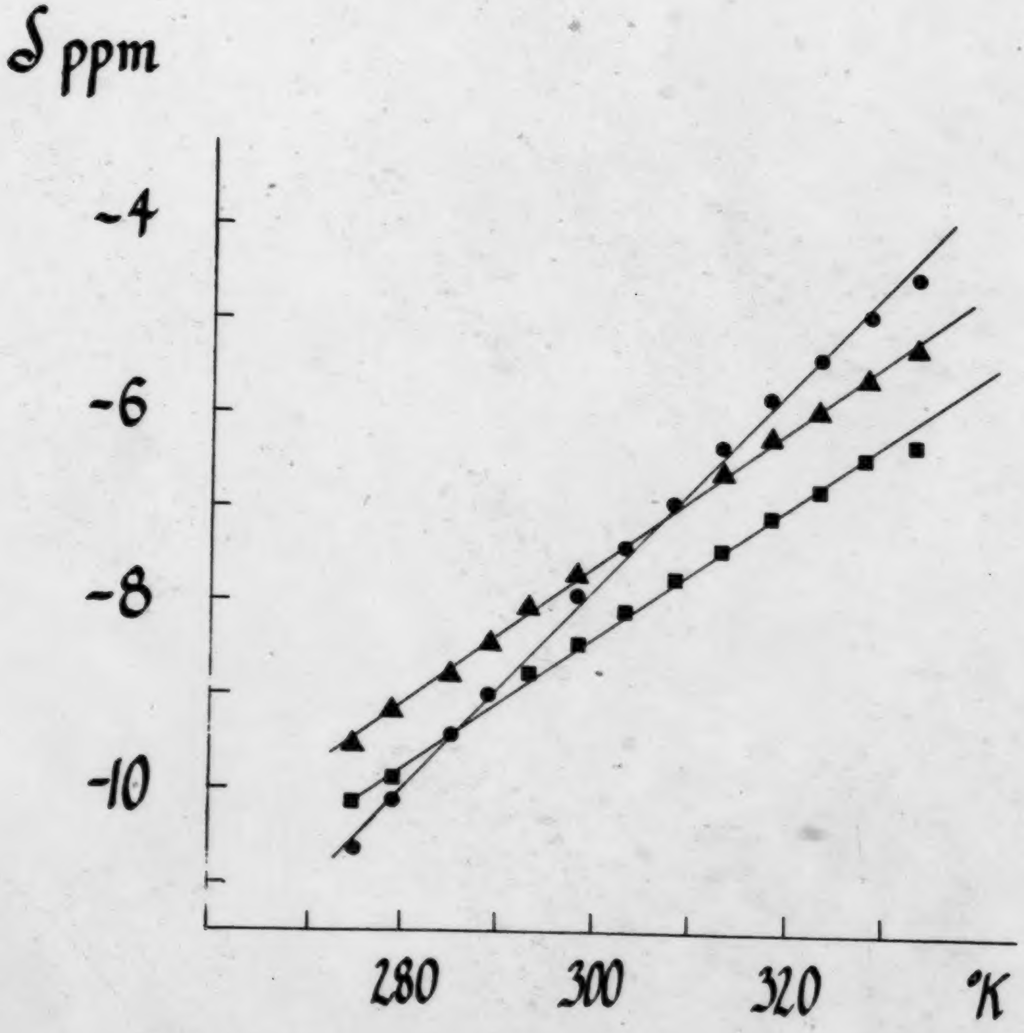

Figure 39. The temperature dependence of the observed shift positions indicated by a plot of the observed shift position vs. temperature. The temperature dependence has been used to sort out overlapping peaks. The symbols used in this figure correspond to resonances similarly labelled in Figure 38.

Table 18

The Temperature Dependence of the Observed Chemical Shift Positions I

Temperature[1]	Resonance[2]				
	1	2	3	4	5
275.0	39.30	39.30	38.22	33.25	30.38
277.1	38.72	38.72	37.51	32.61	29.76
279.0	38.01	38.01	36.86	32.19	29.24
281.0	37.17	37.17	36.15	31.61	28.56
282.8	36.70	36.70	35.52	31.21	28.14
284.8	36.32	36.32	35.05	30.89	27.69
286.7	35.74	35.74	34.45	30.43	27.31
288.7	35.18	35.18	33.85	30.06	26.77
290.6	34.47	34.47	32.93	29.41	26.12
292.6	33.94	33.94	32.49	29.05	25.67

[1] Temperature in °K.
[2] All chemical shift positions are measured in ppm.
Nomenclature corresponds to data presented in Figure 47.

Table 19

The Temperature Dependence of the Observed Chemical Shift Positions II

Temperature[1]	Resonance[2]				
	1	2	3	4	5
282.9	36.13	36.13	34.83	30.76	27.54
287.8	35.22	35.22	33.74	30.02	26.72
292.7	33.76	33.76	32.33	28.99	25.55
297.5	32.75	32.75	31.11	28.10	24.61
302.3	31.61	31.61	29.80	27.16	23.57
307.4	30.64	30.11	28.28	26.04	22.35
312.1	29.61	28.83	26.89	25.03	21.25
317.0	28.63	27.54	25.56	24.05	20.18
321.9	27.76	26.46	24.43	23.16	19.27
326.7	26.84	25.33	23.24	22.28	18.32
331.6	25.98	24.27	22.13	21.46	17.44

[1] temperature in °K.

[2] All chemical shift positions are measured in ppm. Nomenclature corresponds to data in Figure 47.

Table 20

The Temperature Dependence of the Observed Chemical Shift Positions III

Temperature[1]	Resonance[2]				
	6	7	8	9	10
275.0	27.28	23.21	19.57	12.92	13.75
277.1	26.77	22.72	19.18	12.84	13.58
279.0	26.35	22.37	18.84	12.77	13.44
281.0	25.81	21.81	18.42	12.69	13.24
282.8	25.43	21.43	18.12	12.63	13.11
284.8	25.07	21.15	17.86	12.57	13.00
286.7	24.70	20.76	17.56	12.51	12.84
288.7	24.29	20.39	17.27	12.45	12.72
290.6	23.69	19.82	16.82	12.37	12.50
292.6	23.30	19.48	16.53	12.37	12.37

[1] temperature in °K.

[2] All chemical shift positions are measured in ppm. Nomenclature corresponds to data presented in Figure 47.

Table 21

The Temperature Dependence of the Observed Chemical Shift Positions IV

Temperature[1]	Resonance[2]				
	6	7	8	9	10
282.9	24.94	21.03	17.78	12.56	12.95
287.8	24.23	20.34	17.23	12.44	12.70
292.7	23.22	19.40	16.47	12.30	12.30
297.5	22.37	18.63	15.84	12.13	12.13
302.3	21.50	17.79	15.17	12.00	11.75
307.4	20.45	16.80	14.40	11.82	11.38
312.1	19.52	15.93	13.70	11.66	11.05
317.0	18.61	15.08	13.02	11.50	10.72
321.9	17.83	14.35	12.44	11.37	10.47
326.7	17.01	13.60	11.83	11.23	10.16
331.6	16.25	12.89	11.27	11.10	9.89

[1] temperature in °K.

[2] All chemical shift positions are measured in ppm. Nomenclature corresponds to data presented in Figure 47.

Table 22

The Temperature Dependence of the Observed Chemical Shift Positions V

Temperature[1]	Resonance[2]	
	11	41
275.0	12.66	-0.76
277.1	12.48	-0.71
279.0	12.34	-0.67
281.0	12.16	-0.63
282.8	12.01	-0.60
284.8	11.90	-0.56
286.7	11.76	-0.53
288.7	11.63	-0.49
290.6	11.43	-0.47
292.6	11.30	-0.43

[1] Temperature in °K.
[2] All chemical shift positions are measured in ppm. Nomenclature corresponds to data presented in Figures 47 and 48.

Table 23

The Temperature Dependence of the Observed Chemical Shift Positions VI

Temperature[1]	Resonance[2]	
	11	41
282.9	11.87	-0.55
287.8	11.62	-0.49
292.7	11.28	-0.42
297.5	10.98	-0.36
302.3	10.69	-0.27
307.4	10.20	-0.21
312.1	9.93	ND
317.0	9.62	ND
321.9	9.31	ND
326.7	9.00	ND
331.6	8.70	ND

[1] temperature in °K.

[2] All chemical shift positions are measured in ppm. Nomenclature corresponds to data in Figures 47 and 48.

Table 24

The Temperature Dependence of the Observed Chemical Shift Positions VII

Temperature[1]	Resonance[2]				
	43	45	46	48	50
275.0	-0.89	-2.17	-2.07	-3.97	-4.92
277.1	-0.88	-2.12	-2.03	-3.83	-4.74
279.0	-0.87	-2.07	-2.01	-3.71	-4.59
281.0	-0.87	-2.02	-1.97	-3.56	-4.41
282.8	-0.87	-1.97	-1.97	-3.44	-4.28
284.8	-0.86	-1.94	-1.94	-3.36	-4.17
286.7	-0.85	-1.90	-1.90	-3.24	-4.04
288.7	-0.85	-1.86	-1.86	-3.13	-3.90
290.6	-0.85	-1.82	-1.82	-2.96	-3.70
292.6	-0.83	-1.78	-1.78	-2.86	-3.58

[1] Temperature in °K.
[2] All chemical shift positions are measured in ppm. Nomenclature corresponds to data presented in Figure 48.

Table 25

The Temperature Dependence of the Observed Chemical Shift Positions VIII

Temperature[1]	Resonance[2]				
	43	45	46	48	50
282.9	-0.85	-1.92	-1.92	-3.31	-4.12
287.8	-0.84	-1.85	-1.85	-3.11	-3.87
292.7	-0.83	-1.77	-1.77	-2.83	-3.54
297.5	-0.82	-1.70	-1.70	-2.60	-3.26
302.3	-0.80	-1.59	-1.63	-2.33	-2.95
307.4	-0.78	-1.50	-1.57	-2.08	-2.50
312.1	-0.76	-1.40	-1.50	-1.61	-2.29
317.0	-0.74	-1.30	-1.44	-1.30	-1.77
321.9	-0.71	-1.21	-1.36	-1.21	-1.36
326.7	-0.69	-1.12	-1.29	-0.78	-1.12
331.6	-0.67	-1.05	-1.23	-0.48	-0.67

[1] temperature in °K.
[2] All chemical shift positions are measured in ppm. Nomenclature corresponds to data in Figure 48.

Table 26

The Temperature Dependence of the

Observed Chemical Shift Positions IX

Temperature[1]	Resonance[2]				
	51	52	53	54	55
275.0	-4.92	-8.08	-8.08	-8.52	-9.64
277.1	-4.92	-7.84	-7.84	-8.32	-9.35
279.0	-4.88	-7.61	-7.61	-8.16	-9.11
281.0	-4.74	-7.34	-7.34	-7.99	-8.81
282.8	-4.68	-7.17	-7.17	-7.85	-8.59
284.8	-4.63	-6.98	-6.98	-7.70	-8.39
286.7	-4.52	-6.80	-6.80	-7.56	-8.19
288.7	-4.43	-6.60	-6.60	-7.41	-7.99
290.6	-4.32	-6.31	-6.31	-7.19	-7.63
292.6	-4.25	-6.13	-6.13	-7.05	-7.45

---

[1] Temperature in °K.

[2] All chemical shift positions are measured in ppm. Nomenclature corresponds to data presented in Figures 48 and 49.

Table 27

The Temperature Dependence of the Observed Chemical Shift Positions X

Temperature[1]	Resonance[2]				
	51	52	53	54	55
282.9	-4.56	-6.94	-6.94	-7.65	-8.34
287.8	-4.42	-6.57	-6.57	-7.39	-7.94
292.7	-4.22	-6.09	-6.09	-7.02	-7.40
297.5	-4.05	-5.50	-5.69	-6.71	-6.93
302.3	-3.84	-4.99	-5.26	-6.41	-6.41
307.4	-3.64	-4.39	-4.77	-5.95	-5.95
312.1	-3.44	-3.85	-4.32	-5.59	-5.34
317.0	-3.29	-3.29	-3.89	-5.22	-4.83
321.9	-3.05	-2.83	-3.52	-4.94	-4.38
326.7	-2.87	-2.33	-3.13	-4.61	-3.93
331.6	-2.75	-1.89	-2.75	-4.30	-3.53

---

[1] temperature in °K.

[2] All chemical shift positions are measured in ppm. Nomenclature corresponds to data in Figures 48 and 49.

Table 28

The Temperature Dependence of the Observed Chemical Shift Positions XI

Temperature[1]	Resonance[2]				
	56	57	58	59	60
275.0	-9.13	-9.64	-12.71	-11.90	-11.35
277.1	-8.94	-10.85	-12.22	-11.66	-11.19
279.0	-8.82	-10.62	-11.87	-11.43	-11.00
281.0	-8.81	-10.38	-11.52	-11.16	-10.79
282.8	-8.59	-10.20	-11.27	-10.97	-10.67
284.8	-8.39	-10.01	-11.16	-10.81	-10.56
286.7	-8.19	-9.80	-10.61	-10.44	-10.42
288.7	-7.99	-9.62	-10.41	-10.41	-10.23
290.6	-7.88	-9.33	-10.38	-10.12	-9.96
292.6	-7.76	-9.14	-9.46	-9.93	-9.76

[1] Temperature in °K.

[2] All chemical shift positions are measured in ppm. Nomenclature corresponds to data presented in Figure 49.

Table 29

The Temperature Dependence of the Observed Chemical Shift Positions XII

Temperature[1]	Resonance[2]				
	56	57	58	59	60
282.9	-8.34	-9.96	-11.19	-10.76	-10.53
287.8	-7.94	-9.59	-10.38	-10.38	-10.18
292.7	-7.71	-9.08	-9.63	-9.89	-9.75
297.5	-7.43	-8.68	-8.68	-9.48	-9.48
302.3	-7.11	-8.19	-8.19	-9.02	-9.02
307.4	-6.73	-7.68	-7.31	-8.50	-8.68
312.1	-6.42	-7.18	-6.60	-8.03	-8.29
317.0	-6.06	-6.69	-6.06	-7.56	-7.95
321.9	-5.77	-6.21	-5.42	-7.13	-7.58
326.7	-5.47	-5.79	-4.88	-6.71	-7.27
331.6	-5.37	-5.32	-4.23	-6.32	-6.98

[1] temperature in °K.

[2] All chemical shift positions are measured in ppm. Nomenclature corresponds to data in Figure 49.

Table 30

The Temperature Dependence of the Observed Chemical Shift Positions XIII

Temperature[1]	Resonance[2]				
	61	62	64	65	66
275.0	-15.47	-17.16	-19.07	-20.39	-23.40
277.1	-15.15	-16.71	-18.56	-20.04	-22.91
279.0	-14.84	-16.29	-18.13	-19.62	-22.59
281.0	-14.50	-15.82	-17.59	-19.24	-22.28
282.8	-14.25	-15.70	-17.16	-18.91	-21.97
284.8	-14.03	-15.44	-16.82	-18.62	-21.72
286.7	-13.76	-15.05	-16.38	-18.28	-21.41
288.7	-13.50	-14.61	-16.01	-17.96	-21.07
290.6	-13.11	-14.43	-15.39	-17.49	-20.61
292.6	-12.87	-14.07	-14.99	-17.16	-20.33

[1] Temperature in °K.

[2] All chemical shift positions are measured in ppm. Nomenclature corresponds to data presented in Figure 49.

Table 31

The Temperature Dependence of the Observed Chemical Shift Positions XIV

Temperature[1]	Resonance[2]				
	61	62	64	65	66
282.9	-13.94	-15.21	-16.69	-18.55	-21.63
287.8	-13.47	-14.60	-15.97	-17.92	-21.06
292.7	-12.81	-14.07	-14.94	-17.09	-20.24
297.5	-12.26	-13.22	-14.05	-16.40	-19.62
302.3	-11.63	-12.52	-13.16	-15.65	-18.90
307.4	-10.94	-12.04	-12.04	-14.76	-18.10
312.1	-10.29	-11.19	-11.19	-13.94	-17.43
317.0	-9.66	-10.34	-10.34	-13.13	-16.69
321.9	-9.08	-9.82	-9.46	-12.41	-16.05
326.7	-8.49	-9.24	-8.66	-11.65	-15.41
331.6	-7.96	-8.85	-7.96	-10.98	-14.81

---

[1] temperature in °K.

[2] All chemical shift positions are measured in ppm. Nomenclature corresponds to data in Figure 49.

Table 32

Diamagnetic Positions of the Downfield Shifted Resonances in Region I of the ^{1}H NMR Spectrum of the Yb^{3+} Parvalbumin Complex[1]

Resonance[2]	Observed Position[3]	Diamagnetic Position[4]	Paramagnetic Shift[5]
1	31.61	9.35	22.26
2	31.61	5.84	25.77
3	29.80	2.18	27.62
4	27.16	7.06	20.10
5	23.57	1.48	22.09
6	21.50	2.60	18.90
7	17.79	0.10	17.69
8	15.17	1.00	14.17
9	12.00	8.86	3.14
10	11.75	5.13	6.62
11	10.69	3.87	6.82

---

[1] See Figure 46 for the defined limits of region I.
[2] Nomenclature corresponds to data presented in Figure 47.
[3] Observed chemical shift positions (in ppm) for the Yb^{3+} parvalbumin complex (Chapter 5) at 302°K.
[4] These diamagnetic positions (in ppm) were determined by methods described in the Experimental Procedures section.
[5] These paramagnetic shifts (in ppm) were determined by subtracting the diamagnetic position of a given resonance (column 3) from its observed chemical shift position (column 2).

Table 33

Diamagnetic Positions of the Upfield Shifted Resonances in Region II of the ^{1}H NMR Spectrum of the Yb^{3+} Parvalbumin Complex[1]

Resonance[2]	Observed Position[3]	Diamagnetic Position[4]	Paramagnetic Shift[5]
41	-0.27	1.35	-1.62
42	ND	ND	ND
43	-0.80	-0.43	-0.37
44	ND	ND	ND
45	-1.59	0.31	-1.90
46	-1.63	-0.19	-1.44
47	ND	ND	ND
48	ND	ND	ND
49	-2.33	3.60	-5.93
50	-2.95	4.24	-7.19
51	-3.84	0.07	-3.91
52	-4.99	5.76	-10.75
53	-5.26	3.82	-9.08

[1] See Figure 46 for the defined limits of region II. ND indicates not determined.
[2] Nomenclature corresponds to data presented in Figure 48.
[3] Observed shifts (in ppm) for the Yb^{3+} parvalbumin complex (Chapter 5) at 302°K.
[4] These diamagnetic positions (in ppm) were determined by methods described in the Experimental Procedures section.
[5] These paramagnetic shifts (in ppm) were determined by subtracting the diamagnetic position of a given resonance (column 3) from its observed position (column 2).

Table 34

Diamagnetic Positions of the Upfield Shifted Resonances in Region III of the ^{1}H NMR Spectrum of the Yb^{3+} Parvalbumin Complex[1]

Resonance[2]	Observed Position[3]	Diamagnetic Position[4]	Paramagnetic Shift[5]
54	-6.41	0.87	-7.28
55	-6.41	4.02	-10.43
56	-7.11	-0.43	-7.54
57	-8.19	1.12	-9.31
58	-8.19	6.34	-14.53
59	-9.02	0.52	-9.54
60	-9.02	-1.49	-7.53
61	-11.63	1.23	-12.86
62	-12.52	1.64	-14.16
63	ND	ND	ND
64	-13.16	5.92	-19.06
65	-15.65	0.55	-16.20
66	-18.90	-4.30	-14.60

[1] See Figure 46 for the defined limits of region III.

[2] Nomenclature corresponds to data presented in Figure 49.

[3] Observed chemical shift positions (in ppm) for the Yb^{3+} parvalbumin complex (Chapter 5) at 302°K.

[4] These diamagnetic positions (in ppm) were determined by methods described in the Experimental Procedures section.

[5] These paramagnetic shifts (in ppm) were determined by subtracting the diamagnetic position of a given resonance (column 3) from its observed chemical shift position (column 2).

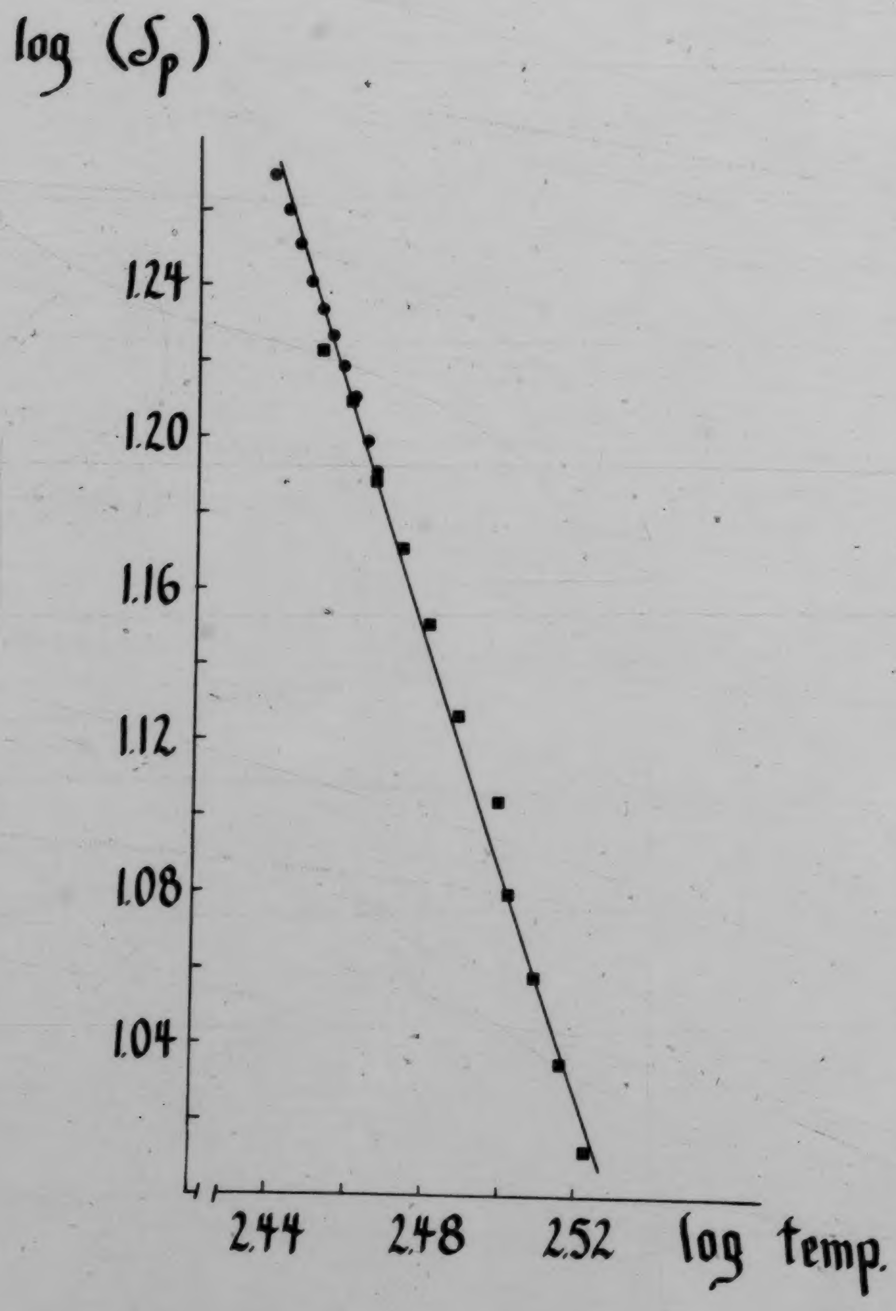

Figure 40. The temperature dependence of the resonance with an observed chemical shift position of 15.17 ppm (at 302°K) indicated by a plot of the log of its paramagnetic shift vs. log temperature. The symbols, ● and ■, represent two separate sets of experiments.

this theory on the basis of data on single crystal susceptibility anisotropies which are non-linearly dependent on T^{-2}, and has observed a T^{-1} dependence of paramagnetic shifts for some Pr^{3+} and Yb^{3+} complexes. de Boer and co-workers (de Boer *et al.*, 1977) have also observed paramagnetic shifts which vary more closely with T^{-1} and suggested that attempts to separate contact from pseudocontact shifts based upon the expected T^{-1} dependence of the former and T^{-2} dependence of the latter are difficult. On the other hand, Stout and Gutowsky (Stout & Gutowsky, 1976) have extended Bleaney's theory for limited crystal field terms and axial symmetry, and conclude that the T^{-3} term is only 10% at most of the T^{-2} term. In addition, McGarvey (McGarvey, 1979) has pointed out that the fitting procedure used by Horrocks is "suspect because it predicts a large shift at infinite temperatures which is contrary to theory". Similar results were obtained by the fitting procedure of de Boer *et al*. McGarvey further derives a general expression for the T^{-3} term for any crystal field, and concludes that the "T^{-2} term of Bleaney does in fact give the pseudocontact term to an accuracy of 10-20% at room temperatures".

In this chapter, the unusual temperature dependence of the Yb^{3+} paramagnetic shift of the shifted protein nuclei is presented. Since the spectra are in the slow exchange limit, (Lee & Sykes, 1980a; Chapter 2), the shift of the complex is observed directly without need to extrapolate as a function of concentration of ligand or metal, as is necessary in the fast exchange limit. In addition, the protein is stable over the temperature range of approximately 0 to 80°C, a range which is particularly large for a protein. All of the resonances have the same temperature dependence as indicated in Figure 40 for the methyl resonance at 15.17 ppm (at 302°K). This resonance has been tentatively assigned to the gamma 2 methyl protons of Val 99 (Lee & Sykes, 1980b; 1980d; Chapter 9). A problem in the slow exchange limit is that the diamagnetic resonance position of these methyl protons is not known *a priori* without separately assigning the resonance in the complex of the protein with a diamagnetic metal such as La^{3+} or Lu^{3+}. However, the valine methyl protons in a diamagnetic protein all resonate in a region near 1.0 ppm. In Figure 40, a plot of the log of the paramagnetic shift of this methyl resonance versus the log of the temperature is presented. The absence of breaks in this plot indicates that no structural conformational changes occur over this temperature range. This plot also provides an indication of which term dominates the series (equation 6.3). The slope in Figure 40 is -3.0. Other choices of diamagnetic positions in the range of 0 to 2.0 ppm lead to values in the slope in the range of -2.8 to -3.2.

As an indication of the effects of different choices of diamagnetic position (equation 6.4) on other resonances, the calculated value of the diamagnetic position for the resonance at 29.80 ppm (at 302°K) was fairly sensitive and varied between 2.18 and 4.13 ppm as the diamagnetic position of the methyl resonance at 15.17 ppm was varied between 1 and 2 ppm. This difference represents only a 7% variation in the paramagnetic shift for the resonance. This analysis is the least solid of the experimental data, but the variations involved do not affect the final conclusions of this project. Only with a temperature dependence of T^{-3} or higher, do most of the shifted nuclei extrapolate at "infinite" temperatures to diamagnetic positions within the known spectrum of the diamagnetic form of the protein.

Although I cannot explain in detail the source of the high dependence on temperature of the lanthanide induced shifts, I have shown in this Chapter, that their observation as a function of temperature is useful in resolving overlapping peaks. In addition, I have demonstrated that the diamagnetic position contributions to the observed chemical shift positions can be evaluated, and the paramagnetic shifts, determined. In Chapter 9, I shall show how these paramagnetic shifts are used to probe the three dimensional structure of the protein.

VII. The Paramagnetic Shifts of Assigned Resonances

A. Introduction

As has been pointed out, the substitution of ytterbium for the calcium bound in the EF site of carp parvalbumin results in a series of resonances shifted far outside the ^{1}H NMR envelope of the diamagnetic form of the protein. Since the protein has high affinity metal binding sites, the spectra are in the slow exchange limit. The main advantage in this limit is that the chemical shifts and relaxation rates of the metal-protein complex are directly and accurately observed; the primary disadvantage is that peaks cannot be assigned. If resonances can be assigned in the diamagnetic and paramagnetic spectra, then an evaluation of the paramagnetic shifts of known nuclei is possible. (A recent paper discusses methods to tackle the problem of assigning ^{1}H NMR resonances (Campbell *et al*., 1975a)).

In this Chapter, I shall discuss the assignment of NMR resonances in the diamagnetic and paramagnetic spectra to the C-2 and C-4 protons of histidine 26, the N acetyl protons of the amino terminus, and the fluorine label of a chemically modified parvalbumin. Subsequently, I shall present the determination of the paramagnetic shifts of these assigned resonances. Later (Chapter 9), I shall describe how the paramagnetic shifts of these assigned resonances, as well as a number of methyl resonances, are used to evaluate and to check the principal elements and orientation of the magnetic susceptibility tensor. These parameters are necessary, because they contain the angular information required to analyze the observed paramagnetic shifts of parvalbumin in terms of the three dimensional structure of the metal binding site.

B. Experimental Procedures

NMR Procedures ^{1}H NMR spectra were obtained on a Bruker HXS-270 spectrometer operating in the Fourier transform mode with quadrature detection. The standard Hahn spin echo pulse sequence, $\pi/2 - \tau - \pi - \tau -$ acquisition (Campbell *et al.*, 1975c), where tau is equal to 25 ms, was used to accumulate data for the ^{1}H NMR spectra shown in Figures 41 and 44. Typical instrumental settings for these spectra were acquisition time 0.8 s, sweep width +/- 2.5 kHz, spectrum size 8192 data points, and 1 Hz linebroadening. Residual HDO was saturated using the pulsed homonuclear decoupling sequence. The sample temperature was 302°K. The ^{1}H NMR chemical shifts were measured relative to the principal resonance of DSS as an internal standard. The standard filters on the HXS-270 were replaced with Bessel filters (Ithaco, model 4302).

The ^{19}F NMR spectra were obtained at 254 MHz using the same spectrometer. Typical settings include 0.8 s acquisition time, sweep width +/- 2.5 kHz, spectrum size 8192 data points, and 5 Hz linebroadening. The sample temperature was 302°K. The ^{19}F chemical shifts were measured relative to 10 mM trifluoroacetic acid in D2O, pH 7.

Sample Preparation The protein and lanthanide solutions were prepared in the same manner as described in Chapter 3. The fluorinated protein was the generous gift of Drs. K. Bose and A. A. Bothner-By (Bose, 1979; Bose & Bothner-By, 1980). The one sulfhydryl of carp parvalbumin, cysteine 18, was chemically modified by the reagent 2-trifluoroacetoxymercuri-4-fluorophenol. The NMR samples were prepared by dissolving the lyophilized protein in the standard D2O buffer consisting of 15 mM Pipes, 0.15 M KCl, 10 mM DTT, 0.5 mM DSS, pH 6.6. pH measurements were made with an Ingold microelectrode (model 6030-04) attached to a Beckman Expandomatic SS-2 or Radiometer 26 pH meter. The pH values quoted are those observed and are not corrected for the deuterium isotope effect. Protein concentrations were determined by amino acid analysis after 24 hr of acid hydrolysis at 110°C.

Histidine Titration Analysis Since the protonation of the histidine is in the fast exchange limit, the observed chemical shift is the sum of the protonated (δ_{AH}) and unprotonated (δ_A) chemical shifts, weighted by their respective fractional populations ($f_{AH} + f_A = 1$) (for a review, see Markley, 1975).

$$\delta_{OBS} = \delta_{A}\left(1 - f_{AH}\right) + \delta_{AH}\left(f_{AH}\right) \qquad (7.1)$$

The equation above is rearranged to the following form:

$$\delta_{OBS} = \delta_{A} + \left(\delta_{AH} - \delta_{A}\right)\left(\frac{[AH]}{[A] + [AH]}\right) \qquad (7.2)$$

When the pH approached the isoelectric point of the protein, the protein started to come out of solution. Thus the complete titration of the sole histidine of parvalbumin 4.25, histidine 26, was unobservable since its pKa is quite low (~5). However, since this study focuses on the structure of the protein at pH's above the histidine pKa, the main object is to determine the deprotonated shift of histidine in the presence and absence of Yb^{3+}. Therefore for the analysis ($\delta_{AH} - \delta_{A}$) is assumed to be equal to standard values of 0.93 ppm and 0.42 ppm for the C-2 and C-4 histidine protons, respectively (Markley, 1975; Edwards & Sykes, 1978). The observed values of (δ_{A}) for the C-2 and C-4 protons are quite close to standard values, indicating a relatively normal and exposed histidine, supporting the above assumptions.

For the simple deprotonation, AH $\rightleftarrows$ H + A, Ka is equal to [H] [A]/[AH]. The above equation simplifies to:

$$\delta_{OBS} = \delta_A + \left(\delta_{AH} - \delta_A\right)\left(\frac{[H]}{K_a + [H]}\right) \qquad (7.3)$$

The pH titration data were fitted by non-linear least squares methods to this equation, resulting in values for both Ka and (δ_A).

C. Results

Titrations of Histidine 26 The C-2 and C-4 protons of His-26 of calcium saturated carp parvalbumin are preferentially observed in the Hahn spin echo spectra shown in Figure 41A because of their relatively narrow linewidths in comparison with the phenylalanine and NH resonances (Campbell *et al*., 1975c). They were further identified as histidine C-2 and C-4 protons by their standard chemical shifts (Markley, 1975; Edwards & Sykes, 1978), the fact that they are the only peaks in this region whose chemical shift is pH dependent over the range pH 5 to 8, and the fact that the C-2 proton shifts more (downfield) than the C-4 proton as a function of pH (see Figures 42 and 43). The observed and calculated data are presented in Tables 35 and 36.

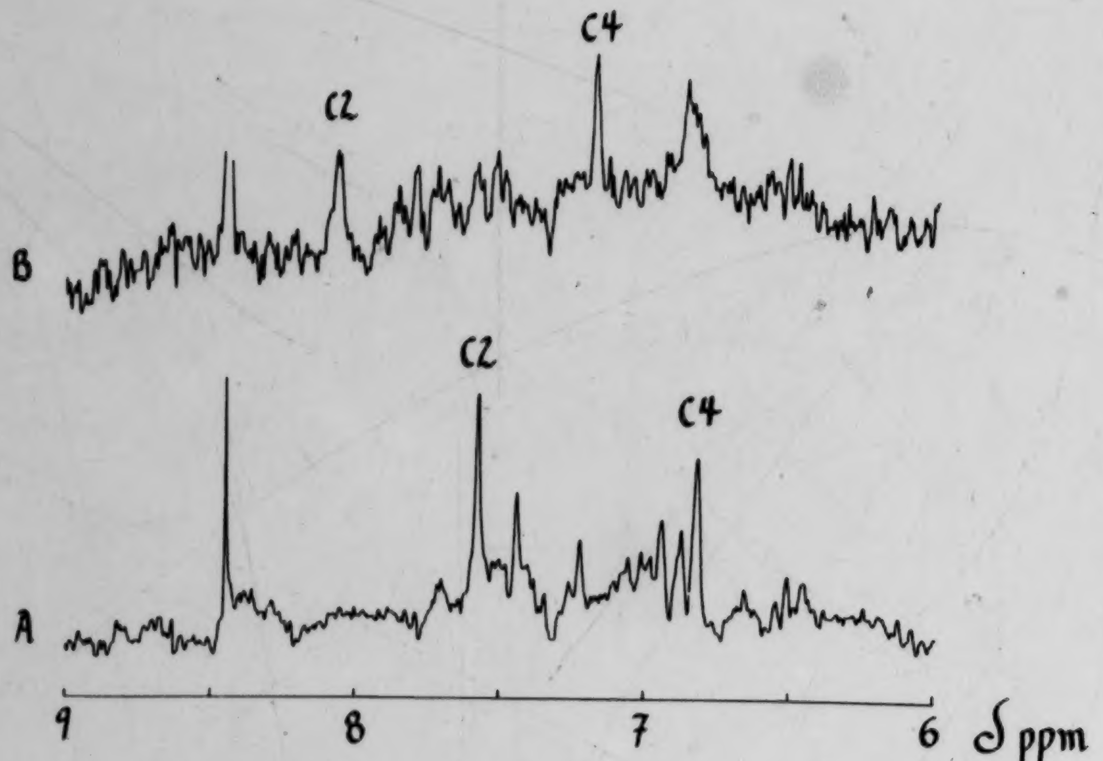

Figure 41. The downfield portion of the 270 MHz ^{1}NMR spectrum of carp parvalbumin.
A. 0.85 mM calcium saturated carp parvalbumin in 15 mM Pipes, 0.15 M KCl, 0.5 mM DSS, 10 mM DTT in D2O, pH 6.35, temperature=302°K.
B. 0.86 mM parvalbumin in 15 mM Pipes, 0.15 M KCl, 0.5 mM DSS, 10 mM DTT, in D2O, pH 6.28, temperature=302°K at a total Yb^{3+} to protein ratio of 0.80.
The symbols C2 and C4 indicate the resonances of protons bonded to carbons C2 and C4 on histidine 26. These spectra were collected by a Hahn spin echo pulse sequence as described in the Experimental Procedures section.

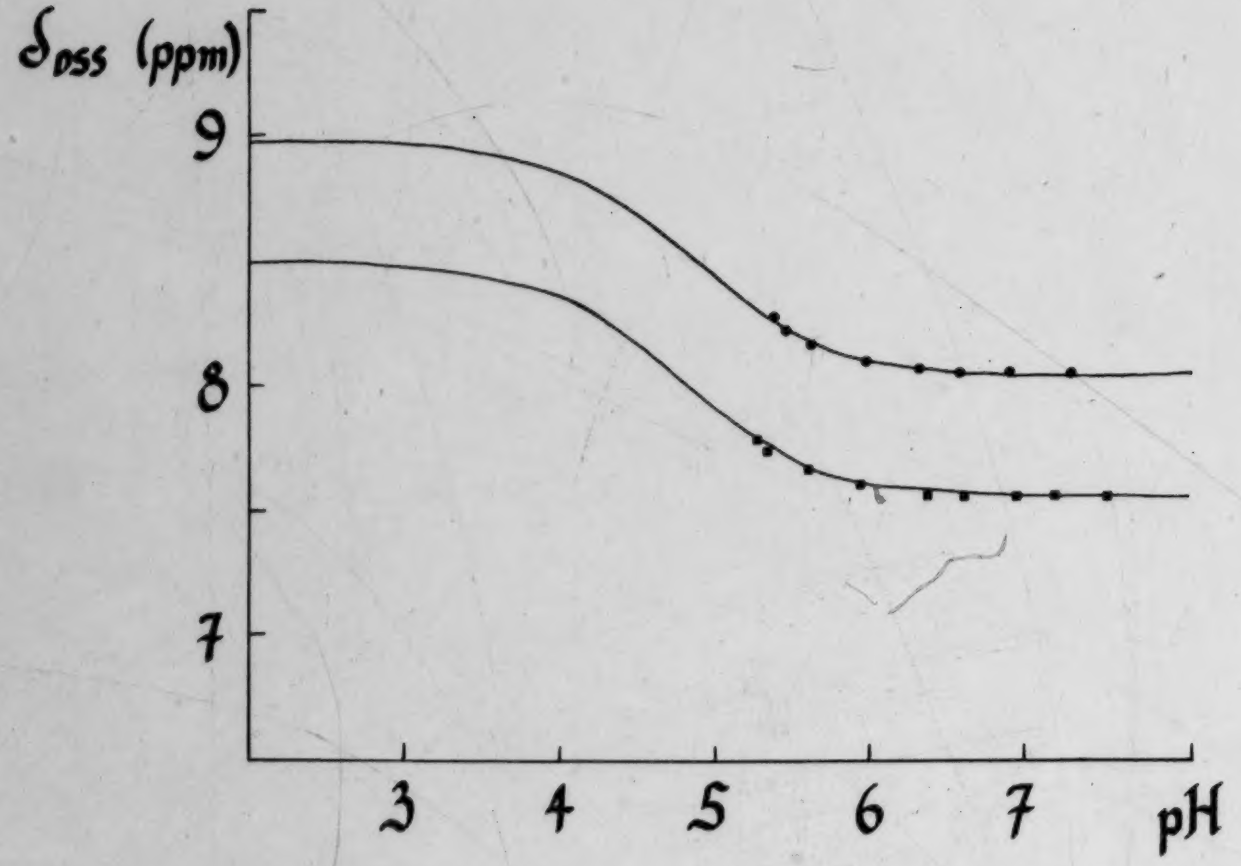

Figure 42. The pH titration curves of the C-2 protons of histidine 26 of carp parvalbumin in the presence of saturating levels of calcium (■) and in the presence of Yb^{3+} (●) at a total Yb^{3+} to total protein ratio of 0.80.

Table 35

The NMR Titration Data for the Histidine C-2 Protons of Carp Parvalbumin in the Presence of Ca^{2+} and Yb^{3+}

	pH	observed shift position[1]	calculated shift position[1]
$+Ca^{2+}$	5.25	7.791	7.778
	5.33	7.736	7.748
	5.59	7.671	7.672
	5.93	7.607	7.612
	6.35	7.576	7.578
	6.59	7.566	7.568
	6.92	7.564	7.561
	7.16	7.561	7.559
	7.50	7.560	7.557
$+Yb^{3+}$	5.36	8.268	8.245
	5.43	8.209	8.220
	5.60	8.155	8.170
	5.96	8.093	8.100
	6.28	8.067	8.069
	6.54	8.057	8.055
	6.84	8.052	8.047
	7.26	8.047	8.041

---

[1] in ppm.

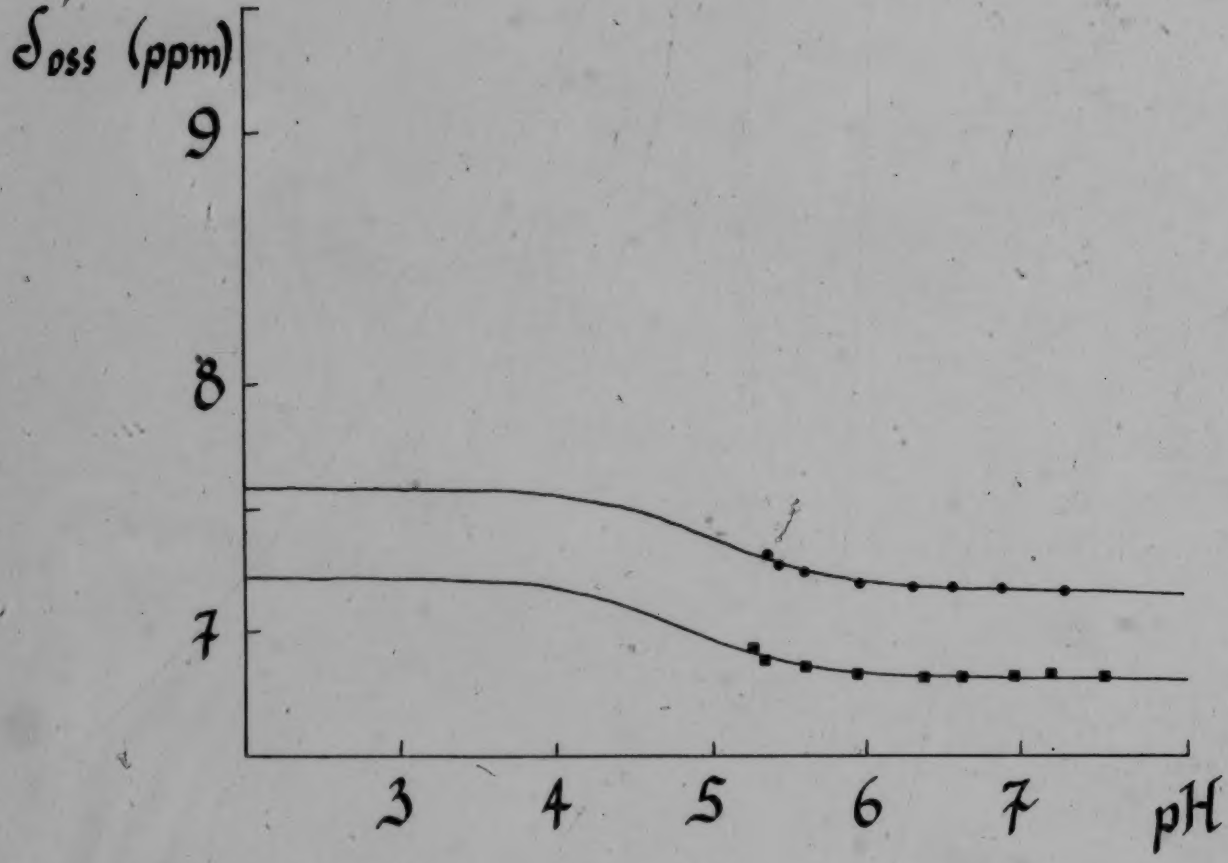

Figure 43. The pH titration curves of the C-4 protons of histidine 26 in the presence of saturating levels of calcium (■) and in the presence of Yb^{3+} (●) at a total Yb^{3+} to total protein ratio of 0.80.

Table 36

The NMR Titration Data for the Histidine C-4 Protons of Carp Parvalbumin in the Presence of Ca^{2+} and Yb^{3+}

	pH	observed shift position[1]	calculated shift position[1]
$+Ca^{2+}$	5.25	6.934	6.919
	5.33	6.894	6.905
	5.59	6.868	6.870
	5.93	6.832	6.842
	6.35	6.821	6.826
	6.59	6.815	6.822
	6.92	6.822	6.819
	7.16	6.827	6.817
	7.50	6.824	6.817
$+Yb^{3+}$	5.36	7.306	7.287
	5.43	7.265	7.273
	5.60	7.233	7.244
	5.96	7.194	7.201
	6.28	7.179	7.180
	6.54	7.171	7.171
	6.84	7.169	7.165
	7.26	7.165	7.161

[1] in ppm.

The resonance at 8.44 ppm is characteristic of the presence of formate ions (Dobson, 1975). These peaks were similarly identified in the spectrum of the protein with Yb^{3+} added to a level where the ratio of total Yb^{3+} to total protein, Yb/P, was 0.80 (Figure 41). Up to a ratio of Yb/P of 1/1, the Yb^{3+} has replaced only the Ca^{2+} bound to the EF hand of parvalbumin (Lee & Sykes, 1980c). The changes in chemical shift observed, which are presented in Table 37, therefore represent the shifts caused by the Yb^{3+} substituted in the EF calcium binding site. Also presented in Figures 42 and 43 are the least squares fits obtained with the assumptions described in the Experimental Procedures section. The pKa's obtained are presented in Table 37.

Observation of the proton NMR resonances of the N acetyl terminus The ^1H NMR spectrum of the acetyl resonance of carp parvalbumin is shown in Figure 44A. This spectrum was obtained using the Hahn spin echo sequence. Again the acetyl protons are preferentially observed because of their relatively narrow linewidth. The peak at 2.050 ppm relative to DSS has been previously assigned to the N acetyl resonance, and the peak at 1.90 ppm results from the presence of acetate ions in the sample (Parello *et al.*, 1974). For comparison, Parello and co-workers (Parello *et al.*, 1974) observe a chemical shift relative to DSS at 2.13 ppm for the N acetyl resonance of parvalbumin 4.25, and at 1.98 ppm for the acetate resonance. The addition of Yb^{3+} to a total Yb^{3+} to total protein ratio of 0.80, results in both

Table 37

Least Squares Analysis of the NMR pH Titration Data For The C-2 and C-4 Protons of Histidine 26 of Carp Parvalbumin

Proton	Metal Occupancy		pKa	Shift[1]
	CD	EF		
C-2	Ca^{2+}	Ca^{2+}	4.75	7.553
	Ca^{2+}	Yb^{3+}	4.82	8.038
C-4	Ca^{2+}	Ca^{2+}	4.80	6.816
	Ca^{2+}	Yb^{3+}	5.00	7.159

[1] observed chemical shift position in ppm.

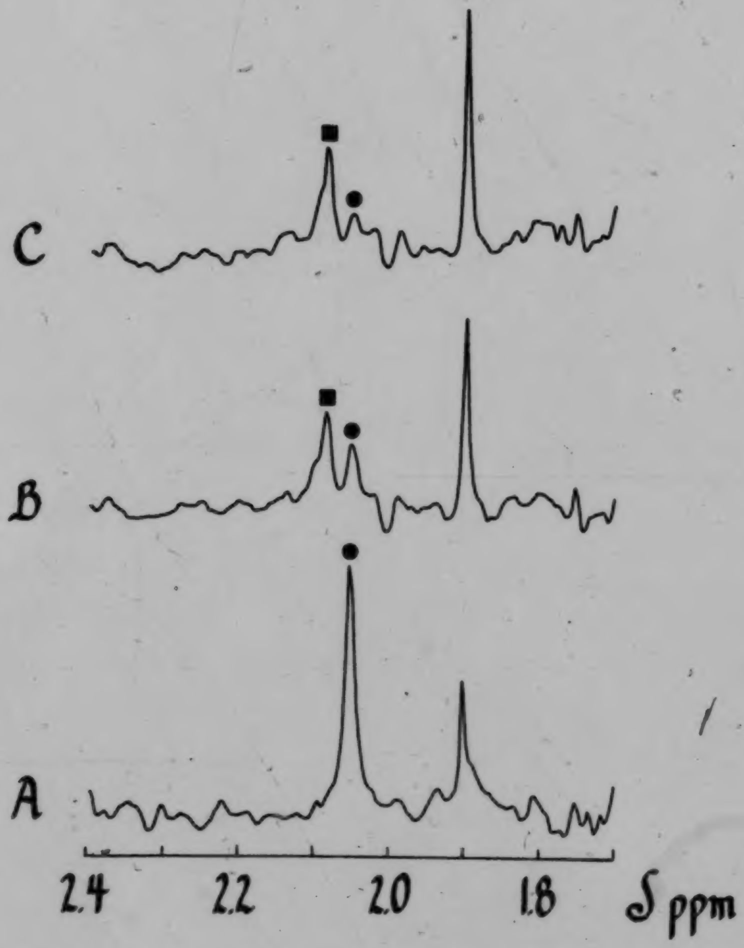

Figure 44. The 270 MHz proton NMR spectrum of the N-acetyl terminus of carp parvalbumin.
A. 0.85 mM calcium saturated carp parvalbumin in the standard D2O buffer, pH 6.72, temperature=301°K.
B. 0.86 mM carp parvalbumin in the standard D2O buffer pH 6.72, temperature=301°K, at a total Yb^{3+} to total protein ratio of 0.80.
C. 0.85 mM carp parvalbumin in the standard D2O buffer, pH 6.77, temperature=301°K, at a total Yb^{3+} to total protein ratio of 1.05. These spectra were acquired using a Hahn spin echo acquisition pulse sequence. The circles (●) indicate the free N-acetyl resonance; the squares (■) indicate the bound resonance.

a free and a bound resonance for the N acetyl protons as shown in Figure 44. This further demonstrates that the metal exchange rates are in the NMR slow exchange limit. A bound chemical shift of 2.083 ppm is observed.

Observation of the fluorine resonance of fluorinated carp parvalbumin The sulfhydryl of cysteine 18 of carp parvalbumin has been chemically modified with 2-trifluoroacetoxymercuri-4-fluorophenol (see Figure 45 insert). The ^{19}F NMR spectrum of the fluorinated protein is shown in Figure 45. In the presence of calcium, a free chemical shift of -49.541 ppm relative to a standard of 10 mM trifluoroacetic acid in D2O pH 7 is observed. When Yb^{3+} is added to a total Yb^{3+} to total protein ratio of 0.66, a resonance representing the fluorine label of the protein with Yb^{3+} bound in the EF Ca^{2+} is observed; its chemical shift is -49.381 ppm (Figure 45B). This represents a paramagnetic chemical shift of 0.16 ppm. Table 38 is a complete list of the paramagnetic shifts for the assigned resonances of carp parvalbumin.

D. Discussion

In Chapter 2, the strategy for the complete analysis of the lanthanide induced ^{1}H NMR chemical shifts of the ytterbium parvalbumin complex in order to determine the three dimensional structure of the EF binding site of carp parvalbumin in solution is outlined. In this Chapter, the focus is on the assignment of the resonances of the C-2 and

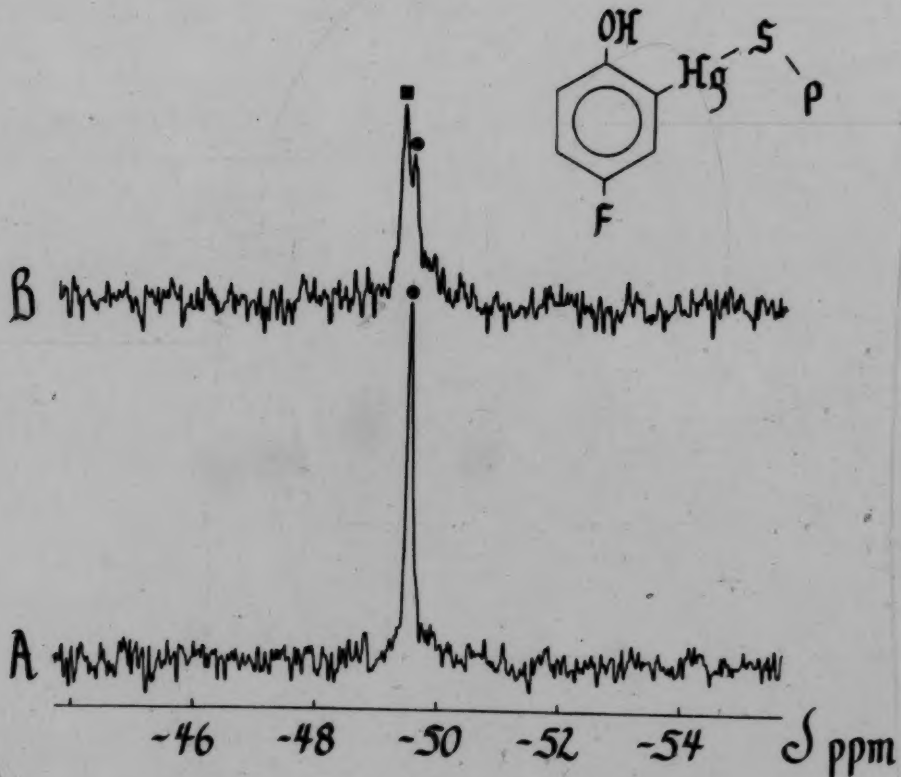

Figure 45. The 254 MHz ^{19}F NMR spectrum of carp parvalbumin chemically modified at cysteine 18 with the reagent 2-trifluoroacetoxymercuri-4-fluorophenol (see insert, P refers to the protein).
A. 0.84 mM fluorinated parvalbumin in 15 mM Pipes, 0.15 M KCl, 0.5 mM DSS, in D2O, pH 6.67, temperature=301°K.
B. 0.82 mM fluorinated parvalbumin in 15 mM Pipes, 0.15 M KCl, 0.5 mM DSS, in D2O, pH 6.65, temperature=301°K at a Yb^{3+} to total protein ratio of 0.66. The chemical shift is measured with respect to 10 mM trifluoroacetic acid in D2O, pH 7. The circles (•) indicate the free fluorine resonance. The squares (▪) indicate the bound fluorine resonance.

Table 38

Paramagnetic Shifts for the Assigned Resonances of Carp Parvalbumin[1]

resonance	diamagnetic position[2]	observed position[3]	paramagnetic shift
His 26 C-2	7.553	8.038	0.485
His 26 C-4	6.816	7.159	0.343
N acetyl	2.050	2.083	0.033
^{19}F label[4]	-49.541	-49.381	0.160

[1] All shifts are measured in ppm relative to DSS, unless otherwise noted.

[2] measured in the presence of Ca^{2+}.

[3] measured in the presence of Yb^{3-}.

[4] in ppm relative to 10 mM trifluoroacetic acid in D2O, pH 7.

C-4 protons of histidine 26, of the N acetylated terminus, and of a sulfhydryl specific fluorinated reporter group, bound to the protein in the diamagnetic and paramagnetic spectra.

The interpretation of NMR results is sometimes hindered by the difficulties in assigning NMR peaks to specific residues in a protein. If the protein contains a single particular residue whose resonance is clearly resolved, then the task of assignment is usually trivial. Since carp parvalbumin 4.25 contains only one histidine, the assignment of its C-2 and C-4 protons is possible.

The characteristic resonance frequency of the two resonances shown in Figure 41 and their chemical shift separation (0.74 ppm) are indicative of the C-2 and C-4 protons of histidine (Markley, 1975). In addition, these assigned C-2 and C-4 resonances of histidine 26 were followed as a function of pH (Figures 42 and 43). At low pH's, the shifts could not be accurately determined, due to the isoelectric precipitation of parvalbumin 4.25. The unusually low pKa's (~4.8) may result from the presence of the nearby positive charge, lys 27. According to X-ray crystallographic coordinates (Protein Data Bank) and proton generated coordinates (Lee & Sykes, 1980b), the lysine NZ to the His C-2 proton distance and the lysine NZ to the histidine C-4 distance are both equal to 6.3A. The least squares analysis also result in the determination of (δ_A) the deprotonated shifts of 7.553 ppm and 6.816 ppm for the

C-2 and C-4 protons respectively; these two observed shift positions represent the diamagnetic shift positions of the histidine resonances. Similar titration behavior has been observed for another parvalbumin isozyme (Birdsall *et al.*, 1979).

To determine the paramagnetic shifts of the histidine protons, Yb^{3+} was added to a sample at a total Yb^{3+} to total protein ratio of 0.80. Analyses similar to those outlined above, demonstrate no significant effect on the pKa's upon addition of Yb^{3+}. However, the chemical shifts differ from their diamagnetic positions (Figures 42 and 43). The chemical shifts (δ_A) for the C-2 and C-4 protons are 8.038 and 7.159 ppm, respectively; the difference between these values and the diamagnetic positions is a measure of the paramagnetic shift contribution. The paramagnetic shifts of the C-2 and C-4 protons are 0.485 and 0.343 ppm respectively.

The resonance of the amino terminal acetyl group was also observed. Since it is the only such group in the protein, its resonance is clearly resolved (Figure 44A) in the region of 2 ppm and easily assigned. This resonance has also been observed in a number of other studies of parvalbumin 4.25 (Parello *et al.*, 1974) and of other parvalbumin isozymes (Birdsall *et al.*, 1979; Cave *et al.*, 1979b). In the presence of Ca^{2+}, the N acetyl resonance is found at 2.050 ppm; in the presence of Yb^{3+}, 2.083 ppm. The difference between these two values represents a paramagnetic shift of 0.033 ppm. In the presence of Yb^{3+}, both forms of the resonances are present in the spectrum (Figures 44B and 44C); this again demonstrates that the metal exchange rates are in the slow exchange limit. From the chemical shift difference between the free (Ca^{2+}) and bound (Yb^{3+}) resonances, and the limits defined by the slow exchange limit, a minimum lifetime of 18 ms is calculated.

Another method for assigning NMR resonances is to chemically modify the protein (Snyder *et al.*, 1975). If the modification reaction is specific, a single, unique probe can be introduced into the protein. The sole sulfhydryl of carp parvalbumin, cys 18, has been so modified. Since it is the only ^{19}F label on the protein, the assignment of its ^{19}F NMR resonance is facilitated.

In this Chapter, I have shown that the unique resonances of carp parvalbumin and of a fluorinated parvalbumin can be easily assigned, and their paramagnetic shifts, determined. The paramagnetic shifts observed are small (0.033 to 0.485 ppm), for the nuclei are far removed from the metal (13.6 Å to 20.1 Å). However the determination of these shifts is essential for the proposed NMR methodology. In Chapter 9, I shall describe how the paramagnetic shifts of the assigned resonances can be used to determine and to check the principal elements and orientation of the magnetic susceptibility tensor.

VIII. Data Summary

A. Introduction

In this chapter, I shall present a summary of the observed data known to date. The total spectrum of the ytterbium parvalbumin complex, presented in Figure 46, is divided into three major Regions I, II, and III.

B. Region I

Figure 47, an expansion of Region I, defines the nomenclature used. The labelling of all resonances is consistent with the system presented in Chapter 5. Table 39 is a summary of the chemical shift data for resonances in Region I; Table 40, the T2 and distance data; Table 41, the T1 and additional data.

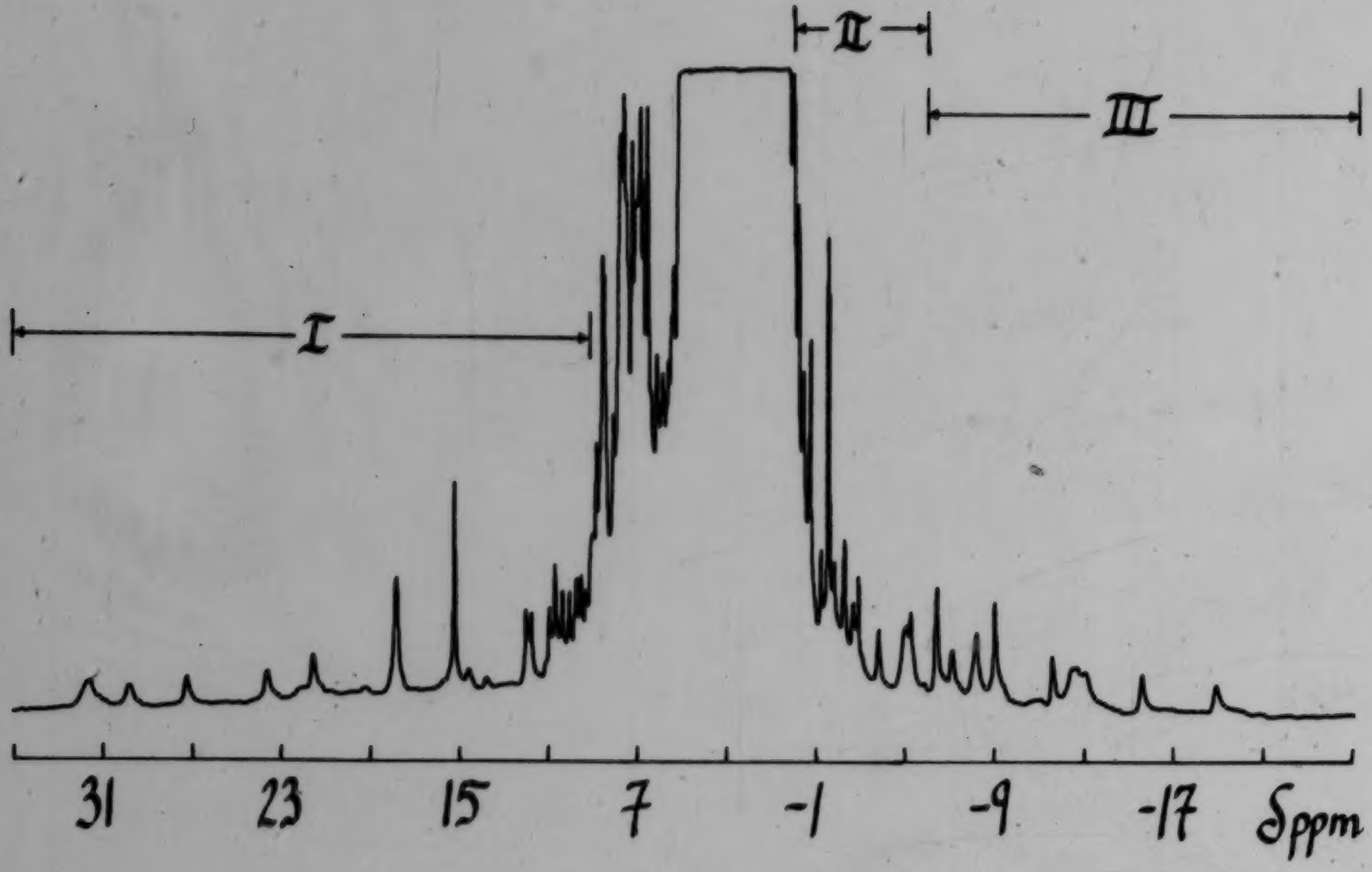

Figure 46. The ^1H NMR spectrum of the Yb^{3+} parvalbumin complex divided into the three Regions I, II, and III. Expansions of these Regions are presented in Figures 47 to 49. The parameters of data acquisition are listed in Figure 29.

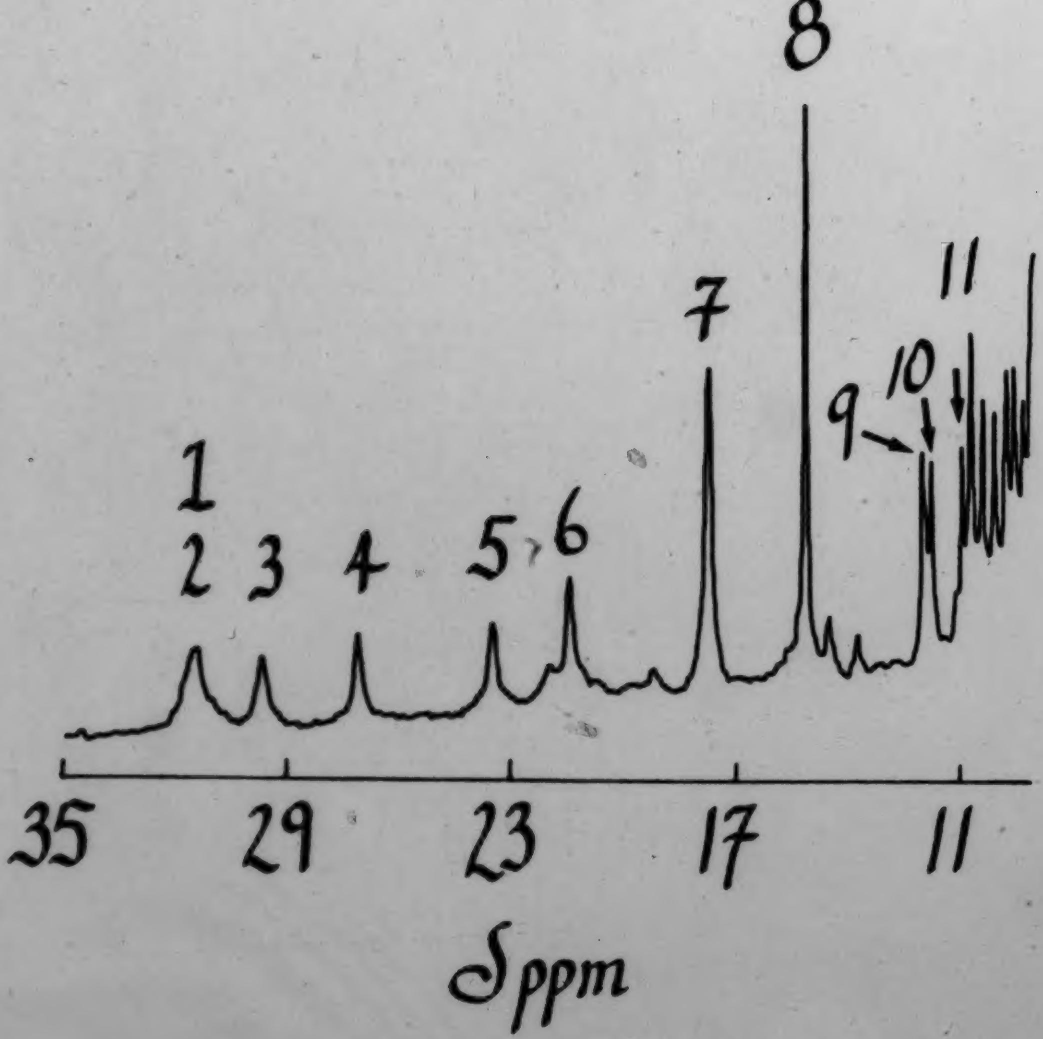

Figure 47. Region I of the ^1H NMR spectrum of the Yb^{3+} parvalbumin complex. The limits of Region I are 35 to 9 ppm. The nomenclature used here is consistent with that presented in Figure 30.

Table 39

Chemical Shifts of the Downfield Shifted Resonances in Region I of the ^1H NMR Spectrum of the Yb^{3+} Parvalbumin Complex[1]

Resonance[2]	Observed Position[3]	Diamagnetic Position[4]	Paramagnetic Shift[5]
1	31.61	9.35	22.26
2	31.61	5.84	25.77
3	29.80	2.18	27.62
4	27.16	7.06	20.10
5	23.57	1.48	22.09
6	21.50	2.60	18.90
7	17.79	0.10	17.69
8	15.17	1.00	14.17
9	12.00	8.86	3.14
10	11.75	5.13	6.62
11	10.69	3.87	6.82

---

[1] See Figure 46 for the defined limits of region I.
[2] Nomenclature corresponds to data presented in Figure 47.
[3] Observed chemical shift positions (in ppm) for the Yb^{3+} parvalbumin complex at 302°K (Chapter 5).
[4] These diamagnetic positions (in ppm) were determined by methods described in Chapter 6.
[5] These paramagnetic shifts (in ppm) were determined by subtracting the diamagnetic positions of a given resonance (column 3) from its observed chemical shift position (column 2).

Table 40

Metal to Proton Distances of the Downfield Shifted Resonances in Region I of the ^{1}H NMR Spectrum of the Yb^{3+} Parvalbumin Complex[1]

Resonance[2]	1/T2┌*OBS*┐[3]	1/T2┌*DD*┐[4]	1/T2┌*X*┐[5]	r[6]
1	ND	ND	ND	ND
2	ND	ND	ND	ND
3	325	184	141	5.8 -0.1/+0.1
4	230	91	139	5.9 -0.1/+0.1
5	263	161	102	6.2 -0.1/+0.2
6	235	157	78	6.5 -0.2/+0.3
7	199	98	101	6.2 -0.2/+0.2
8	95	71	24	7.9 -0.7/+1.8
9	ND	ND	ND	ND
10	112	100	12	8.8 -1.2/+1.4
11	ND	ND	ND	ND

[1] See Figure 46 for the defined limits of Region I. ND indicates not determined.

[2] Nomenclature corresponds to data presented in Figure 47.

[3] 1/T2┌*OBS*┐ (in s^{-1}) are the observed spin spin relaxation rates (Chapter 5).

[4] 1/T2┌*DD*┐ (in s^{-1}) are the calculated dipole dipole contributions to the observed spin lattice relaxation rates (Chapter 5) measured by linear least squares methods.

[5] 1/T2┌*X*┐ (in s^{-1}) was measured by linear least squares methods. 1/T2┌*DD*┐ was subtracted from the best fit 1/T2┌*OBS*┐ at 270 MHz to yield 1/T2┌*X*┐.

[6] r, the metal to proton distance (Table 13).

Table 41

Additional Data of the Downfield Shifted Resonances in Region I of the ^{1}H NMR Spectrum of the Yb^{3+} Parvalbumin Complex[1]

Resonance[2]	T1[3]	Proton Type[4]	EF[5]	CD[6]
1	ND	CH	+	ND
2	.032 ± .002	CH	+	ND
3	.054 ± .004	CH	+	-
4	.046 ± .003	CH	+	+
5	.046 ± .003	CH	+	+
6	.043 ± .003	CH	+	+
7	.046 ± .001	CH3	+	+
8	.145 ± .008	CH3	+	+
9	.408 ± .028	NH	+	ND
10	.347 ± .031	CH	+	ND
11	ND	NH	+	ND

---

[1] See Figure 46 for the defined limits of Region I. ND indicates not determined.

[2] Nomenclature corresponds to data presented in Figure 47.

[3] The observed T1's (in s) were measured at 270 MHz by inversion recovery pulse sequences (Chapter 5).

[4] CH3 refers to methyl protons; CH, to carbon bound protons: NH, to nitrogen bound protons. The temperature dependence of the shifted resonances (Chapter 6) has been used to sort out overlapping peaks and to confirm the contributions to the areas of overlapping peaks.

[5] A + sign indicates that the resonance is in the vicinity of the EF site; a - sign indicates that it is not.

[6] A - sign indicates that the resonance is in the vicinity of the CD site; a - sign indicates that it is not.

C. Region II

Figure 48 is an expansion of Region II. Additional resonances have been labelled. Table 42 is a summary of the chemical shift data for selected resonances in Region II; Table 43, T2 and distance data; Table 44, T1 and additional data.

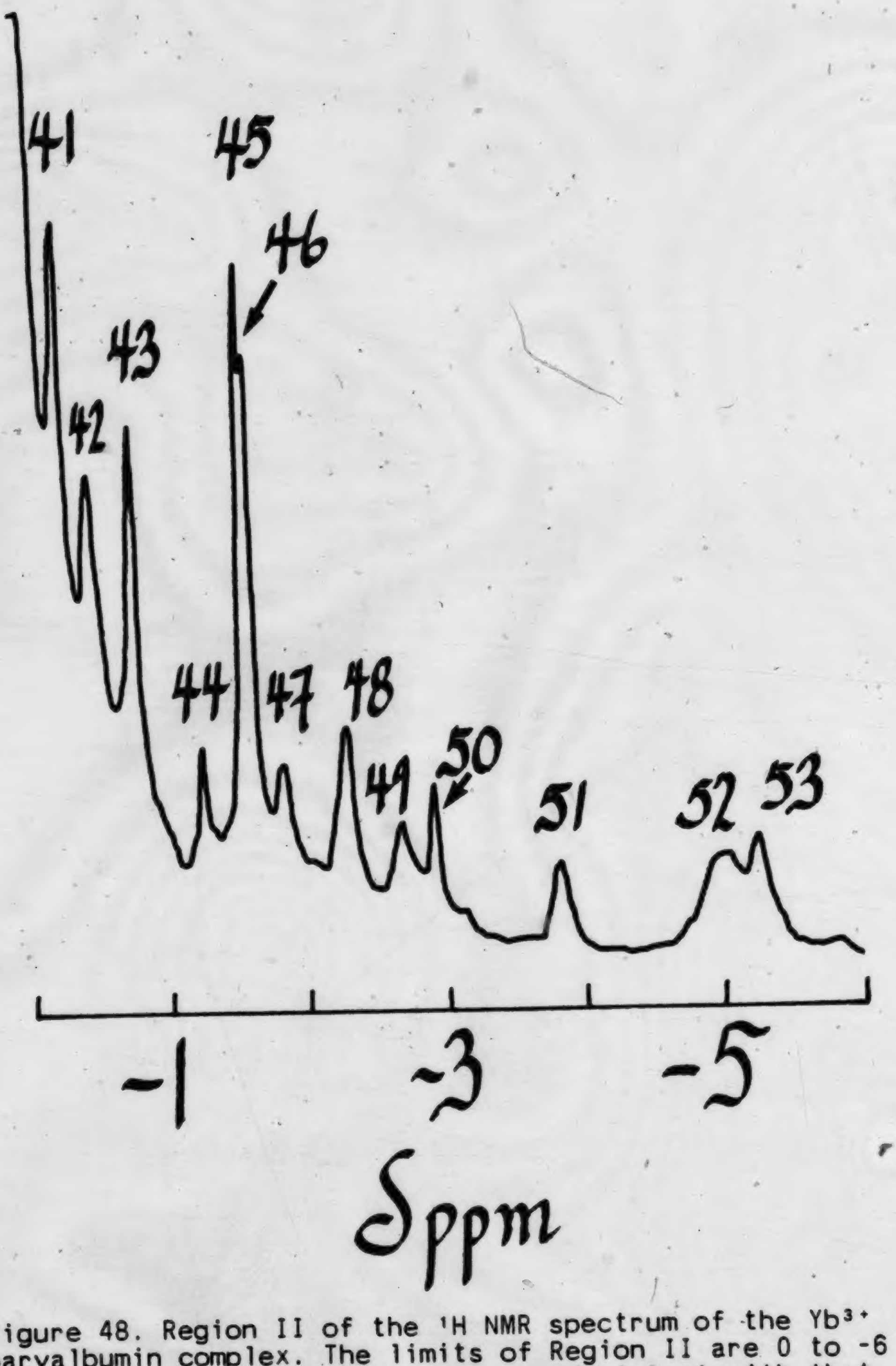

Figure 48. Region II of the ^{1}H NMR spectrum of the Yb^{3+} parvalbumin complex. The limits of Region II are 0 to -6 ppm. the nomenclature used here is consistent with that presented in Figure 30; however additional resonances have been labelled.

Table 42

Chemical Shifts of the Upfield Shifted Resonances in Region II of the ^1H NMR Spectrum of the Yb^{3+} Parvalbumin Complex[1]

Resonance[2]	Observed Position[3]	Diamagnetic Position[4]	Paramagnetic Shift[5]
41	-0.27	1.35	-1.62
42	ND	ND	ND
43	-0.80	-0.43	-0.37
44	ND	ND	ND
45	-1.59	0.31	-1.90
46	-1.63	-0.19	-1.44
47	ND	ND	ND
48	ND	ND	ND
49	-2.33	3.60	-5.93
50	-2.95	4.24	-7.19
51	-3.84	0.07	-3.91
52	-4.99	5.76	-10.75
53	-5.26	3.82	-9.08

[1] See Figure 46 for the defined limits of region II. ND indicates not determined.

[2] Nomenclature corresponds to data presented in Figure 48.

[3] Observed chemical shift positions (in ppm) for the Yb^{3+} parvalbumin complex at 302°K (Chapter 5).

[4] These diamagnetic positions (in ppm) were determined by methods described in Chapter 6.

[5] These paramagnetic shifts (in ppm) were determined by subtracting the diamagnetic positions of a given resonance (column 3) from its observed chemical shift position (column 2).

Table 43

Metal to Proton Distances of the Upfield Shifted Resonances in Region II of the ^{1}H NMR Spectrum of the Yb^{3+} Parvalbumin Complex[1]

Resonance[2]	$1/T2_{OBS}$[3]	$1/T2_{DD}$[4]	$1/T2_{X}$[5]	r[6]
41	ND	ND	ND	ND
42	ND	ND	ND	ND
43	ND	ND	ND	ND
44	ND	ND	ND	ND
45	ND	ND	ND	ND
46	ND	ND	ND	ND
47	ND	ND	ND	ND
48	ND	ND	ND	ND
49	ND	ND	ND	ND
50	ND	ND	ND	ND
51	116	90	26	7.7 -0.6/+1.5
52	ND	ND	ND	ND
53	ND	ND	ND	ND

---

[1] See Figure 46 for the defined limits of Region II. ND indicates not determined.

[2] Nomenclature corresponds to data presented in Figure 48.

[3] $1/T2_{OBS}$ (in s^{-1}) are the observed spin spin relaxation rates (Chapter 5).

[4] $1/T2_{DD}$ (in s^{-1}) are the calculated dipole dipole contributions to the observed spin lattice relaxation rates (Chapter 5) measured by linear least squares methods.

[5] $1/T2_{X}$ (in s^{-1}) was measured by linear least squares methods. $1/T2_{DD}$ was subtracted from the best fit $1/T2_{OBS}$ at 270 MHz to yield $1/T2_{X}$.

[6] r, the metal to proton distance (Table 13).

Table 44

Additional Data of the Upfield Shifted Resonances in Region II of the ^1H NMR Spectrum of the Yb^{3+} Parvalbumin Complex[1]

Resonance[2]	T1[3]	Proton Type[4]	EF[5]	CD[6]
41	ND	CH3	+	ND
42	ND	CH	+	ND
43	ND	CH3	+	ND
44	ND	CH	+	+
45	ND	CH3	+	ND
46	ND	CH3	+	ND
47	ND	CH	+	-
48	ND	CH	+	+
49	ND	CH	+	+
50	ND	CH	+	+
51	.240 ± .020	CH	+	+
52	ND	CH	+	-
53	ND	CH	+	-

---

[1] See Figure 46 for the defined limits of Region II. ND indicates not determined.

[2] Nomenclature corresponds to data presented in Figure 48.

[3] The observed T1's (in s) were measured at 270 MHz by inversion recovery pulse sequences (Chapter 5).

[4] CH3 refers to methyl protons; CH, to carbon bound protons; NH, to nitrogen bound protons. The temperature dependence of the shifted resonances (Chapter 6) has been used to sort out overlapping peaks and to confirm the contributions to the areas of overlapping peaks.

[5] A + sign indicates that the resonance is in the vicinity of the EF site; a - sign indicates that it is not.

[6] A - sign indicates that the resonance is in the vicinity of the CD site; a - sign indicates that it is not.

D. Region III

Figure 49 is an expansion of Region III. Table 45 is a summary of the chemical shift data for selected resonances in Region III; Table 46, T2 and distance data; Table 47, T1 and additional data.

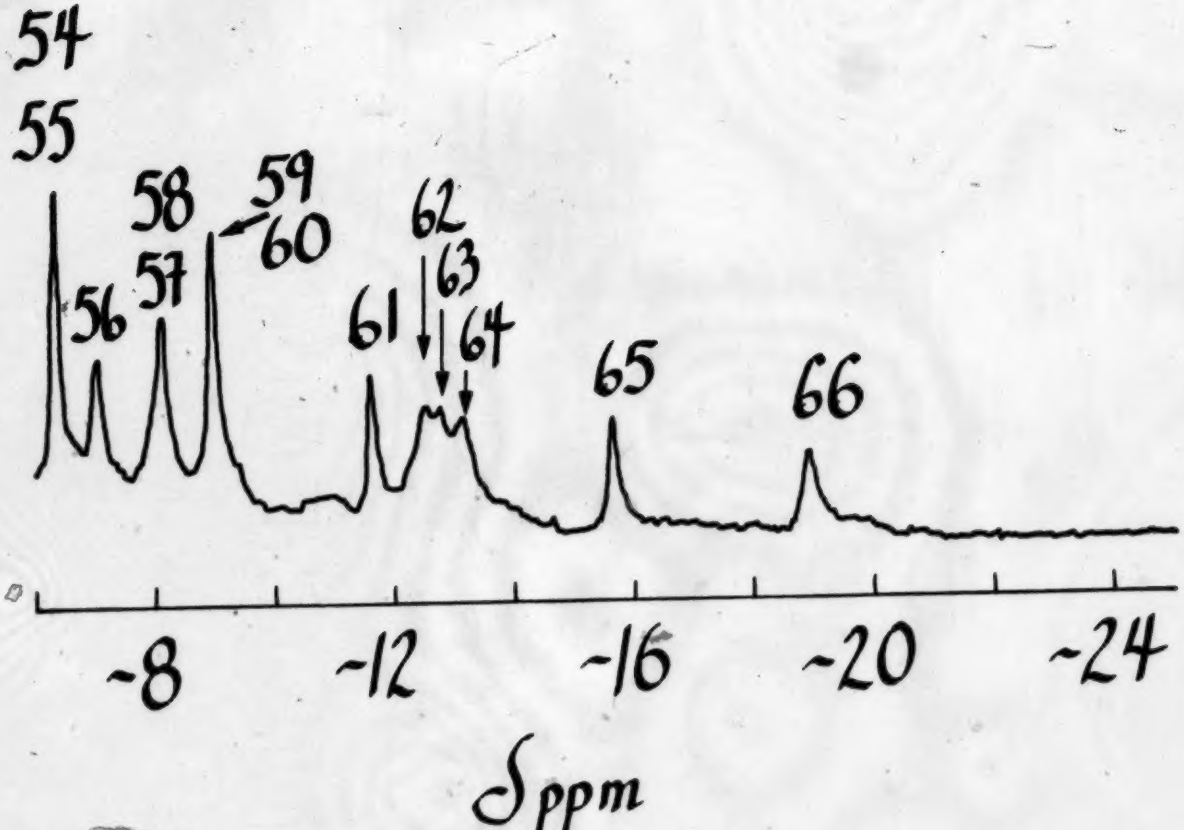

Figure 49. Region III of the ^1H NMR spectrum of the Yb^{3+} parvalbumin complex. The limits of Region III are -6 to -25 ppm. The nomenclature used here is consistent with that presented in Figure 31.

Table 45

Chemical Shifts of the Upfield Shifted Resonances in Region III of the ^1H NMR Spectrum of the Yb^{3+} Parvalbumin Complex[1]

Resonance[2]	Observed Position[3]	Diamagnetic Position[4]	Paramagnetic Shift[5]
54	-6.41	0.87	-7.28
55	-6.41	4.02	-10.43
56	-7.11	-0.43	-7.54
57	-8.19	1.12	-9.31
58	-8.19	6.34	-14.53
59	-9.02	0.52	-9.54
60	-9.02	-1.49	-7.53
61	-11.63	1.23	-12.86
62	-12.52	1.64	-14.16
63	ND	ND	ND
64	-13.16	5.92	-19.06
65	-15.65	0.55	-16.20
66	-18.90	-4.30	-14.60

---

[1] See Figure 46 for the defined limits of region III.

[2] Nomenclature corresponds to data presented in Figure 49.

[3] Observed chemical shift positions (in ppm) for the Yb^{3+} parvalbumin complex at 302°K (Chapter 5).

[4] These diamagnetic positions (in ppm) were determined by methods described in Chapter 6.

[5] These paramagnetic shifts (in ppm) were determined by subtracting the diamagnetic positions of a given resonance (column 3) from its observed chemical shift position (column 2).

Table 46

Metal to Proton Distances of the Upfield Shifted Resonances in Region III of the ^{1}H NMR Spectrum of the Yb^{3+} Parvalbumin Complex[1]

Resonance[2]	$1/T2_{OBS}$[3]	$1/T2_{DD}$[4]	$1/T2_{X}$[5]	r[6]
54	ND	ND	ND	ND
55	ND	ND	ND	ND
56	195	93	102	6.2 -0.2/+0.2
57	ND	ND	ND	ND
58	ND	ND	ND	ND
59	ND	ND	ND	ND
60	ND	ND	ND	ND
61	143	97	46	7.0 -0.4/+0.6
62	ND	ND	ND	ND
63	ND	ND	ND	ND
64	ND	ND	ND	ND
65	194	127	67	6.6 -0.2/+0.3
66	235	56	179	5.6 -0.1/+0.1

---

[1] See Figure 46 for the defined limits of Region III. ND indicates not determined.

[2] Nomenclature corresponds to data presented in Figure 49.

[3] $1/T2_{OBS}$ (in s^{-1}) are the observed spin spin relaxation rates (Chapter 5).

[4] $1/T2_{DD}$ (in s^{-1}) are the calculated dipole dipole contributions to the observed spin lattice relaxation rates (Chapter 5) measured by linear least squares methods.

[5] $1/T2_{X}$ (in s^{-1}) was measured by linear least squares methods. $1/T2_{DD}$ was subtracted from the best fit $1/T2_{OBS}$ at 270 MHz to yield $1/T2_{X}$.

[6] r, the metal to proton distance (Table 13).

Table 47

Additional Data of the Upfield Shifted Resonances in Region III of the ^{1}H NMR Spectrum of the Yb^{3+} Parvalbumin Complex[1]

Resonance[2]	T1[3]	Proton Type[4]	EF[5]	CD[6]
54	ND	CH	+	+
55	ND	CH	+	+
56	.138 ± .012	CH	+	-
57	ND	CH	+	+
58	ND	CH	+	+
59	ND	CH	+	+
60	ND	CH	+	+
61	.252 ± .011	CH	+	+
62	ND	CH	+	+
63	ND	CH	+	+
64	ND	CH	+	-
65	.164 ± .011	CH	+	+
66	.098 ± .012	CH	+	+

[1] See Figure 46 for the defined limits of Region III. ND indicates not determined.
[2] Nomenclature corresponds to data presented in Figure 49.
[3] The observed T1's (in s) were measured at 270 MHz by inversion recovery pulse sequences (Chapter 5).
[4] CH3 refers to methyl protons; CH, to carbon bound protons; NH, to nitrogen bound protons. The temperature dependence of the shifted resonances (Chapter 6) has been used to sort out overlapping peaks and to confirm the contributions to the areas of overlapping peaks.
[5] A + sign indicates that the resonance is in the vicinity of the EF site; a - sign indicates that it is not.
[6] A - sign indicates that the resonance is in the vicinity of the CD site; a - sign indicates that it is not.

IX. The Elucidation of the Principal Axis System

A. Introduction

In Chapter 7, I discussed the assignment of the NMR resonances of the C-2 and C-4 protons of histidine 26, of the N acetyl protons of the amino terminus, and of a fluorine label in the diamagnetic spectrum of carp parvalbumin in the presence of Ca^{2+}, and in the paramagnetic spectrum of the protein in the presence of Yb^{3+}. In this Chapter, I shall demonstrate how these paramagnetic shifts and the shifts of a number of methyl resonances are used to evaluate and to check the principal elements and orientation of the magnetic susceptibility tensor of the Yb^{3+} parvalbumin complex, and to view the coordination geometry of the lanthanide in the EF binding site. With these parameters, I am able to compare the observed spectrum of the nuclei surrounding the EF calcium binding site of parvalbumin with that calculated from the X-ray crystallographic structure. The implications of these results on the protein structure are discussed.

B. Theory of the Lanthanide Induced Shifts

The paramagnetic shifts result from the influence of the lanthanide 4f electrons and consist of two contributions, dipolar and contact shifts. In this application, contact shifts are neglected (Chapter 5).

Dipolar Shifts The first contribution, the dipolar (or pseudocontact) shift results from the 'through space' interaction between the magnetic moment of the unpaired electrons of the metal and neighboring, interacting nuclei. The magnitude of the pseudocontact shift is a function of the metal ion involved and of the geometry of the nucleus relative to the metal ion. The paramagnetic shift of the nucleus from its diamagnetic position written in the principal axis system of the magnetic susceptibility tensor of the metal ion (Bleaney, 1972) is given in equation 9.1.

$$\delta_p = A1 \left\langle \frac{3\cos^2\Theta - 1}{r^3} \right\rangle + A2 \left\langle \frac{\sin^2\Theta \cos 2\phi}{r^3} \right\rangle \qquad (9.1)$$

$$= A1 \cdot G1 + A2 \cdot G2$$

θ, ϕ, and r are the spherical coordinates of the nucleus in the principal axis system (Figure 50). The brackets < > indicate that the appropriate time averaged geometry of the nucleus must be used. A1 and A2 are ligand field parameters which are related to the principal elements of the magnetic susceptibility tensor (equations 9.2 and 9.3).

$$A1 = (\chi_{zz} - \bar{\chi})/2 \qquad (9.2)$$

$$A2 = (\chi_{xx} - \chi_{yy})/2 \qquad (9.3)$$

where χ_{xx}, χ_{yy}, and χ_{zz} and $\bar{\chi}$ are the principal elements and

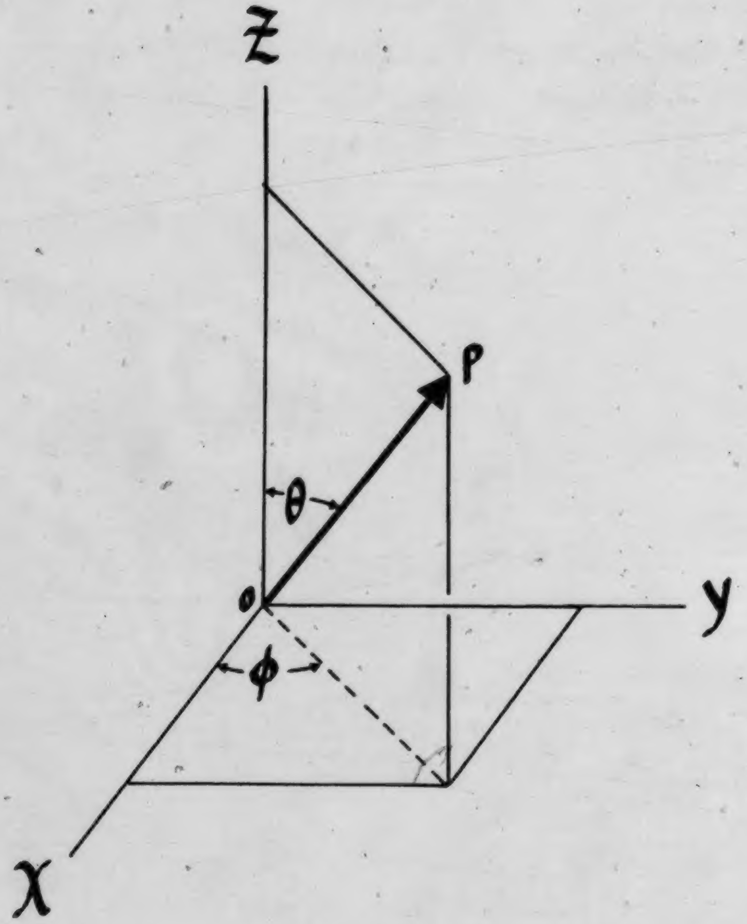

Figure 50. Definitions of the spherical coordinates. The three values r, θ, and ϕ define the spherical coordinates of a nucleus P in the principal axis system of the magnetic susceptibility tensor of the metal O. The length of the vector OP is r.

trace respectively of the magnetic susceptibility tensor. Three situations may arise in relating the shift to geometry.

1. If $X_{xx}=X_{yy}=X_{zz}$, the symmetry is cubic. Since both A1 and A2 are equal to zero, no pseudocontact shifts are observed; equation 9.1 is equal to zero.

2. If $X_{xx}=X_{yy}\neq X_{zz}$, the condition is known as axial symmetry. Since $X_{xx}=X_{yy}$, the value of A2 is equal to zero. Thus equation 9.1 is simplified, for the second term is neglected; the shift is then a function of only two variables, the distance r, and the angle θ. The pseudocontact shifts for different nuclei (i and j) in a given molecule can then be expressed as a ratio of the two shifts (equation 9.4), thereby eliminating A1.

$$\frac{\delta_p^i}{\delta_p^j} = \frac{\left(3\cos^2\theta_i - 1\right) / r_i^3}{\left(3\cos^2\theta_j - 1\right) / r_j^3} \tag{9.4}$$

If the axial symmetry assumption is valid, the ratios can then be analyzed to determine the three dimensional structure of a molecule.

3. If $X_{xx}\neq X_{yy}\neq X_{zz}$, the symmetry is called non-axial. In this case, shift ratios may not be used in the analysis, since the constant A2 is non-zero. Because there are no assumptions made, equation 9.1 is not simplified; the complete expression of equation 9.1 must then be used to analyze the shifts in terms of a three dimensional

structure.

The determination of the principal elements and orientation of the magnetic susceptibility tensor is essential, because they contain the unknowns required to relate the paramagnetic shift to the three dimensional structure of the protein metal binding site. The aim is to evaluate the orientation of the principal axis system of the magnetic susceptibility tensor and the two parameters A1 and A2. In this analysis, neither cubic nor axial symmetry is assumed, however, the following assumptions are made. Yb^{3+} is in the same position as the Ca^{2+}. Coordinates of ^{1}H nuclei can be calculated based upon the coordinates observed by X-ray crystallographic methods, standard C-H and N-H bond lengths, and C-C-H and C-N-H bond angles. There are five unknowns (Marinetti *et al.*, 1977): three to describe the orientation of the principal axis system and two, to define the parameters A1 and A2. In this study, the orientation of the principal axis system is described in terms of direction cosines L1, L2, and L3 (with $L1^2 + L2^2 + L3^2 = 1$) (Figure 51), relative to the X-ray axis system, and of a rotation axis and a rotation angle α (alpha) for the transformation of the coordinates of the protons from the X-ray structure axis system to a new axis system. The set of unknowns will be represented as (L1, L2, and alpha).

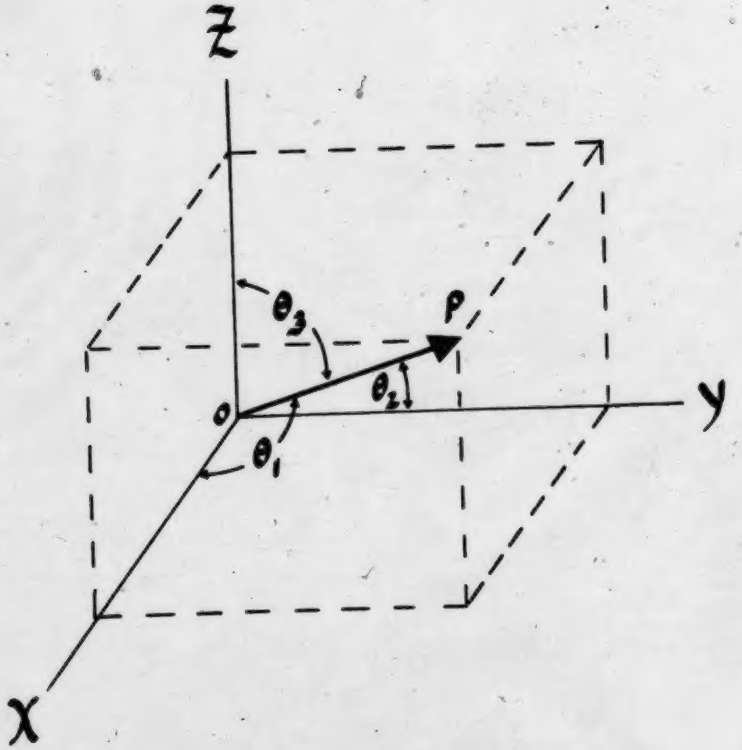
Z
Y
X
0
P
θ_1
θ_2
θ_3

Figure 51. Definitions of the direction cosines. A point in space P is defined by the three angles L1, L2, and L3 (or θ1, θ2, and θ3 as shown in this figure).

C. Experimental Procedures

Data Acquisition The NMR samples were prepared and the data acquired according to the methods described in the experimental procedures section of Chapter 5. Experiments with spectral widths of ± 50 KHz insure that all the resonances observable are present within the ±10 KHz sweep width range used in this study.

Fitting Procedure A computer program was written to determine the best fit of the five unknowns, A1, A2, L1, L2, and alpha, to the paramagnetic shifts of the C-2 and C-4 protons of histidine 26, of the N acetyl terminus, and of a number of methyl resonances. The paramagnetic shift of a fluorine probe was used to check the final calculation. The fitting procedure is described below.

Several attempts were made to solve the relationship between the observed shifts of nuclei near the metal ion and their geometry with respect to the metal ion. This requires the determination of five unknowns; L1, L2, and alpha specify the orientation of the principal axis system of the magnetic susceptibility tensor, centered at the metal; A1 and A2 are two scaling parameters which are related to the principal elements of the tensor.

One useful set of resonances is the six shifted methyl resonances (Figure 52). There are only seven methyls within 10A of the EF metal binding site. Two of these methyls are shifted more downfield than 10 ppm, and appear at 17.79 ppm (paramagnetic shift of 17.69 ppm) and 15.17 ppm

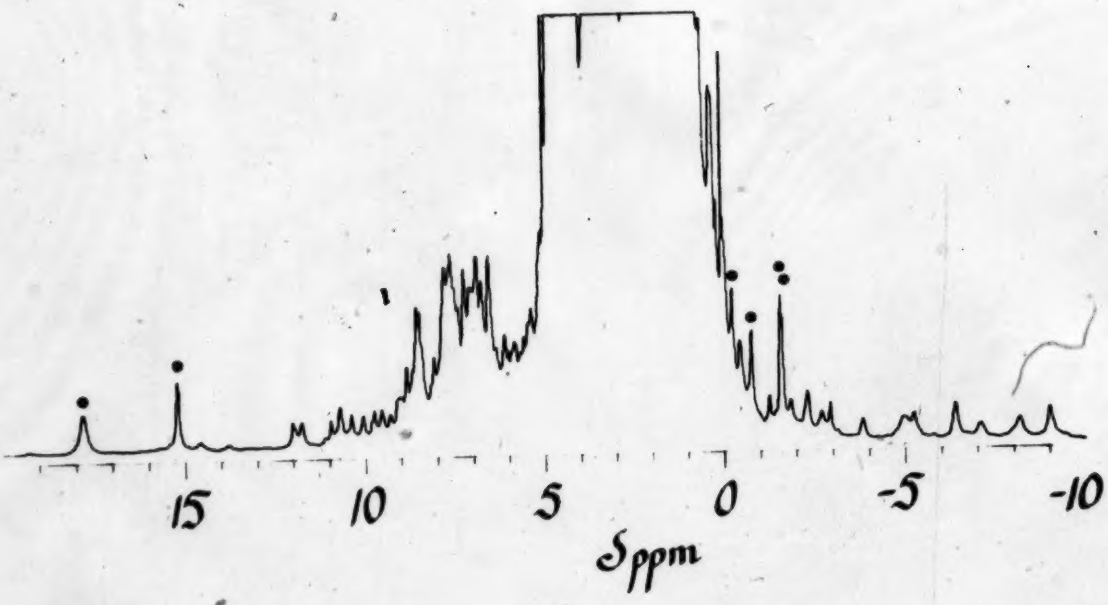

Figure 52. The ^1H NMR spectrum of the methyl resonances observed for the parvalbumin-Yb^{3+} complex. The 0.68 mM protein sample was prepared in 15 mM Pipes, 0.15 M KCl, 10 mM DTT, 0.5 mM DSS in D2O, pH 6.65 at a total metal to total protein ratio of 0.8. The sample temperature was 302°K.

(paramagnetic shift of 14.17 ppm). The other four observed methyls are shifted upfield, the most upfield appearing at -1.59 ppm (paramagnetic shift of -1.90 ppm). Two of the upfield shifted methyls are seen overlapping in Figure 52. The coordinates of the protons surrounding the metal are needed to calculate the spectra based upon the X-ray structure. The last Diamond refined X-ray structure of parvalbumin (Moews & Kretsinger, 1975a) was chosen as the most appropriate starting point. Proton coordinates were generated from the structure assuming standard bond lengths and geometries. In the case of methyl groups, the methyl proton centroid model (Rowan *et al.*, 1974) was used to determine the average methyl proton positions. For various choices of A1, A2, L1, L2, and alpha, spectra were calculated from the X-ray based proton coordinates. These calculated spectra were then compared with the observed paramagnetic shifts. Several criteria based upon the observed shifted methyl resonances were used in an attempt to assess the goodness of fit between the calculated and observed spectra in order to determine the best fit choices of the five unknown parameters. After no unambiguous fit was calculated, a second approach to the fitting procedure was initiated.

The resonances of the C-2 and C-4 protons of histidine 26 and the amino terminal acetyl protons have been assigned, and their paramagnetic shifts, determined. The determination of the paramagnetic shifts of the methyl resonances or of the three assigned resonances alone is insufficient for the fitting procedure. However, the paramagnetic shifts of the three assigned resonances, in conjunction with the paramagnetic shifts of the methyl resonances, can be used to determine the five NMR unknowns. The search for the best fit solution to the unknowns was made in the following manner. For a given choice of L1, L2, and alpha, the geometric factors G1 and G2 (equation 9.1) were calculated for the His C-2, His C-4, and N acetyl methyl protons. The parameters A1 and A2 for this particular choice of axis system were then taken as those giving the best least squares fit of the calculated paramagnetic shifts to the experimentally determined shifts for these nuclei. If the resultant calculated paramagnetic shifts for the assigned resonances were in good agreement with the experimentally determined shifts, the paramagnetic shifts of the methyl groups near the EF site were then calculated from their geometry in this axis system and the best fit A1 and A2. The choice of axis system was then rejected if it did not meet the criteria of having only two methyl groups shifted more downfield than 10 ppm, and having no methyl resonance shifted more upfield than -5 ppm. If the solution passed the above criteria, the goodness of the solution was tested by calculating a chi value comparing the two calculated most downfield methyl shifts with the paramagnetic shifts of 17.69 and 14.17 ppm, and the most upfield methyl shift with a paramagnetic shift of -1.9 ppm. One best fit solution was identified on the basis of the best fit of the calculated shifts to the His C-2, His C-4, and N acetyl shifts and the three shifted methyls discussed above. In fact 24 solutions were found corresponding to the various possible permutations of the labelling of the principal axis system (Agresti *et al.*, 1977). The final solution was selected by adopting the convention that $|A1|$ be maximal, and that $0<|A2/A1|<1$. The assigned nuclei are relatively far removed from the metal (13-20 A); this turned out to be an advantage, for their calculated geometric factors, G1 and G2, from equation 9.1, were not sensitive to inaccuracies in the X-ray structure. In addition, the histidine and the N acetyl nuclei are also located at diverse angular orientations, which is advantageous for the fitting procedure (Figure 53).

Generation of Proton Coordinates Proton coordinates based upon the X-ray crystallographic coordinates available from the Brookhaven Protein Data Bank were generated using the computer program written by P.D. Cradwick. The following bond lengths were assumed: CH (aromatic) 1.08 A; CH (aliphatic) 1.09 A; NH (peptide) 1.02 A (Kennard, 1970; Gordon & Ford, 1972).

Methyl proton centroid model Proton positions of the three protons of methyl resonances are difficult to determine, because of the presence of internal rotation. For the methyl groups, the methyl proton centroid model was used (Rowan *et al.*, 1974) to determine the average methyl proton positions. Figure 54 illustrates this model for the amino

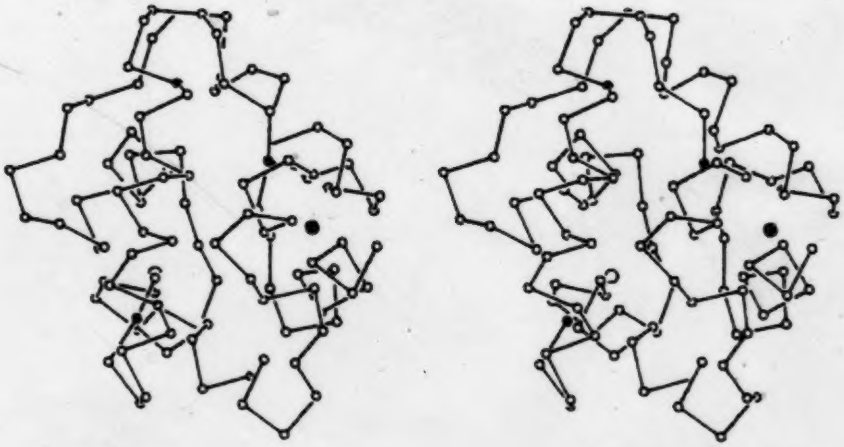

Figure 53. A stereodiagram of the alpha carbon backbone of parvalbumin indicating the diverse angular orientation of residues 1, 18, and 26. The atoms labelled correspond to the alpha carbon position of Ala 1, the approximate position of the amino acetyl terminus; of Cys 18, the fluorine label; of His 26, the C-2 and C-4 protons.

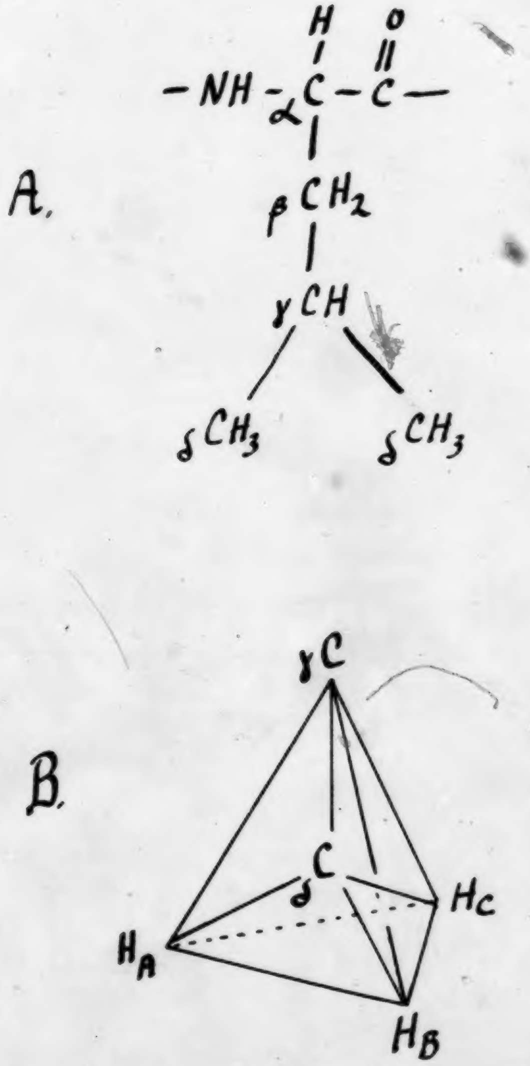

Figure 54. The methyl proton centroid model. The amino acid leucine is used as an illustration of the methyl proton centroid model.
A. The atom names of leucine.
B. The basis for the methyl proton centroid model.
The three protons HA, HB, and HC are all bonded to the delta carbon of leucine. To determine the average methyl proton position, a perpendicular is drawn from the gamma carbon through the delta carbon to a point in the plane determined by the three proton positions HA, HB, and HC. This point is considered the average methyl proton position.

acid leucine. To determine the average methyl proton position of a leucine methyl group, a perpendicular is drawn from the gamma carbon, through the delta carbon, to a point in the plane determined by the three proton positions HA, HB, and HC (Figure 54B). This position is considered the average methyl proton position. A 1.09 A CH bond length and a 109.3° H-C-H bond angle was assumed. The distance from the delta carbon atom to the average methyl proton position is 0.366 A. Similarly, positions for all other methyls were determined based upon the coordinates available from the Brookhaven Protein Data Bank.

Calculation of Paramagnetic Shifts A computer program was written to calculate the predicted paramagnetic shifts of nuclei, based upon the best fit parameters determined by the fitting procedure described above. The coordinates of parvalbumin (Protein Data Bank) were rotated in the new axis system defined by the parameters L1, L2, and alpha. The geometric factors G1 and G2 and the proton to metal distances were measured. The predicted paramagnetic shifts were then calculated according to equation 9.1.

D. Results

The values for the best fit solution are L1=-0.60, L2=-0.77, L3=-0.217, and alpha = 4.11 radians with A1 and A2 equal to -5450 ppm A^3 and -3360 ppm A^3, respectively. The observed paramagnetic shifts of the His 26 C-2, His 26 C-4, and N acetyl protons of parvalbumin are listed in Table 48.

Table 48

Paramagnetic Shift Data of the Assigned Histidine and N-acetyl Resonances of Parvalbumin

	Observed[1]	Calculated	
Nucleus	shift[1]	shift[1]	r(A)[2]
His 26 C2	0.485	0.488	13.6
His 26 C4	0.343	0.337	15.1
N-acetyl	0.033	0.042	20.1

[1] Paramagnetic chemical shifts in units of ppm.

[2] Distances to the EF metal are calculated from the X-ray structure (Kretsinger & Nockolds, 1973).

The list of their calculated chemical shifts, based upon the best fit parameters listed above, demonstrates that there is excellent agreement between the experimentally determined and calculated paramagnetic shifts, indicated by a standard deviation of ±0.008 ppm. The observed paramagnetic shifts for the seven methyl groups within approximately 10 A of the EF binding site and the metal to proton distances, obtained from their linewidths, are listed in Table 49. Also listed are the calculated paramagnetic shifts, and the distances based upon the X-ray structure. There is fair agreement for the two most downfield shifted methyl groups (17.69 vs. 18.075 ppm) and (14.17 vs. 11.297 ppm). The predicted distances 6.1 A and 9.0 A correspond well with the observed distances (6.2 ± 0.2 and 7.9 +1.8/-0.7 A which were calculated from the linewidths of the resonances (Chapter 5). However there is less agreement between the observed and calculated chemical shifts for the remaining five methyl resonances.

A list of the most downfield and most upfield experimentally determined and calculated paramagnetic shifts is presented in Table 50. The experimentally determined chemical shifts of the six most upfield shifted resonances are -12.68 to -19.06 ppm. Sixteen resonances with paramagnetic shifts more upfield than -19.06 ppm are calculated. The predicted linewidths of the shifted resonances relative to the linewidth of the resonance with an observed chemical shift position of 29.80 ppm are also

Table 49

A Comparison Between the Observed and Calculated Paramagnetic Shifts and Distances for the Seven Methyl Groups Within 10 Å of the EF Site

Observed		Calculated		
shift[1]	r(Å)[2]	shift[1]	nucleus	r(Å)[5]
17.690	6.2 +0.2/-0.2	18.075	LEU 86 δ 1	6.1
14.170	7.9 +1.8/-0.7	11.297	VAL 99 γ 2	9.0
[3]	[4]	9.807	ILE 97 γ 2	6.0
-0.365	[4]	6.270	ILE 97 δ 1	7.2
-1.440	[4]	6.120	LEU 86 δ 2	8.4
-1.621	[4]	-1.037	ILE 58 δ 1	10.2
-1.900	[4]	-3.793	ILE 58 γ 2	9.6

[1] Paramagnetic shifts, in ppm, ranked in decreasing order.
[2] Calculated from linewidths.
[3] Not shifted outside the diamagnetic spectrum.
[4] Calculated from the X-ray structure (Kretsinger & Nockolds, 1973).

Table 50

A Comparison of the Most Upfield and Most Downfield Observed and Calculated Paramagnetic Shifts

Observed	Calculated		
shift[1]	shift[1]	Nucleus	Relative Broadening[2]
	47.473	ASP 90β	3.50
	35.445	GLU 101β	2.71
	32.949	ASP 94β	3.66
27.62	27.191	GLY 95α	0.64
25.77	26.634	ASP 90β	1.36
22.26	26.011	GLY 93α	1.69
22.09	25.914	ASP 94α	0.78
20.10	24.024	ILE 97γ	3.64
18.90	17.618	GLU 101γ	4.41
-12.86	-13.332	PHE 57α	0.25
-14.16	-13.536	LYS 96ε	0.10
-14.53	-13.628	GLU 59γ	0.08
-14.60	-17.281	LYS 96ε	0.12
-16.20	-17.921	PHE 57β	0.14
-19.06	-20.128	ASP 92δ	3.81
	-28.628	LYS 96α	0.59
	-28.814	SER 91β	0.44
	-29.154	SER 91γ	0.29
	-30.477	LYS 96γ	0.59
	-31.068	GLU 101β	3.91
	-33.090	PHE 57α	0.44
	-35.307	ASP 92δ	1.01
	-39.388	LYS 96γ	0.68
	-40.338	LYS 96α	0.59
	-41.793	LYS 96β	2.12
	-50.889	ASP 92ε	4.83
	-53.348	PHE 57β	14.11
	-57.797	SER 91β	1.25
	-95.357	PHE 57δ	3.98
	-119.548	LYS 96β	8.60
	-148.459	LYS 96β	7.46

---

[1] Paramagnetic shifts measured in ppm.

[2] This column indicates the predicted line broadening relative to the linewidth of the resonance with an observed chemical shift of 29.80 ppm and r=5.85 A (which was calculated from its linewidth); this line broadening is based on a r^6 dependence.

listed. This calculation is based upon an r^6 dependence of the linewidths and the distance of 5.9 A calculated from the linewidth observed for the resonance at 29.80 ppm.

E. Discussion

This Chapter describes how the paramagnetic shifts of four assigned resonances and of a number of methyl resonances are used to evaluate and to check the principal elements and orientation of the magnetic susceptibility tensor of the Yb^{3+} parvalbumin complex. With these parameters, I am able to view the coordination geometry of the lanthanide in the EF binding site and to compare the observed spectrum of nuclei surrounding the EF metal binding site of parvalbumin, with that calculated from the X-ray crystallographic coordinates. The NMR fitting procedure results in the determination of a set of parameters which generates excellent agreement between the experimentally determined and calculated paramagnetic shifts of the His 26 C-2, His 26 C-4, and N acetyl methyl resonances. These resonances are far removed (13-20 A) from the metal ion, so that there is little possibility of a contact contribution to the shifts. In addition, small errors in the X-ray structure such as the less well defined electron density in the region of the amino terminus (Moews & Kretsinger, 1975a) are not going to greatly influence the calculated shifts. Also the diamagnetic positions of these assigned resonances were independently determined (Chapter 7). Therefore the choice of best fit is not ambiguous, nor are any of the assumptions made likely to be incorrect for these resonances.

The paramagnetic shift for the modified parvalbumin fluorine probe, which also meets the above criteria, has been measured. Because its exact position is unknown, it is not useful for the fitting procedure. However, it serves as a check on the best fit parameters, if the position of the probe is assumed to be equivalent to the position of the sulfur atom of cysteine 18. If the best fit parameters of L1, L2, alpha, A1, and A2 are used, and the above assumption made, a predicted paramagnetic chemical shift of 0.182 ppm is calculated. Since this value is comparable to the observed value of 0.16 ppm, this experiment serves to confirm the determination of the best fit NMR parameters. Therefore for these four resonances, which are in the approximate range of 13-23 A from the metal, there is excellent agreement between the calculated and experimentally determined spectra (Table 48).

The agreement is fair for nuclei such as the methyl groups which are closer to the metal, 6-10 A, especially considering potential inaccuracies in the determination of the diamagnetic positions and the use of the methyl proton centroid model. The observed metal to proton distances measured from the linewidths (Chapter 5) also agree quite well with the distances calculated based upon the X-ray coordinates of the best fit assigned methyl groups (Table

49). These data indicate the correctness of the best fit solution.

However, the agreement between the calculated and observed paramagnetic shifts is poor for nuclei very close to the metal. In all the fitting attempts for which reasonable criteria were invoked, calculated paramagnetic shifts far outside the range of the observed shifts were predicted. It is possible that resonances outside of the observed range were broadened beyond detection (see the relative linewidth prediction listed in Table 50); it is possible that very nearby nuclei may have contact shift contributions. However, neither of these two explanations can account for the large number of nuclei which have extraordinary large calculated paramagnetic shifts. There may be a problem from the NMR standpoint. The foremost possibility is the presence of internal motions. In this case, the observed NMR shifts would be too large rather than too small; such a prediction reflects the unequal weighting of closer conformations in the average of the sort $\langle 1/r^3 \rangle$.

There may be problems due to structural differences between the calcium substituted and ytterbium substituted proteins. Discrepancies may result from structural changes due to the +3 charge vs. the +2 charge of Ca^{2+}. However several lines of evidence fail to support this hypothesis (Chapter 4). The protons would be in a more compact conformation near the metal, due to the increased charge; which would result in the observed shifts being much larger than the predicted paramagnetic shifts.

The disagreement in paramagnetic shifts may result from inaccuracies in the generation of proton coordinates; the use of standard bond lengths and geometries may be invalid.

However, the largest source of errors I feel is inaccuracies in the X-ray based proton coordinates at a level below the resolution of the X-ray method (1.9 Å in this case). That is, errors on the order of 0.5 Å of a nuclei position as close as 3-4 Å greatly influence the NMR results, whereas they may not be detectable by X-ray crystallographic methods.

In the future, I shall generate a refined structure of carp parvalbumin with the aid of the NMR data which is at a level of resolution presently unobtainable by X-ray methods (Chapter 10).

The orientation of ligands in the EF calcium binding site of carp parvalbumin in the principal axis system of the magnetic susceptibility tensor of the metal ion is shown as a stereodiagram in Figure 55. An examination of this arrangement of oxygen atoms (Figure 56) reveals that the coordination resembles a distorted trigonal antiprism with the Z axis intercepting the opposite trigonal faces. Few examples of the geometry of six coordinate lanthanide complexes are available for comparison and the question remains as to the participation of the other carboxyl oxygens in the metal coordination (Moews & Kretsinger, 1975a; Sowadski *et al.*, 1978). The exact structure of the

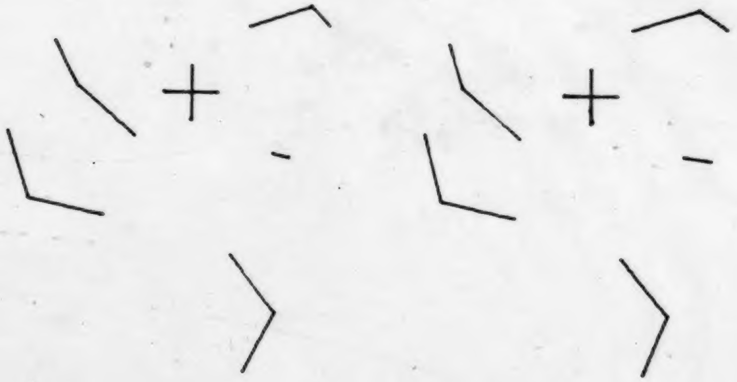

Figure 55. The orientation of the ligands in the EF metal binding site of carp parvalbumin in the principal axis system of the magnetic susceptibility tensor of the ytterbium ion. This is a stereodiagram of the oxygen ligands in the EF metal binding site. The origin is at the metal ion position. The positive Z axis is pointed out of the page, the positive Y axis is vertical, and the positive X axis points to the right.

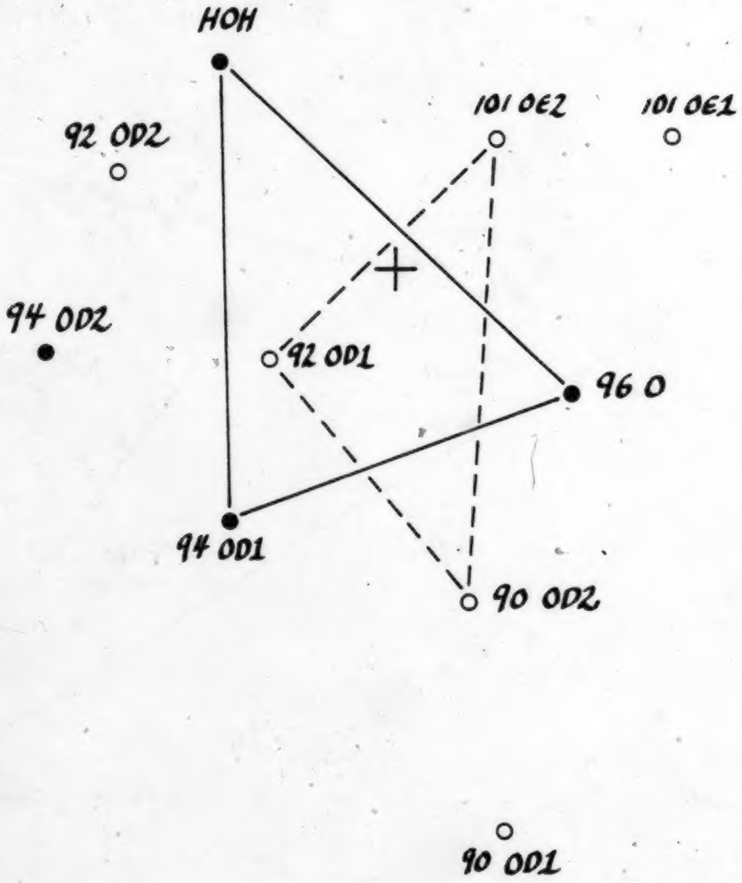

Figure 56. The orientation of the ligands in the EF metal binding site of carp parvalbumin in the principal axis system of the magnetic susceptibility tensor of the ytterbium ion. This is a projection of the oxygen atoms in the EF metal binding site in the XY plane. The origin is at the metal ion position. The positive Z axis is pointed out of the page, the positive Y axis is vertical, and the positive X axis points to the right. The nomenclature of Kretsinger & Nockolds, 1973, is used. Those atoms represented by open circles (o) are in the positive Z direction, above the plane of the paper; those atoms represented by filled circles (•) are in the negative Z direction, below the plane of the paper. The values of Z are listed below (in A): (HOH, -1.0; 90 OD2, 1.2; 90 OD1, 0.2; 92 OD2, 0.8; 92 OD1, 1.7; 94 OD2, -1.9; 94 OD1, -1.2; 96 O, -1.4; 101 OE2, 2.0; 101 OE1, 0.3).

ligands around the Yb^{3+} in the principal axis system of the magnetic susceptibility tensor must therefore await the refinement of the protein structure. Figure 56 however seems stereochemically reasonable and therefore is a suggestive indicator that the appropriate principal axis system has been determined.

X. Conclusions

A. Introduction

In this thesis, I have demonstrated that the paramagnetic ^{1}H NMR shifts of ytterbium substituted parvalbumin can be used to determine the three dimensional solution structure of the EF binding site. Significant differences exist between the observed paramagnetic shifts of the protons nearby the metal and the paramagnetic shifts calculated based upon proton coordinates generated from the X-ray crystallographic structure of parvalbumin (Moews & Kretsinger, 1975a).

B. Discussion

The differences between the calculated and observed spectra may be due to either trivial or non-trivial causes. A number of possible explanations is listed below: a) the effects of temperature on the NMR shifts and on the X-ray structural determination, b) changes in the protein structure as a result of differences in solvents used in the NMR and X-ray crystallographic studies, c) the presence of significant contact shift contributions to the NMR paramagnetic shifts, d) the neglect, for the moment, of the effects of internal motions in the protein on the calculation of NMR shifts, e) structural changes caused by Yb^{3+} replacing the larger Ca^{2+} ion, f) real differences between the crystallographic and solution structure, or g) errors in the X-ray generated proton coordinates.

The effects of temperature on the NMR shifts and on the X-ray structure determination The discrepancy may result from the effects of temperature. The paramagnetic shifts of parvalbumin at 302°K have been analyzed to yield the structure of the protein at 302°K. Differences are observed between the structure indicated by NMR methods and by X-ray methods, for which the data was collected at an unspecified temperature (Kretsinger & Nockolds, 1973). However, none of the observed paramagnetic shifts determined between 2° and 59°C approach the range of calculated shifts based upon the X-ray structure. The effects of temperature apparently cannot explain the observed disagreement between the NMR structure and the X-ray structure.

Changes in the protein structure as a result of differences in solvents used in the NMR and X-ray crystallographic studies The introduction of the deuterated solvent D2O may induce structural changes in the protein. However, the observed chemical shift positions of the parvalbumin Yb^{3+} complex in the presence of D2O and in the presence of H2O are identical (not shown); the structure of the protein in D2O and H2O are apparently identical. Any minor differences between the two observed spectra cannot explain the rather major differences between the observed and calculated spectra. The NMR experiment could be repeated in the 4.0 M phosphate buffer used in the X-ray study (Kretsinger & Nockolds, 1973), but the lanthanide would precipitate in the form of lanthanide phosphates. Also, the protein sample could possibly crystallize. The difference in pH, 6.8 in the X-ray study and 6.7 in the NMR study, is too small to cause major structural changes.

The presence of contact shift contributions to the NMR paramagnetic shifts The contact shift contribution has been neglected in this study because 1) the 4f electrons are inner core electrons and are not highly delocalized (when compared to the transition metal valence 3d electrons, 2) all protons under consideration are several bonds removed from the metal, 3) of all the lanthanides, ytterbium contributes the smallest contact contribution (Reuben, 1973b), and 4) the ratio of pseudocontact to contact shift is smallest for Yb^{3+} (Reuben, 1973b). Contact shifts are possible; however for the above reasons, their contributions to the paramagnetic shift would be small. The contact shifts could not account for the large disagreement between the observed and calculated spectra. As an indication of the magnitude of contact contributions previously observed, ^1H NMR studies of the interaction of alanine with Yb^{3+} (Sherry & Pascual, 1977) indicate that the contact shifts of the alpha and beta protons of alanine are ~10% of the pseudocontact shift.

The neglect of the effects of internal motions in the protein on the calculation of NMR shifts The surface residues of parvalbumin as well as other proteins are not immobile, (Robson, 1977; Huber, 1979) but are known to undergo motions. Such motions often result in poorly defined residues and coordinates in the X-ray structure (Moews & Kretsinger, 1975a). These motions could very well explain the extraordinary large paramagnetic shifts calculated for seven of the protons of Lys 96 (Table 50), for example. Also the flipping of phenylalanine rings (Snyder *et al.*, 1975; Roberts, 1975) about the C beta and C gamma bonds occurs on the timescale of 10^{-3} s in parvalbumin (Cave *et al.*, 1976). This flipping may result in inaccuracies in the proton positions; the shifts of the phenylalanine protons would be and are observed to be incorrect (Table 50). The rotation of methyl groups is another example of internal motion. However, the problem for this set of protons is less serious, for no extraordinary large shifts are calculated for any of the seven methyl groups within 10 A of the EF metal (Table 49).

However, the major question involves the residues not expected to undergo the motions as described above, such as the residues involved in the loop around the metal. Since the metal is tightly bound to the protein, any motions occurring in the amino acid side chains of the metal binding loop are expected to be constrained. Since many of the residues known to be mobile are internal, their flipping or rotating would require large scale motions of the protein to occur (Gelin & Karplus, 1975; McGammon *et al.*, 1977; McGammon & Karplus, 1979). Such motions would affect the NMR spectrum. Even if one considers only the $1/r^3$ dependence of the shift, the effects of motional averaging on the observed chemical shifts is not straightforward. However, the $1/r^3$ dependence would be expected to weight the closer contacts more heavily than the distant contacts. That is, if motional averaging were to occur around a local minimum defined by the X-ray positions, the shifts would be weighted more heavily for those conformations in which the nuclei are closer to the metal. Because of this dependence, large shifts should be observed. However, the range of paramagnetic chemical shifts observed is much less than the one calculated based upon the crystallographic coordinates. Although these motions must be considered, their contribution cannot explain the observed discrepancy.

The presence of internal motions may be a major problem if the motional averaging in solution is not the same averaging process occurring in the crystal. The position of an atom in a crystal represents a minimum about which there may be some vibrational averaging. The protein in solution may be undergoing different motional averaging which would result in a time averaged protein structure different from the crystallographic structure (see below). These differences may explain the disagreement between the observed and calculated spectra.

Structural changes caused by Yb^{3+} replacing Ca^{2+} The substitution of the smaller tripositive Yb^{3+} (0.87 Å) for the larger dipositive Ca^{2+} (0.99 Å) ion, may result in structural changes in the protein such as compacting or expansion of the metal binding site, because of the increased charge density or change in coordination number. However the X-ray crystallographic structure of the terbium substituted parvalbumin indicates no major structural changes (Sowadski *et al.*, 1978). In another crystallographic application, the substitution of a series of selected lanthanides (Matthews & Weaver, 1974) for the calcium ions bound in sites 1, 3, and 4 of thermolysin results in no major structural changes in the protein. However, since the technique described herein is more sensitive to errors at short distances than X-ray crystallographic methods, one cannot argue that no changes occur, because none are observed in the X-ray structure. Indeed some minor changes in the ^{1}H NMR spectrum are observed upon binding of the diamagnetic Lu^{3+} to parvalbumin (Chapter 2). The substitution of Yb^{3+} for Ca^{2+} may result in structural changes due to an increase in coordination number. The laser induced luminescence studies (Horrocks & Sudnick, 1979) of Tb^{3+} and Eu^{3+} substituted parvalbumins indicate that there is only one water molecule bound to the EF site of parvalbumin, as is observed in the X-ray structure, even though lanthanides generally prefer a higher coordination number. These results suggest that the structures of the Ca^{2+} substituted and lanthanide substituted parvalbumins are identical.

Differences between the crystallographic and solution structure The discrepancy may be due to differences in the solution and crystal structure. If the tightening of the metal binding site were to occur due to the increased charge density, this compacting would affect the results in the opposite direction. That is, if protons were closer to the metal than suggested by the X-ray structure, then the observed range in paramagnetic shifts would be much larger than the range of paramagnetic shifts calculated based upon the X-ray crystallographic structure. However, the opposite is observed; the calculated paramagnetic shifts are far larger than the observed range of paramagnetic shifts. This observation then suggests that the structure of the metal binding site is actually more open and expanded than the X-ray crystallographic structure suggests. The enlargened metal binding site may reflect the differences in motional averaging in solution and in the crystalline state.

Errors in the X-ray generated proton coordinates I feel the most probable source of the observed differences lies in the X-ray generated proton coordinates. The errors may be due to either the proton generated coordinates or the original X-ray crystallographic coordinates. Inaccuracies may arise in the proton generated coordinates, because idealized geometries were assumed. How valid and correct are standard bond lengths and angles? Although there is no definite answer to this query, it is indicated as a possible source of the discrepancy. The other conceivable explanation lies in the original X-ray crystallographic determination of parvalbumin. The structure with the best R factor (F6h, R =

0.27; Protein Data Bank) has distorted molecular geometries due to the unconstrained refinement of the coordinates. The observed phenylalanine rings were distorted and non-planar. The generated protons of glycine residues involved in the metal binding loop point directly to the metal; this observation indicates an unreasonable structure. Because the bond angles and geometries of the amino acids are known *a priori* to a greater accuracy than the 1.85 Å determination can yield, the last refined structure (F6d, R = 0.34) that had standard geometries was used. However, this structure is not one of the better refined structures known to date. A more highly refined parvalbumin structure may explain the discrepancy.

C. The Future

In the preceeding section, I have discussed a number of possibilities to explain the differences between the observed paramagnetic shifts and the calculated paramagnetic shifts based upon the X-ray crystallographic structure. In this section, I shall discuss what the future holds for this methodology and the study.

The NMR data and the X-ray crystallographic data indicate that there is a disagreement between the solution and solid state structure. In the future I hope to refine the X-ray based proton coordinates of carp parvalbumin. I shall try to determine what specific movements in the X-ray crystallographic structure are necessary to yield calculated paramagnetic shifts which approach the observed paramagnetic shifts. I feel that minor changes in the proton coordinates should minimize the observed disagreement. However, to date, I cannot state quantitatively the magnitude of position changes needed. It may be possible that small changes on the order of 0.5 A to 1.0 A in the positions of carbon, oxygen, and nitrogen atoms and small changes in bond rotations may result in significant changes in the proton coordinates. These proton position changes may then account for the disagreement in the observed and calculated spectra. I shall make an initial attempt at refinement by using a graphics display system. Using the experimentally determined magnitude and orientation of the principal axes of the magnetic susceptibility tensor, I shall introduce specific bond rotations to determine the magnitude of changes in position needed to minimize the discrepancy. This will be a first approximation at a better structure. Secondly, in collaboration with Dr. Brian F.P. Edwards, I am determining the X-ray crystallographic structure of parvalbumin to the highest resolution possible, using the methods of Hendrickson & Konnert (Hendrickson & Konnert, 1980). A more highly refined structure of the protein may be the answer to the observed discrepancy. A final refinement incorporating both the NMR data and the X-ray crystallographic data should yield the true solution structure of the carp parvalbumin.

Bibliography

Abragam, A. (1961) *The Principles of Nuclear Magnetism*, p 264, Oxford University Press, Oxford.

Abragam, A., & Bleaney, B. (1970) *Electron Paramagnetic Resonance of Transition Ions*, Oxford University Press, Oxford.

Agresti, D.G., Lenkinski, R.E., & Glickson, J.D. (1977) *Biochem. Biophys. Res. Commun. 76*, 711.

Barker, W.C., Ketcham, L.K., & Dayhoff, M.O. (1978) in *Atlas of Protein Sequence and Structure* (M.O. Dayhoff, Ed.), Vol. 5, Supplement 3, p 273, National Biomedical Research Foundation, Washington, D.C.

Barry, C.D., North, A.C.T., Glasel, J.A., Williams, R.J.P., & Xavier, A.V. (1971) *Nature 232*, 236.

Bauer, D.R., Opella, S.J., Nelson, D.J., & Pecora, R. (1975) *J. Am. Chem. Soc. 97*, 2580.

Benzonana, G., Capony, J.-P., & Pechere, J.-F. (1972) *Biochim. Biophys. Acta 278*, 110.

Bernstein, F.C., Koetzle, T.F., Williams, G.J.B., Meyer,Jr., E.F., Brice, M.D., Rodgers, J.R., Kennard, O., Shimanouchi, T., & Tasumi, M. (1978) *Arch. Biochem. Biophys. 185*, 584.

Birdsall, W.J., Levine, B.A., Williams, R.J.P., Demaille, J.G., Haiech, J., & Pechere, J.-F. (1979) *Biochimie 61*, 741.

Birnbaum, E.R., & Sykes, B.D. (1978) *Biochemistry 17*, 4865.

Bleaney, B., Dobson, C.M., Levine, B.A., Martin, R.B., Williams, R.J.P., & Xavier, A.V. (1972) *J.C.S. Chem. Commun.*, 791.

Bleaney, B. (1972) *J. Magn. Reson. 8*, 91.

Bloembergen, N. (1957a) *J. Chem. Phys. 27*, 572.

Bloembergen, N. (1957b) *J. Chem. Phys. 27*, 595.

Blum, H.E., Lehky, P., Kohler, L., Stein, E.A., & Fischer, E.H. (1977) *J. Biol. Chem. 252*, 2834.

Bose, K. (1979) *Ph.D. Thesis*, Carnegie-Mellon University, Pittsburgh, Pennsylvania.

Bose, K., & Bothner-By, A.A. (1980) *Fed. Proc. Fed. Amer. Soc. Exp. Biol. 39*, 1626.

Boudreaux, E.A. & Mulay, L.N. (1976) *Theory and Applications of Molecular Paramagnetism*, John Wiley & Sons, New York.

Briggs, J.M., Moss, G.P., Randall, E.W., & Sales, K.D. (1972) *Chem. Commun.* 1180.

Campbell, I.D., Dobson, C.M., Williams, R.J.P., & Xavier, A.V. (1973a) *J. Magn. Reson. 11*, 172.

Campbell, I.D., Dobson, C.M., Williams, R.J.P., & Xavier, A.V. (1973b) *Ann. N. Y. Acad. Sci. 222*, 163.

Campbell, I.D., Dobson, C.M., & Williams, R.J.P. (1975a) *Proc. R. Soc. Lond. Ser. A. 345*, 23.

Campbell, I.D., Dobson, C.M., & Williams, R.J.P. (1975b) *Proc. R. Soc. London Ser A. 345*, 41.

Campbell, I.D., Dobson, C.M., Williams, R.J.P., & Wright, P.E. (1975c) *FEBS Lett. 57*, 96.

Capony, J.-P., Pina, C., & Pechere, J.-F. (1976) *Eur. J. Biochem. 70*, 123.

Carrington, A., & McLachlan, A.D. (1967) *Introduction to Magnetic Resonance*, Harper & Row, New York.

Carver, J.P., Barber, B.H., & Fuhr, B.J. (1977) *J. Biol. Chem. 252*, 3141.

Cave, A., Dobson, C.M., Parello, J., & Williams R.J.P. (1976) *FEBS Lett. 65*, 190.

Cave, A., Parello, J., Drakenberg, T., Thulin, E., & Lindman, B. (1979a) *FEBS Lett. 100*, 148.

Cave, A., Pages, M., Morin, P., & Dobson, C.M. (1979b) *Biochimie 61*, 607.

Cave, A., Daures, M.-F., Parello, J., Saint-Yves, A., & Sempere, R. (1979c) *Biochimie 61*, 755.

Cheung, W.Y. (1980) *Science 207*, 19.

Coffee, C.J., & Bradshaw, R.A. (1973) *J. Biol. Chem. 248*, 3305.

Coffee, C.J., Bradshaw, R.A., & Kretsinger, R.H. (1974) in *Advances in Experimental Medicine and Biology* (M.

Friedman, Ed.) p 48, Plenum Press, New York.

Coffee, C.J., & Solano, C. (1976) *Biochim. Biophys. Acta 453*, 67.

Collins, J.H., Potter, J.D., Horn, M.J., Wilshire, G., & Jackman, N. (1973) *FEBS Lett. 36*, 268.

Collins, J.H. (1974) *Biochem. Biophys. Res. Commun. 58*, 301.

Collins, J.H. (1976) *Nature 259*, 699.

Collins, J.H., Greaser, M.L., Potter, J.D., & Horn, M.J. (1977) *J. Biol. Chem. 252*, 6356.

Cox, J.A., Wnuk, W., & Stein, E. (1977) in *Calcium Binding Proteins and Calcium Function* (R.H. Wasserman, R.A. Corradino, E. Carafoli, R.H. Kretsinger, D.H. MacLennan, & F.L. Siegel, Eds.) p 302, Elsevier, New York.

Cox, J.A., Winge, D.R., & Stein, E.A. (1979) *Biochimie 61*, 601.

Dabrowska, R., Sherry, J.M.F., Aromatorio, D.K., & Hartshorne, D.J. (1978) *Biochemistry 17*, 253.

Darnall, D.W., & Birnbaum, E.R. (1970) *J. Biol. Chem. 245*, 6484.

de Boer, J.W.M, Sakkers, P.J.D., Hilbers, C.W., & de Boer, E. (1977) *J. Magn. Reson. 25*, 455.

Dedman, J.R., Jackson, R.L., Schreiber, W.E., & Means, A.R. (1978) *J. Biol. Chem. 253*, 343.

Demaille, J., Dutruge, E., Eisenberg, E., Capony, J.-P., & Pechere, J.-F. (1974) *FEBS Lett. 42*, 173.

Derancourt, J., Haiech, J., & Pechere, J.-F. (1978) *Biochim. Biophys. Acta 532*, 373.

Dobson, C.M. (1975) *Biochemistry 14*, 4905.

Dobson, C.M., & Levine, B.A. (1976) in *New Techniques in Biophysics and Cell Biology* (R.H. Pain, & B.J. Smith, Eds.), 3, p 19, John Wiley & Sons, London.

Dobson C.M., Geraldes, C.F.G.C., Ratcliffe, G., & Williams, R.J.P. (1978) *Eur. J. Biochem. 88*, 259.

Donato, Jr.,H., & Martin, R.B. (1974) *Biochemistry 13*, 4575.

Drakenberg T., Lindman, B., Cave, A., & Parello, J. (1978) *FEBS Lett. 92*, 346.

Dwek, R.A., Richards, R.E., Morallee, K.G., Nieboer, E., Williams, R.J.P., & Xavier, A.V. (1971) *Eur. J. Biochem. 21*, 204.

Edwards, B.F.P., & Sykes, B.D. (1978) *Biochemistry 17*, 684.

Elgavish, G.A., & Reuben, J. (1974) *J. Magn. Reson. 16*, 360.

Enfield, D.L., Ericcson, L.H., Blum, H.E., Fischer, E.H., & Neurath, H. (1975) *Proc. Nat. Acad. Sci. USA 72*, 1309.

Flaschka, H.A. (1964) *EDTA Titrations*, p 64, Pergamon Press, Oxford.

Frank, G., & Weeds, A.G. (1974) *Eur. J. Biochem. 44*, 317.

Fullmer, C.S., & Wasserman, R.H. (1977) in *Calcium Binding Proteins and Calcium Function*, (R.H. Wasserman, R.A. Corradino, E. Carafoli, R.H. Kretsinger, D.H. MacLennan, & F.L. Siegel, Eds.) p 302, Elsevier, New York.

Geisow, M.J. (1978) *Nature 276*, 211.

Gelin, B.R., & Karplus, M. (1975) *Proc. Nat. Acad. Sci. USA 72*, 2002.

Geraldes, C.F.G.C., & Williams, R.J.P. (1978a) *Eur. J. Biochem. 85*, 463.

Geraldes, C.F.G.C., & Williams, R.J.P. (1978b) *Eur. J. Biochem. 85*, 471.

Geraldes, C.F.G.C. (1979) *J. Magn. Reson. 36*, 89.

Geraldes, C.F.G.C., & Williams, R.J.P. (1979) *Eur. J. Biochem. 97*, 93.

Goodman, M., & Pechere, J.-F. (1977) *J. Mol. Evol. 9*, 131.

Gordon, A.J., & Ford, R.A. (1972) *The Chemist's Companion*, John Wiley & Sons, New York.

Gueron, M. (1975) *J. Magn. Reson. 19*, 58.

Haiech, J., Derancourt, J., Pechere, J.-F., & Demaille, J.G. (1979a) *Biochimie 61*, 583.

Haiech, J., Derancourt, J., Pechere, J.-F., & Demaille, J.G. (1979b) *Biochemistry 18*, 2752.

Handbook of Chemistry and Physics (1970), (R.C. Weast, Ed.), The Chemical Rubber Co., Cleveland, Ohio.

Hasselbach, W. (1964) *Prog. Biophys. Mol. Biol. 14*, 167.

Heizmann, C.W., & Strehler, E.E. (1979) *J. Biol. Chem. 254*, 4296.

Hendrickson, W.A., & Karle, J. (1973) *J. Biol. Chem. 248*, 3327.

Hendrickson, W.A., & Konnert, J.H. (1980) in *Biomolecular Structure, Function, Conformation, and Evolution* (R. Srinivasan, Ed.) p 43, Pergamon, Oxford.

Hincke, M.T., McCubbin, W.D., & Kay, C.M. (1978) *Can. J. Biochem. 56*, 384.

Hinckley, C.C. (1969) *J. Am. Chem. Soc. 91*, 5160.

Hofmann, T., Kawakami, M., Hitchman, A.J.W., Harrison, J.E., & Dorrington, K.J. (1979) *Can. J. Biochem. 57*, 737.

Horrocks, Jr., W. DeW. (1977) *J. Magn. Reson. 26*, 333.

Horrocks, Jr., W. DeW., & Sudnick, D.R. (1979) *J. Am. Chem. Soc. 101*, 334.

Huber, R. (1979) *Nature 280*, 538.

Hüfner, S. (1978) *Optical Spectra of Transparent Rare Earth Compounds*, Academic Press, New York.

Jarrett, H.W., & Penniston, J.T. (1978) *J. Biol. Chem. 253*, 4676.

Jauregui-Adell, J., & Pechere, J.-F. (1978) *Biochim. Biophys. Acta 536*, 263.

Kennard, O. (1970) in *Handbook of Chemistry and Physics*, (R.C. Weast, Ed.), The Chemical Rubber Co., Cleveland, Ohio.

Klee, C.B., Crouch, T.H., & Richman, P.G. (1980) *Annu. Rev. Biochem. 49*, 489.

Konosu, S., Hamoir, G., & Pechere, J.-F. (1965) *Biochem. J. 96*, 98.

Korbl, J., & Pribil, R. (1956) *Chemist-Analyst 45*, 102.

Kretsinger, R.H., Dangelat, D., & Bryan, R.F. (1971) *J. Mol. Biol. 59*, 213.

Kretsinger, R.H., & Nockolds, C.E. (1973) *J. Biol. Chem. 248*, 3313.

Kretsinger, R.H., & Parry, C.D. (1975) *Biochim. Biophys. Acta 405*, 40.

Kretsinger, R.H. (1976) *Annu. Rev. Biochem. 45*, 239.

LaMar, G.N., Horrocks, Jr., W. deW., & Holm, R.H., Eds. (1973) *NMR of Paramagnetic Molecules: Principles and Applications*, New York, Academic Press.

Lee, L., Sykes, B.D., & Birnbaum, E.R. (1979a) *FEBS Lett. 98*, 169.

Lee, L., Birnbaum, E.R., & Sykes, B.D. (1979b) *Biophys. J. 25*, 247a.

Lee, L., & Sykes, B.D. (1980a) *Adv. Inorg. Biochem. 2*, 183.

Lee, L., & Sykes, B.D. (1980b) *Biophys. J. 33*, 000.

Lee, L., & Sykes, B.D. (1980c) *Biochemistry 19*, 3208.

Lee, L., & Sykes, B.D. (1980d) in *Biomolecular Structure Determination by NMR*, (A.A. Bothner-By, J.D. Glickson, & B.D. Sykes, Eds.), p 000, Marcel Dekker, New York.

Lee, L., & Sykes, B.D. (1980e) *Biochemistry 19*, 000.

Lee, L., & Sykes, B.D. (1980f) *J. Magn. Reson. 00*, 000.

Lehky, P., Comte, M., Fischer, E.H., & Stein, E.A. (1977) *Anal. Biochem. 82*, 158.

Lehky, P., & Stein, E.A. (1979) *Comp. Biochem. Physiol. 63*, 253.

Lenkinski, R.E., & Reuben, J. (1976) *J. Magn. Reson. 21*, 47.

Lenkinski, R.E., Agresti, D.G., Chen, D.M., & Glickson, J.D. (1978) *Biochemistry 17*, 1463.

Lin, Y.M., Liu, Y.P., & Cheung, W.Y. (1974) *J. Biol. Chem. 249*, 4943.

Lynch, T.J., & Cheung, W.Y. (1979) *Arch. Biochem. Biophys. 194*, 165.

Marinetti, T.D. (1975) *Ph.D. Thesis*, Harvard University, Cambridge, Massachusetts.

Marinetti, T.D., Snyder, G.H., & Sykes, B.D. (1975) *J. Am. Chem. Soc. 97*, 6562.

Marinetti, T.D., Snyder, G.H., & Sykes, B.D. (1976) *Biochemistry 15*, 4600.

Marinetti, T.D., Snyder, G.H., & Sykes, B.D. (1977) *Biochemistry 16*, 647.

Markley, J.L. (1975) *Acc. Chem. Res. 8*, 70.

Martin, R.B., & Richardson, F.S. (1979) *Quart. Rev. Biophys. 12*, 181.

Matthews, B.W., & Weaver, L.H. (1974) *Biochemistry 13*, 1719.

McConnell, H.M., & Robertson, R.E. (1958) *J. Chem. Phys. 29*, 1361.

McCubbin, W.D., & Kay, C.M. (1980) *Acc. Chem. Res. 13*, 185.

McDonald, C.C., & Phillips, W.D. (1969) *Biochem. Biophys. Res. Commun. 35*, 43.

McGammon, J.A., Gelin, B.R., & Karplus, M. (1977) *Nature 267*, 585.

McGammon, J.A., & Karplus, M. (1979) *Proc. Nat. Acad. Sci. USA 76*, 3585.

McGarvey, B.R. (1979) *J. Magn. Reson. 33*, 445.

Means, A.R., & Dedman, J.R. (1980) *Nature 285*, 73.

Moews, P.C., & Kretsinger, R.H. (1975a) *J. Mol. Biol. 91*, 201.

Moews, P.C., & Kretsinger, R.H. (1975b) *J. Mol. Biol. 91*, 229.

Morris, A.T., & Dwek, R.A. (1977) *Quart. Rev. Biophys. 10*, 421.

Murray, J.M., & Weber, A. (1974) *Sci. Am. 230*, 56.

Nelson, D.J., Opella, S.J., & Jardetzsky, O. (1976) *Biochemistry 15*, 5552.

Nelson, D.J., Miller, T.L., & Martin, R.B. (1977) *Bioinorg. Chem. 7*, 325.

Nelson, D.J. (1978) *Inorg. Chim. Acta 27*, L71.

Nelson, D.J., Theoharides, A.D., Nieburgs, A.C., Murray, R.K., Gonzalez-Fernandez, F., & Brenner, D.S. (1979) *Int. J. Quantum Chem. 16*, 159.

Newman, R.H. (1974) *Tetrahedron 30*, 969.

Nockolds, C.E., Kretsinger, R.H., Coffee, C.J., & Bradshaw, R.A. (1972) *Proc. Nat. Acad. Sci. USA 69*, 581.

Parello, J., & Pechere, J.-F. (1971) *Biochimie 53*, 1079.

Parello, J. Cave, A., Puigdomenech, P., Maury, C., Capony, J.-P., & Pechere, J.-F. (1974) *Biochimie 56*, 61.

Parello, J., Lilja, H., Cave, A., & Lindman, B. (1978) *FEBS Lett. 87*, 191.

Pechere, J.-F., Demaille, J., & Capony, J.-P. (1971a) *Biochim. Biophys. Acta 236*, 391.

Pechere, J.-F., Capony, J.-P., & Ryden, L. (1971b) *Eur. J. Biochem. 23*, 421.

Pechere, J.-F., Capony, J.-P., & Demaille, J. (1973) *Syst. Zool. 22*, 533.

Pechere, J.-F., Derancourt, J., & Haiech, J. (1977) *FEBS Lett. 75*, 111.

Perkins, S.J., & Wüthrich, K. (1978) *Biochim. Biophys. Acta 536*, 406.

Potter, J.D., Johnson, J. D., Dedman, J.R., Schreiber, W.E., Mandel, F., Jackson, R.L., & Means, A.R. (1977a) in *Calcium Binding Proteins and Calcium Function* (R.H. Wasserman, R.A. Corradino, E. Carafoli, R.H. Kretsinger, D.H. MacLennan, & F.L. Siegel, Eds.), p 239, Elsevier, New York.

Potter, J.D. Dedman, J.R., & Means, A.R. (1977b) *J. Biol. Chem. 252*, 5609.

Potter, J.D., Johnson, J.D., & Mandel, F. (1978) *Fed. Proc. Fed. Amer. Soc. Exp. Biol. 37*, 1608.

Protein Data Bank, Department of Chemistry, Brookhaven National Laboratory, Associated Universities, Inc., Upton, L.I., New York, 11973.

Raiford, D.S., Fisk, C.L., & Becker, E.D. (1979) *Anal. Chem. 51*, 2050.

Rao, K.S.P., & Gerday, C. (1973) *Comp. Biochem. Physiol. 44*, 931.

Rasmussen, H., Goodman, D.B.P., & Tenehouse, A. (1972) *Crit. Rev. Biochem. 1*, 95.

Reuben, J. (1973a) *Prog. Nuc. Magn. Reson. Spectros. 9*, 1.

Reuben, J. (1973b) *J. Mag. Reson. 11*, 103.

Roberts, G.C.K. (1975) *Nature 258*, 112.

Robson, B. (1977) *Nature 267*, 577.

Rowan III, R., McGammon, J.A., & Sykes, B.D. (1974) *J. Am. Chem. Soc. 96*, 4773.

Schwarzenbach, G., & Flaschka, H. (1969) in *Complexometric Titrations*, p 146, Methuen & Co., London.

Shannon, R.D. (1976) *Acta Crystallogr. A32*, 751.

Shenolikar, S., Cohen, P.T.W., Cohen, P., Nairn, A.C., & Perry, S.V. (1979) *Eur. J. Biochem. 100*, 329.

Sherry, A.D., & Pascual, E. (1977) *J. Am. Chem. Soc. 99*, 5871.

Sherry, A.D., Yang, P.P., & Morgan, L.O. (1980) *J. Am. Chem. Soc. 00*, 000.

Slichter, C.P. (1978) *Principles of Nuclear Magnetic Resonance*, Springer-Verlag, New York.

Smith, S.J. (1977) *Nature 268*, 400.

Snyder, G.H., Rowan R., Karplus, S., & Sykes, B.D. (1975) *Biochemistry 14*, 3765.

Solomon, I. (1955) *Phys. Rev. 99*, 559.

Sowadski, J. Cornick, G., & Kretsinger, R.H. (1978) *J. Mol. Biol. 124*, 123.

Stevens, F.D., Walsh, M., Ho, H.C., Teo, T.S., & Wang, J.H. (1976) *J. Biol. Chem. 251*, 4495.

Stout, Jr., E.W., & Gutowsky, H.S. (1976) *J. Magn. Reson. 24*, 389.

Swift, T.J., & Connick, R.E. (1962) *J. Chem. Phys. 37*. 307.

Tanswell, P., Thornton, J.M., Korda, A.V., & Williams, R.J.P. (1975) *Eur. J. Biochem. 57*, 135.

Taylor, E.W. (1972) *Annu. Rev. Biochem. 41*, 577.

Tufty, R.M., & Kretsinger, R.H. (1975) *Science 187*, 167.

Vanaman, T.C., Sharief, F., & Watterson, D.M. (1977) in *Calcium Binding Proteins and Calcium Function* (R.H. Wasserman, R.A. Corradino, E. Carafoli, R.H. Kretsinger, D.H. MacLennan, & F.L. Siegel, Eds.), p 107, Elsevier, New York.

van Eerd, J.-P., & Takahashi, K. (1976) *Biochemistry 15*, 1171.

Van Geet, A.L. (1968) *Anal. Chem. 40*, 2227.

Van Geet, A.L. (1969) Abstracts of the 10th Experimental NMR Conference, Mellon Institute, Pittsburgh, Pennsylvania.

Van Geet, A.L. (1970) *Anal. Chem. 42*, 679.

Van Vleck, J.H. (1932) *The Theory of Electric and Magnetic Susceptibilities*, Clarendon Press, Oxford.

Vega, A.J., & Fiat, D. (1976) *Mol. Phys. 31*, 347.

Vogel, A.I. (1961) in *Quantitative Inorganic Analysis*, p 899, Longmans, London.

Wagner, P.D. & Weeds, A.G. (1977) *J. Mol. Biol. 109*, 455.

Warshel, A., & Levitt M. (1976) *J. Mol. Biol. 106*, 421.

Watterson, D.M., Sharief, F., & Vanaman, T.C. (1980) *J. Biol. Chem. 255*, 962.

Weeds, A.G., & McLachlan, A.D. (1974). *Nature 252*, 646.

Weeds, A., Wagner, P., Jakes, R., & Kendrick-Jones, J. (1977) *Calcium Binding Proteins and Calcium Function* (R.H. Wasserman, R.A. Corradino, E. Carafoli, R.H. Kretsinger, D.H. MacLennan, & R.L. Siegel, Eds.), p 222, Elsevier, New York.

Westcott, K.R., LaPorte, D.C., & Storm, D.R. (1979) *Proc. Nat. Acad. Sci. USA 76*, 204.

White, H., & Closset, J. (1979) *Biophys. J. 25*, 247a.

Wong, P.Y.-K., & Cheung, W.Y. (1979) *Biochem. Biophys. Res. Commun. 90*, 473.

Yagi, K., Yazawa, M., Kakiuchi, S., Oshima, M., & Uenishi, K. (1978) *J. Biol. Chem. 253*, 1338.

Zeppezauer, M., Eklund, H., & Zeppezauer, E.S. (1968) *Arch. Biochem. Biophys. 126*, 564.

Appendix 1

Amino Acid Nomenclature[1]

Amino Acid	Three letter Abbreviation	One letter Abbreviation
Alanine	Ala	A
Arginine	Arg	R
Asparagine	Asn	N
Aspartic Acid	Asp	D
(Aspartic Acid or Asparagine)	Asx	B
Cysteine	Cys	C
Glutamine	Glu	Q
Glutamic Acid	Glu	E
(Glutamic Acid or Glutamine)	Glx	Z
Glycine	Gly	G
Histidine	His	H
Isoleucine	Ile	I
Leucine	Leu	L
Lysine	Lys	K
Methionine	Met	M
Phenylalanine	Phe	F
Proline	Pro	P
Serine	Ser	S
Threonine	Thr	T
Tryptophan	Trp	W
Tyrosine	Tyr	Y
Valine	Val	V

---

[1] (1969) *Biochem. J. 113*, 1.

Appendix 2

Chemical Structures for Buffers and Indicators

1. Pipes

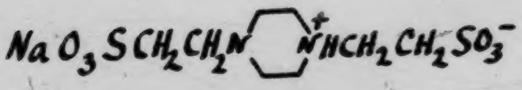
NaO3SCH2CH2N
+
NHCH2CH2SO3-

2. Mes

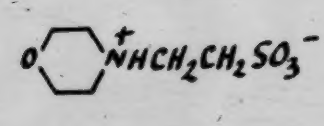
O
+
NHCH2CH2SO3-

3. dithizone

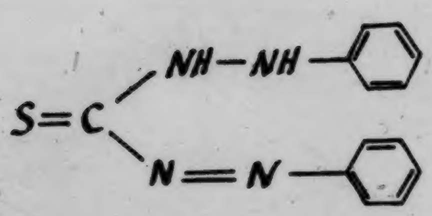

4. xylenol orange

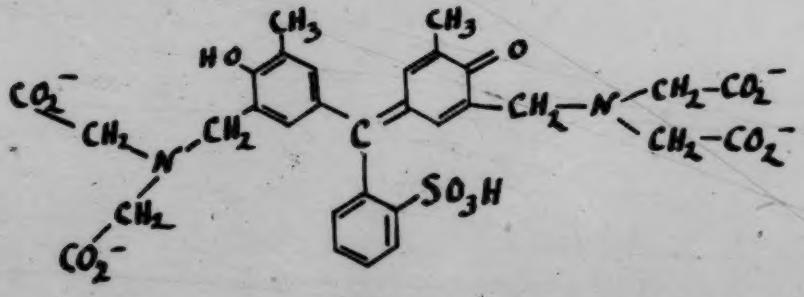
CH3
HO
CH3
O
CO2-
CH2
N
CH2
C
CH2—N
CH2—CO2-
CH2—CO2-
CH2
CO2-
SO3H

Appendix 3

Numerical Values for Some Important Physical Constants[1]

Planck's constant	$h = 6.6256 \times 10^{-27}$ erg sec
Planck's constant	$\hbar = 1.05443 \times 10^{-27}$ erg sec
Boltzmann's constant	$k = 3.8044 \times 10^{-16}$ erg/deg
Gyromagnetic ratio(^{1}H)	$\gamma = 2.6753 \times 10^{4}$ rad/sec gauss
Nuclear magneton	$\mu_N = 0.50504 \times 10^{-23}$ erg/gauss
Bohr magneton	$\beta = 0.92731 \times 10^{-20}$ erg/gauss

---

[1] Abbreviations used: sec, seconds; deg, degree; rad, radians (Carrington & McLachlan, 1967).